

Three Dimensional Finite Element Optimization Using the Partial p-Adaptive Method for
Stress Analysis of Underground Excavations with Prismatic Cross-sections

Rasha Ibrahim

A Thesis
in
The Department
of
Building, Civil and Environmental Engineering

Presented in Partial Fulfillment of the Requirements
For the Degree of Master of Applied Science (Civil Engineering) at
Concordia University
Montreal, Quebec, Canada

July 2014

© Rasha Ibrahim, 2014

CONCORDIA UNIVERSITY

School of Graduate Studies

This is to certify that the thesis prepared

By: Rasha Ibrahim

Entitled: Three Dimensional Finite Element Optimization Using the Partial p-Adaptive Method for Stress Analysis of Underground Excavations with Prismatic Cross-sections

and submitted in partial fulfillment of the requirements for the degree of:

MASc Civil Engineering

complies with the regulations of the University and meets the accepted standards with respect to originality and quality.

Signed by the final examining committee:

Dr. A. M. Hanna _____ Chair

Dr. C. Alecsandru _____ Examiner

Dr. A. Dolatabadi _____ Examiner

Dr. A. M. Zsaki _____ Supervisor

Approved by _____
Chair of Department or Graduate Program Director

Dean of Faculty

ABSTRACT

Three Dimensional Finite Element Mesh Optimization Using the Partial p-Adaptive Method for Stress Analysis of Underground Excavations with Prismatic Cross-sections

Rasha Ibrahim

As the complexity and challenges in the field of geomechanics rise, reducing computational costs has become a major theme to be investigated. This thesis evaluates the p-adaptive mesh optimization method's performance for problems in the 3D finite element stress analysis of underground excavations with prismatic cross-sections. The p-adaptivity changes the element formulation within the finite element mesh, based on the concept of excavation disturbed zone. The changes in element formulation require the use of transition elements to connect linear hexahedral finite elements with quadratic ones. The forthcoming research was conducted using sim|FEM (Zsaki 2010), a research computer code intended for excavation design, which solves 2D plane strain and 3D problems. It was written in C++ and its key feature is its capability to test models with transition elements, which is not found in other analysis software. The research project started with an overview of 3D element formulations, both normal and transitional, which were implemented in the code then simple, yet practical models were tested and the

results were analyzed. For some models, the results were compared to commercial software to prove that a correct behavior of the elements tested was obtained. Finally, the p-adaptive method was developed for this class of excavations and it was applied to a linear elastic medium with two circular excavations in a triaxial stress field representing a practical scenario of perhaps a transportation tunnel with a service tunnel running beside it excavated in intact rock. Mesh optimized and non-optimized models were compared and the results showed that optimization results in a reduction of the global stiffness matrix size on average by 82 percent and a reduction of solution times by about 82 percent for optimized models tested using 12-node and 16-node transitional elements, respectively, as compared to non-optimized models.

ACKNOWLEDGEMENTS

It is a pleasure to express my gratitude to all those people who have supported me and had their contributions in making this thesis possible.

First and foremost, I would like to express my gratitude to my supervisor Dr. Attila Michael Zsaki for his continuous support and his patience. I sincerely appreciate his organized supervision and that he was always available to answer my questions and guide me through my research.

I would also like to thank Concordia University, especially the Building, Civil and Environmental Engineering Department for providing me with all the tools to ease my research process.

A deep gratitude goes to my parents: Emet Habib and Abdolrahman Ibrahim. Nothing would have been possible without their unconditional love and unlimited help. Not to forget my dear sister Dima and my brothers Basem and Firas who have always been there for me. To my family, I dedicate this thesis.

I am deeply thankful to my husband Waseem Hasan for his great companion and for providing a loving environment for me to get through all the challenges in this chapter of my life. Not forgetting to express my appreciation to my husbands' family for their encouragement. I would also like to send my love to my precious unborn daughter who gives me the inspiration and motivation to work hard.

Last, but not the least, I thank my colleagues Arghya Kamal Chatterjee and Ram Adhikari for their help and for making my graduate studies enjoyable. My thanks also go to my best friends: Sarah Nizam, Alida Salman and Somaia Alwassouf for their sincere friendship.

TABLE OF CONTENTS

LIST OF FIGURES	ix
LIST OF TABLES	xiii
NOMENCLATURE	xvi
1. Introduction	1
1.1 Thesis General Objective	4
1.2 Detailed Objectives	4
2. Literature Review - Numerical Stress Analysis in Geomechanics	5
2.1 Finite Difference Method (FDM).....	5
2.2 Discrete Element Method (DEM)	7
2.3 Boundary Element Method (BEM)	8
2.4 Finite Element Method (FEM).....	10
2.4.1 Displacement Approximation and Shape Functions	12
2.5 Mesh Optimization.....	13
2.5.1 h-Adaptivity.....	14
2.5.2 p-Adaptivity.....	14
2.5.3 r-Adaptivity	14
2.5.4 hp-Adaptivity.....	15
2.6 Excavation Disturbed Zone (EDZ)	15
2.7 Percentage of Disturbance.....	16
3. The Application of Partial p-Adaptive Mesh Optimization	17
3.1 Determination of the Excavation Disturbed Zone (EDZ)	20
4. Formulation of First Order, Second Order and Transition Hexahedral Elements	24

4.1	Shape Functions	24
4.1.1	8-Node Linear Hexahedral Elements	24
4.1.2	20-Node Quadratic Hexahedral Elements	26
4.1.3	Construction of Shape Functions for Transitional Hexahedral Elements	30
4.1.4	Shape Functions for Transitional Hexahedral Elements	34
4.2	Displacement, Strain and Stress for Hexahedral Elements	37
4.2.1	Element Equation - Displacement	37
4.2.2	Element Strain Matrix	39
4.2.3	Element Stiffness Matrix	41
4.2.4	The Direct Stiffness Assembly Method.....	43
5.	Performance Evaluation of Transition Elements.....	44
5.1	Type I Models	47
5.1.1	Type I Models Using (STRHEX08L) - Results	50
5.1.2	Type I Models Using (STRHEX20Q) - Results	54
5.1.3	Type I Models Using (STRHEX12T) and (STRHEX16T) – Results	60
5.2	Type II Models	64
5.2.1	Type II Models Using (MHex08L) and (MHex20Q) - Results.....	65
5.2.2	Type II Models Using (MHex12T) and (MHex16T) - Results	70
6	Verification of Practical Performance of Transitional Elements – Pressurized Cavity Problem	77
6.2	Cases 1 through 4 – Baseline cases	82
6.3	Cases 5 through 10: The use of transitional elements	95
6.4	Benefits of mesh optimization.....	97

7. Application of Partial p-Adaptive Mesh Optimization to Underground Excavations with Prismatic Cross-sections	101
7.1 Results of the Non-optimized Model	102
7.2 Results of the Optimized Models	112
7.2.1 Case 1 Results	113
7.2.2 Case 2 Results	117
7.3 Non-optimized and Optimized Models Comparison	121
7.4 Benefits of Mesh Optimization	129
8. Conclusion	132
9. Recommendations for Further Work	133
10. List of References	134
Appendix 1	137
Appendix 2	145
Appendix 3	148

LIST OF FIGURES

Figure 2.1 BEM Model (Katsikadelis 2002).....	9
Figure 2.2 Typical 2D Finite Elements (Potts & Zdravkovic 1999).....	11
Figure 2.3 Continuity of Displacement Field (Potts & Zdravkovic 1999)	13
Figure 2.4 Mesh refinement methods. From left to right: 1) Original mesh 2) Uniform h-refinement 3) Uniform p-refinement 4) r-refinement, (Garcia Rosero 2011)	15
Figure 3.1 Frontal View of Underground Excavation Model.....	19
Figure 3.2 Zoomed View of Excavations 1 and 2	19
Figure 3.3 Circular hole in an infinite plate (After Kirsch, 1898) as found in (Jaeger et al. 2007)	20
Figure 3.4 Transition Band Determination	23
Figure 4.1 First Order Hexahedral Element.....	25
Figure 4.2 Second Order Hexahedral Element	27
Figure 4.3 The (8 to 26)-Node Hexahedral Element	30
Figure 4.4 Location of Nodes 9 to 26	32
Figure 4.5 12-Node and 16-Node Transitional Elements	36
Figure 5.1 Type I and II Models	46
Figure 5.2 Equivalent Nodal Forces	49
Figure 5.3 Type I Model - STRHEX08L.....	50
Figure 5.4 Illustration of Corner Node (0,0,2) location for the STRHEX08L Model	51
Figure 5.5 Displacement Vector Magnitude at Corner Node (0,0,2).....	52
Figure 5.6 Type I Model - STRHEX20Q	55
Figure 5.7 Illustration of Corner Node (0,0,2) location for the STRHEX20Q Model	56

Figure 5.8 Displacement Vector Magnitude at the Corner Node (0,0,2) Model STRHEX20	56
Figure 5.9 Illustration of Mid-Side Nodes (1,0,2) and (0,0,1) location for STRHEX20Q Model	57
Figure 5.10 Displacement Vector Magnitude at the Mid-Side Node (1,0,2) Model STRHEX20Q	58
Figure 5.11 Displacement Vector Magnitude at the Mid-Side Node (0,0,1) Model STRHEX20Q	59
Figure 5.12 Type I Model - STRHEX12T Figure 5.13 Type I Model - STRHEX16T	61
Figure 5.14 Displacement Vector Magnitude at the Corner Node (0,0,2) with respect to sim FEM Models: STRHEX08LR, STRHEX12T, STRHEX16T, STRHEX20QF	62
Figure 5.15 Displacement Vector Magnitude at the Mid-Side Node (1,0,2) with respect to sim FEM Models: STRHEX12T, STRHEX16T, STRHEX20QF	62
Figure 5.16 Displacement Vector Magnitude at Node (0,0,1) with respect to sim FEM Models: STRHEX16T, STRHEX20QF	63
Figure 5.17 Mesh With Only Linear Hexahedral Elements - MHex08L	66
Figure 5.18 Mesh With Only Quadratic Hexahedral Elements - MHex20.....	67
Figure 5.19 Illustration of Nodes (0,0,3), (3,0,3), (3,3,3), (0,3,3), (2,0,3), (2,3,3), (0,1,3) and (3,1,3) location	68
Figure 5.20 Mesh With (12) Transition Hexahedral Elements - MHex12T	72
Figure 5.21 Mesh With (16) Transition Hexahedral Elements - MHex16	73
Figure 5.22 Displacement Vector Magnitude at Node (0, 0,3).....	75

Figure 5.23 Displacement Vector Magnitude at Node (2, 0, 3).....	75
Figure 5.24 Displacement Vector Magnitude at Node (0, 1, 3).....	76
Figure 6.1 Frontal View of Boundary Conditions and Transition Bands Used in the Pressurized Cavity Problem.....	80
Figure 6.2 3D View of the Pressurized Cavity Problem Summarizing the Boundary Conditions.....	80
Figure 6.3 Model with HEX08L Elements - Undeformed Mesh.....	83
Figure 6.4 Model with HEX20Q Elements - Undeformed Mesh	83
Figure 6.5 Plot of Displacement Magnitude (m) – Case 1 (sim FEM)	86
Figure 6.6 Plot of Displacement Magnitude (m) – Case 2 (ABAQUS)	87
Figure 6.7 Plot of σ_{xx} Stress Contours (kPa) – Case 1 (sim FEM)	87
Figure 6.8 Plot of σ_{xx} (or S11 in ABAQUS) Stress Contours (kPa) – Case 2 (ABAQUS)	88
Figure 6.9 Plot of Displacement Magnitude (m) – Case 3 (sim FEM)	91
Figure 6.10 Plot of Displacement Magnitude (m) – Case 4 (ABAQUS)	91
Figure 6.11 Plot of σ_{yy} Stress Contours (kPa) – Case 3 (sim FEM)	92
Figure 6.12 Plot of σ_{yy} Stress Contours (kPa) – Case 4 (ABAQUS).....	92
Figure 6.13 Plot of Displacement Magnitude at Lower Boundary – Cases 1 through 4 ..	94
Figure 6.14 Plot of displacement magnitude at the Left Boundary – Cases 1 through 4 .	94
Figure 6.15 Frontal View of Typical Mesh Using Transition Zone	96
Figure 6.16 Plot of Displacement Magnitude at the Lower Boundary for Cases 5-10....	96
Figure 6.17 Plot of Displacement Magnitude at the Left Boundary for Cases 5-10	97

Figure 6.18 Memory Usage and Solution Time Savings for Cases 5 through 10 in Comparison to Case 3.....	100
Figure 7.1 Underground Excavation Model	101
Figure 7.2 Ellipsoidal Approximation of an Excavation (Zsaki 2005).....	102
Figure 7.3 Summary of the Boundary Conditions of the Non-optimized Model	103
Figure 7.4 Zoomed View of Frontal Plot of σ_{zz} (kPa) of the Non-optimized Model ...	111
Figure 7.5 The Boundary Conditions of Optimized Models	112
Figure 7.6 Memory Usage and Solution Time Savings for Cases 1 and 2 in Comparison to the Non-optimized Model.....	131

LIST OF TABLES

Table 3.1 Model Material Properties of Underground Excavation Model	18
Table 3.2 Location, Radii and Dimensions of Underground Excavations Model	18
Table 4.1 Node Coordinates for the Linear Hexahedral Element in the Natural Coordinate System.....	26
Table 4.2 Shape Functions and Their Derivatives for First Order Hexahedral Elements (Morton et al. 1995)	26
Table 4.3 Node Coordinates for 20-Node Quadratic Hexahedral Element in the Natural Coordinate System.....	28
Table 4.4 Shape Functions and Their Derivatives for the 20-Node Quadratic Hexahedral Element (Dhondt 2004).....	28
Table 4.5 The Coordinates of Nodes (1 to 8) in a Natural Coordinate System	31
Table 4.6 Shape Functions and Their Derivatives for Nodes (1 to 8) (Morton et al. 1995)	31
Table 4.7 The Coordinates of Nodes (9 to 26) in a Natural Coordinate System	32
Table 4.8 Shape Functions and their Derivatives for Nodes (9 to 20).....	33
Table 4.9 Shape functions and their derivatives for Nodes (21 to 26)	34
Table 4.10 12-Node Transitional Hexahedral Element Shape Functions.....	36
Table 4.11 16-Node Transitional Hexahedral Element Shape Functions.....	37
Table 4.12 Locations of Integration Points in Hexahedral Elements	42
Table 5.1 Material Properties of Type I and Type II Models	47

Table 5.2 Displacement Percentage Difference at the Corner Node (0,0,2) for the STRHEX08L Element	52
Table 5.3 Displacement Percentage Difference at Corner Node (0,0,2) for STRHEX20Q Element	57
Table 5.4 Displacement Percentage Difference at Mid-Side Node (1,0,2) for the STRHEX20Q Element.....	58
Table 5.5 Displacement Percentage Difference at the Mid-Side Node (0,0,1) for the STRHEX20Q Element.....	59
Table 5.6 Percentage Difference of Reduced Integrated Models in Respect to Fully Integrated Models	68
Table 5.7 Percentage Differences of Models with Transition Elements in Respect to Linear and Quadratic Models.....	74
Table 6.1 Material Properties.....	79
Table 6.2 Summary of Models for Pressurized Cavity Analysis.....	81
Table 6.3 Comparison of Displacement Results for Cases 1 and 2 – Lower Boundary ...	85
Table 6.4 Comparison of Displacement Results for Cases 1 and 2 – Left Boundary.....	86
Table 6.5 Comparison of Displacement Results for Cases 3 and 4 – Lower Boundary...	89
Table 6.6 Comparison of Displacement Results for Cases 3 and 4 – Left Boundary.....	90
Table 6.7 Use of Computational Resources Comparison for Pressurized Cavity Models	99
Table 6.8 Ratio of Computational Resource Requirements for Pressurized Cavity Models	99
Table 7.1 Non-optimized Model Displacement Results at the Border of Excavation 1.	104
Table 7.2 Non-optimized Model Displacement Results at the Border of Excavation 2.	106

Table 7.3 Optimized Model Displacement Results at the Border of Excavation 1- Case 1	113
Table 7.4 Optimized Model Displacement Results at the Border of Excavation 2 - Case 1	115
Table 7.5 Optimized Model Displacement Results at the Border of Excavation 1 - Case 2	117
Table 7.6 Optimized Model Displacement Results at the Border of Excavation 2 - Case 2	119
Table 7.7 Comparison of displacement results for Non-optimized Model and Optimized Model Case 1 at the borders of Excavation 1	121
Table 7.8 Comparison of Displacement Results for Non-optimized Model and Optimized Model Case 1 at the Borders of Excavation 2.....	123
Table 7.9 Comparison of Displacement Results for Non-optimized Model and Optimized Model Case 2 at the Borders of Excavation 1.....	125
Table 7.10 Comparison of Displacement Results for Non-optimized Model and Optimized Model Case 2 at the Borders of Excavation 2.....	127
Table 7.11 Use of Computational Resources Comparison for Underground Excavation Models.....	130
Table 7.12 Ratio of Computational Resource Requirements for Underground Excavation Models.....	130

NOMENCLATURE

a	Radius of a circular opening (m)
B	Compatibility, deformation-displacement, strain-displacement matrix
D	Disturbance
E	Modulus of Elasticity (MPa)
K	Stiffness matrix
J	Jacobian matrix
N_i	Shape function for the i^{th} node
r	Radial distance from center of an opening (m)
R	Vector of forces
u, d	Vector of displacements
γ	Unit Weight (kN/m^3)
ξ	Natural coordinate for hexahedral elements
η	Natural coordinate for hexahedral elements
ζ	Natural coordinate for hexahedral elements
ν	Poisson's ratio
σ_r	Radial stress (MPa)
σ_θ	Tangential stress (MPa)
σ_H	Horizontal in situ stress (MPa)
σ_V	Geostatic overburden stress (MPa)
$\tau_{r\theta}$	Shear stress related to σ_r and σ_θ (MPa)
σ_{xx}	Horizontal stress (MPa)

σ_{zz}	Vertical stress (MPa)
τ_{xz}	Shear stress related to σ_{xx} and σ_{zz} (MPa)
ux	Displacement in horizontal plane along x-axis (m)
uy	Displacement in horizontal plane along y-axis (m)
uz	Displacement in vertical direction along z-axis (m)

1. Introduction

Computational science is considered to be a powerful tool that tries to solve many issues faced by engineers in all fields through building, analyzing and implementing algorithms used to solve mathematical models that simulate engineering phenomena. Many numerical methods have been developed that provide some of the tools needed to face increasing challenges in engineering.

Geomechanics, for instance, is a field intended to deal with complex material behavior of soil and rock where problems involve “nonlinear and time dependent behavior, arbitrary geometries, initial or in situ conditions, multi-phase media, different loadings (static, quasi-static, cyclic and dynamic), and such environmental factors as temperature, fluids and pollutant movement.” (Desai & Gioda 1990)

Applying numerical analysis allows engineers to simplify related problems and find approximate solutions. However, in spite of all the benefits of numerical methods, processing time and memory are expensive. This can be a major issue in large and complex geomechanics projects, especially when 3D analysis is needed. Therefore, a lot of research has attempted to develop more cost effective numerical techniques.

As an introduction to this thesis, a brief description of the most popular numerical methods: the Finite Difference Method (FDM), the Discrete Element Method (DEM), the Boundary Element Method (BEM) and finally the Finite Element Method (FEM) is presented in Chapter 2. More focus is given to the Finite Element Method (FEM), since it is the method implemented to analyze all of the models throughout this thesis.

That is followed by a general explanation of mesh adaptivity techniques. Despite the advanced computer software used, complex geomechanics problems still take a considerable amount of processing time and a large amount of memory. They also, in some cases, require parameter changes during the analysis process, such as material properties, boundary and geometry conditions (for example, to simulate the process of mining, excavation and material removal) that might lead to high engineering costs. To address these issues, mesh optimization techniques can be implemented.

Mesh optimization techniques are applied by reducing the number of nodes or relocating the nodes or changing the formulation of elements in a mesh that results in reducing the number of degrees of freedom that in turn reduces the size of vectors and matrices required to solve the problem. In this thesis, a p-type adaptivity technique was implemented. The main application of which is presented in Chapter 7. A linear elastic medium containing two underground excavations was tested as a practical problem, perhaps representing a common scenario of an underground transportation tunnel with a smaller service tunnel parallel to it excavated in a homogeneous rock mass. To optimize the mesh with a p-type refinement, first the stresses caused by these excavations in the medium were calculated analytically by applying Kirsch equations (Kirsch 1898) that were found in the references to represent an “infinite plate with circular opening” by (Ramamurthy 2007). Then, the p-type procedure was implemented by determining the Excavation Disturbed Zone (EDZ) in order to determine the location of a transition band. The EDZ was defined by (Zsaki 2005) as the zone of a mesh that is undergoing more than a percentage of disturbance of 5% in comparison with the initial in situ stress in the studied medium. The p-adaptivity procedure applied to the underground excavations

problem is explained in Chapter 3. The transition band consisted of transition elements (12-node and 16-node hexahedral elements were chosen to be tested in this thesis) separating the mesh into two regions. In one region, the elements stayed quadratic and in the other region the quadratic elements were transformed to linear ones by removing the mid-side nodes. Three models were tested; one non-optimized mesh, as the benchmark, and two optimized meshes as explained later in Chapter 7.

Few numerical modeling programs were used to test the models in this thesis, but only one of them was able to test both the non-optimized and the optimized models. This program was sim|FEM (Zsaki 2010). sim|FEM is a computer code intended for research in excavation design, written in C++, that solves 2D plane strain problems and 3D models and is capable of testing models with transition elements (Zsaki 2010). This code also enables a 2D visualization of the results, but it does not support a 3D visualization yet. For this reason, a set of TCL scripts were written to use the Visualization Toolkit (VTK) (Kitware Inc. 2010) and the results of the 3D models were rendered with either linear or quadratic hexahedral elements.

Before applying the p-adaptivity technique, all the formulations of the 3D elements programmed in sim|FEM code (8-node, 20-node, 12-node and 16-node hexahedral elements) are presented in Chapter 4.

Chapters 5 and 6 are dedicated to the evaluation of the performance of transition elements in three simple, yet representative scenarios: the evaluation of transition elements as single elements, the evaluation of transition elements as part of simple assemblage of elements and finally, the evaluation of transition elements in a pressurized cavity problem, representing a simple, yet practical engineering problem.

1.1 Thesis General Objective

The objective of this thesis is to study the possibility of reducing computation time and computer memory usage without affecting solution accuracy. This is attempted by using mesh optimization via a p-type mesh adaptivity technique when solving 3D models analysed with the finite element method.

The p-type technique is performed by removing nodes from certain regions are located outside of the EDZ (Zsaki 2005).

1.2 Detailed Objectives

This thesis also aims to:

- Evaluate the behavior of transition elements. The transition elements chosen to be tested in this thesis were: 12-node and 16-node hexahedral elements. The formulations of these elements were based on Morton et al. (1995).
- Determine disturbance percentage (Zsaki 2005) in the studied medium to define the EDZ by applying an analytical solution (Kirsch 1898). Certain nodes that belong to the elements outside the EDZ were removed. As a result, those elements were transferred to linear elements and the band of transition elements was created. The band linked the quadratic elements inside the EDZ with the linear ones outside the EDZ. A model of two underground excavations was analyzed as an example application.
- Test three kinds of meshes; quadratic, linear and meshes with transition elements to compare the accuracy of solution and computational resources usage.

2. Literature Review - Numerical Stress Analysis in Geomechanics

The main objective of this thesis was to study the possibility of reducing computational resources while solving 3D models by implementing the Finite Element Method (FEM) and without affecting the solution's accuracy. Hence, this chapter will review the numerical methods most used in geomechanics. The methods summarized are: the Finite Difference Method (FDM), the Discrete Element Method (DEM), the Boundary Element Method (BEM) and the Finite Element Method (FEM). More details will be presented about FEM since it is the method implemented in this study. Following that, the review will provide a brief explanation about mesh optimization techniques: r-adaptivity, h-adaptivity, p-adaptivity and hp-adaptivity. More extended explanations are given about the p-type method that is applied in this thesis.

The use of the p-adaptivity technique for underground excavations, which were tested in Chapter 7, requires the determination of the region of interest in the studied medium. Hence, it is necessary to understand the definition of the percentage of disturbance (Zsaki 2005) to find the EDZ.

2.1 Finite Difference Method (FDM)

Before the Finite Element Method (FEM) was developed, the Finite Difference Method (FDM) was the main numerical method used in geotechnical engineering (Desai & Christian 1977). This technique was implemented by discretizing the studied domain as a grid. The nodes comprising this grid should have the same distance between each other ($\Delta x=\Delta y$) as shown in Figure 2.1 (Desai & Christian 1977). The functions' derivatives in the differential equations governing the physical problem were replaced

with finite difference approximation of the functions' values between given values of the variables on a discretized domain.

$$\frac{du}{dx} = \lim_{\Delta x \rightarrow 0} \frac{\Delta u}{\Delta x} \approx \frac{\Delta u}{\Delta x} \quad (\text{Desai \& Christian 1977}) \quad (1)$$

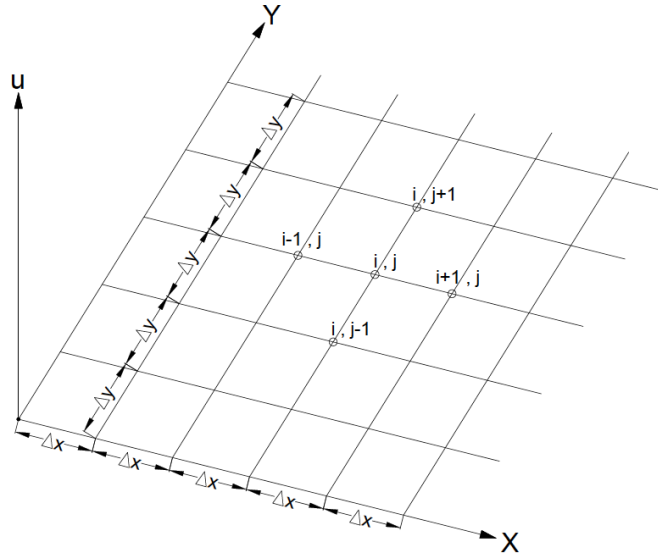


Figure 2.1 Finite Difference Method (Desai & Christian 1977)

As a result, the differential equations are converted into a set of difference equations that can be evaluated by these approximations. For example, for the first derivative in the direction of the x-axis, the approximations are:

$$\text{Central difference: } \frac{du}{dx} = \frac{u_{i+1,j} - u_{i-1,j}}{2\Delta x} + O(\Delta x)^2 \quad (\text{Desai \& Christian 1977}) \quad (2)$$

$$\text{Forward difference: } \frac{du}{dx} = \frac{u_{i+1,j} - u_{i,j}}{\Delta x} + O(\Delta x) \quad (\text{Desai \& Christian 1977}) \quad (3)$$

$$\text{Backward difference: } \frac{du}{dx} = \frac{u_{i,j} - u_{i-1,j}}{\Delta x} + O(\Delta x) \quad (\text{Desai \& Christian 1977}) \quad (4)$$

Where $O(\Delta x)$ “represents the error introduced in approximating the derivatives which can be called discretization error.” (Desai & Christian 1977). Equations (2), (3) and (4) can be solved by including the points of interest and then finding the displacement value u at those points.

The FDM is efficient to be used to solve many geotechnical problems, such as laterally loaded piles, one-dimensional consolidation and two or three dimensional seepage (Desai & Christian 1977). However, as the geological media usually involves non-homogenous materials, it is relatively difficult to obtain finite difference equations to account for the variation of the material properties (Desai & Christian 1977). Also, implementing the FDM in case of irregular boundaries is more complicated than in case of simple ones (Desai & Christian 1977). Dealing with simple boundaries allows the mesh points to be adjusted to coincide with the boundaries, while with irregular boundaries, special procedures should be taken to account for the uneven meshes created in that case. For the previous two examples, the finite element method is more efficient to be used than the FDM, where such special procedures are not required (Desai & Christian 1977).

2.2 Discrete Element Method (DEM)

As stated by Jing and Stephansson (2007), the Discrete Element Method (DEM) includes: “all numerical methods treating the problem domain as an assemblage of independent units and is mainly applied for problems of fractured rocks, granular media and multi body systems in mechanical engineering.” The essence of DEM formulation depends on the contact between the individual objects, their kinematics and their

deformation mechanism, where each object has different displacements and rotations (Jing & Stephansson 2007).

The three main aspects of the DEM for mechanical analysis are:

1. Creating a block assemblage, recording its topology and updating it throughout the deformation process.
2. Selecting a proper form of motion equations and constitutive models and solution techniques.
3. Updating the geometry and mechanical behavior of contact between the blocks during the deformation process. (Jing & Stephansson 2007).

The DEM is efficiently used for rock mechanics problems. Yet, it has a major shortcoming, which is the unknown characteristics before setting up the analysis, like the location, orientation and dimensions of the fractures (Jing & Stephansson 2007). This causes uncertainty about the feature system geometry of the problem (Jing & Stephansson 2007).

2.3 Boundary Element Method (BEM)

The Boundary Element method (BEM) is a numerical technique for analyzing the behavior of engineering structures subjected to external loads (Katsikadelis 2002). In this method only the boundaries of the problem are discretized, as shown in Figure 2.2. The solution of the governing integral equations is found at the boundary first. Then, the solution inside the problem boundaries can be found numerically.

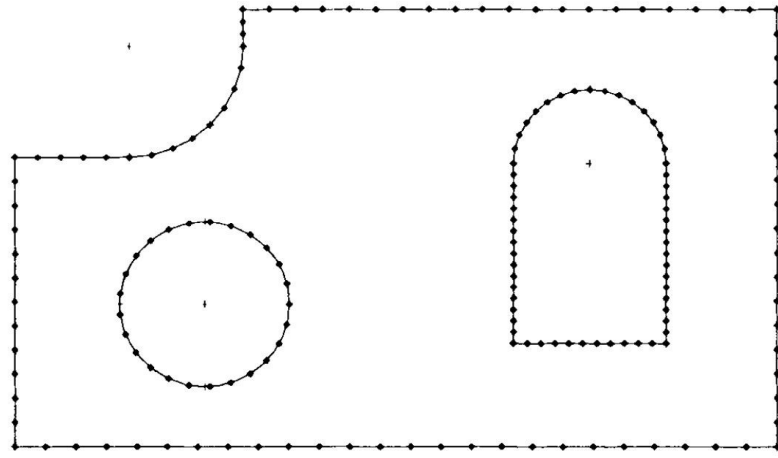


Figure 2.1 BEM Model (Katsikadelis 2002)

Using BEM has important advantages that can be summarized as follows (Katsikadelis 2002):

1. As the discretization happens only at the boundary of the studied problem, the number of unknowns is reduced. Therefore, BEM is considered an easy and fast technique that allows any modification process caused by any change of the problem conditions to be simple.
2. BEM is suitable for analyzing problems with geometric peculiarities such as cracks.
3. BEM enables the solution to be found at any point of the problem domain at any time instant.

In spite of its advantages, BEM still has some shortcomings when compared to FEM. As a simple example, the coefficient matrices in BEM are non-symmetric and dense, as opposed to FEM, which are usually symmetric and sparse matrices (Katsikadelis 2002).

2.4 Finite Element Method (FEM)

The Finite Element Method (FEM) or what is also called Finite Element Analysis (FEA) refers to a wide range of techniques used in geomechanics. It is a computational method used to approximate solutions of boundary and initial value problems. As stated by Hutton (2005), a boundary value problem is “a mathematical problem in which one or more dependent variables must satisfy a differential equation everywhere within a known domain of independent variables and satisfy specific conditions on the boundary of the domain.” The general procedures of FEM can be summarized as follows (Potts & Zdravkovic 1999):

1. Element discretization: the domain is divided into finite elements, as shown in Figure 2.3, that have nodes defined in the element boundaries or within the element.
2. Primary variable approximation: a primary variable should be selected (e.g. displacements, stresses, etc.) and this variable is to be computed at the nodes.

The solution in the FEM method is approximated locally within the element that is performed by the element’s shape functions (interpolation functions).

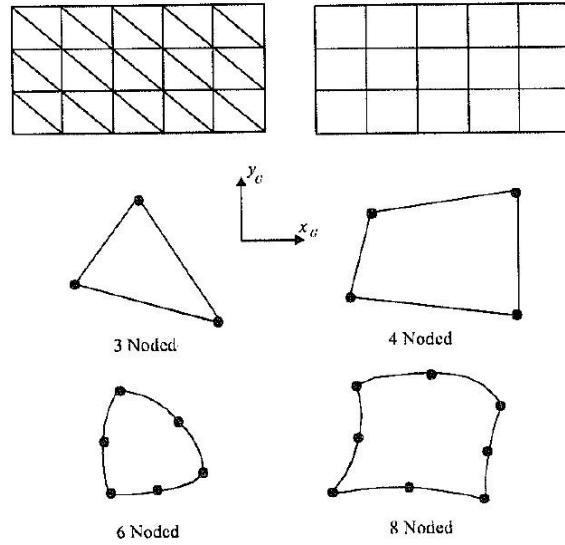


Figure 2.2 Typical 2D Finite Elements (Potts & Zdravkovic 1999)

3. Element equations: the appropriate variational principle (e.g. minimum potential energy) should be used to derive element the equations:

$$[\mathbf{K}_E] \cdot \{\Delta \mathbf{d}_E\} = \{\Delta \mathbf{R}_E\} \quad (5)$$

Where:

$[\mathbf{K}_E]$: The element stiffness matrix.

$\{\Delta \mathbf{d}_E\}$: The vector of incremental element nodal displacements.

$\{\Delta \mathbf{R}_E\}$: The vector of incremental element nodal forces.

4. Global equations: combine the element equation to form global equations:

$$[\mathbf{K}_G] \cdot \{\Delta \mathbf{d}_G\} = \{\Delta \mathbf{R}_G\} \quad (6)$$

Where:

$[\mathbf{K}_G]$: The global stiffness matrix.

$\{\Delta \mathbf{d}_G\}$: The vector of all incremental element nodal displacements.

$\{\Delta \mathbf{R}_G\}$: The vector of all incremental element nodal forces.

5. Boundary conditions: modify the global equations by applying the boundary conditions such as the loadings effect $\{\Delta R_G\}$ and the displacement effect $\{\Delta d_G\}$.
6. Solve the global equations: by solving the global equations, the displacements at all nodes can be computed and from that any secondary quantities can be calculated such as stresses and strains.

2.4.1 Displacement Approximation and Shape Functions

The field variables are found at the nodes and used to approximate the values at the non-nodal points, meaning within the element by interpolating the nodal values:

$$\{U_G\} = [N] \cdot \{U\}_{nodes} \quad (7)$$

Where:

$[N]$: The matrix of shape functions.

$\{U_G\}$: The vector of global nodal displacements.

$\{U\}_{nodes}$: The vector of local nodal displacements.

The displacement approximation must satisfy the compatibility conditions that are summarized by (Potts & Zdravkovic 1999) as follows:

1. Continuity of the displacement field which means that the displacements must vary continuously within each element by ensuring that the displacement at each element side depends only on the nodal displacements of that side, as illustrated in Figure 2.4.

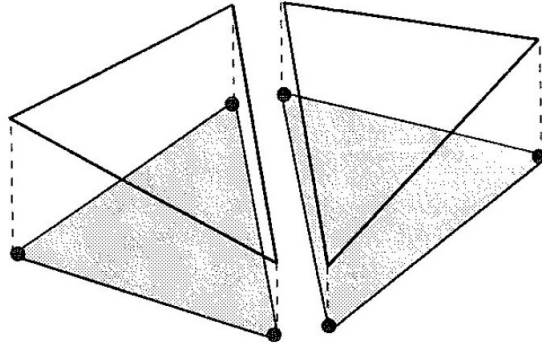


Figure 2.3 Continuity of Displacement Field (Potts & Zdravkovic 1999)

2. The displacement approximation should be able to represent rigid body movement.
3. The displacement approximation should be able to represent constant strain rates.

2.5 Mesh Optimization

The base criterion in engineering problems is to define a limit of the error computed in the energy norm (Zienkiewicz & Taylor 2013). Yet, improving the mesh quality and the accuracy of results, especially at the regions of interest, is possible by implementing some methods that are called mesh optimization or mesh adaptivity techniques.

Those techniques can be applied in many ways, such as changing the size of elements everywhere in mesh or only in specific regions of it with the necessity of respecting the quality of a mesh, as measured by element aspect ratio for example, or by changing the order of all or some elements by removing certain nodes, and thus reducing the degree of interpolation.

In this section, the following adaptivity methods were covered: h-adaptivity, p-adaptivity, r-adaptivity and finally, h-p adaptivity, which is a combination of both the h and p method.

2.5.1 h-Adaptivity

In h-adaptivity, the same element formulation is used but it is changed in size, creating a denser/coarser mesh. The elements are made larger in some locations (reducing mesh density), while in others they are made smaller (increasing mesh density) to provide the maximum economy in reaching the desired solution (Zienkiewicz & Taylor 2013). This method can be applied by subdividing existing elements or by regenerating a new mesh (Zienkiewicz & Taylor 2013).

2.5.2 p-Adaptivity

In p-adaptivity, the same element size is used and the order of the polynomial used in element definition is increased/decreased (Zienkiewicz & Taylor 2013). That can be done either uniformly throughout the whole domain or locally at some regions of the mesh. But as stated by Zienkiewicz & Taylor (2013), neither of cases “has a direct procedure developed, which allows the prediction of the best refinement to be used to obtain a given error. Here the procedures generally require more resolutions and tend to be more costly. However, the convergence for a given number of variables is more rapid with p-refinement and it has much to recommend it.”

2.5.3 r-Adaptivity

In r-adaptivity, the total number of nodes stays constant, but the nodes’ location is adjusted to obtain an optimal approximation (Zienkiewicz & Taylor 2013). The r-adaptivity method is considered a subclass of h-adaptivity. Its procedure is difficult to use

in practice since the relocation of nodes might lead to higher aspect ratio for some elements and thus deteriorating element quality.

2.5.4 hp-Adaptivity

This technique combines h and p adaptivity methods, where both the sizes of the elements and their order are changed (Zienkiewicz & Taylor 2013). This method might be applied in steps by first, using h-adaptivity to obtain acceptable accuracy and then, by applying p-adaptivity to obtain more accurate results in the region of interest.

Figure 2.4 shows a summary of the four mesh optimization techniques explained above.

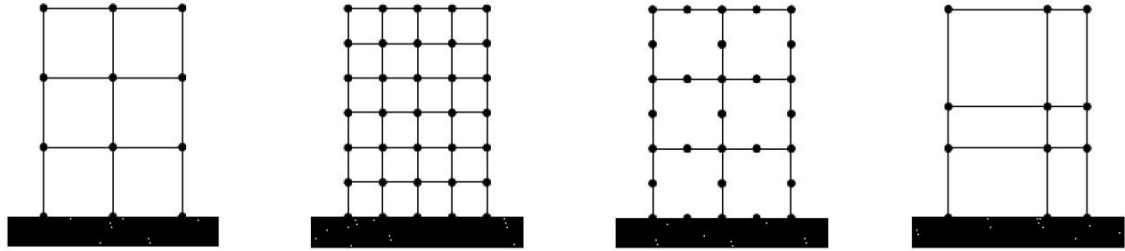


Figure 2.4 Mesh refinement methods. From left to right: 1) Original mesh 2) Uniform h-refinement 3) Uniform p-refinement 4) r-refinement, (Garcia Rosero 2011)

2.6 Excavation Disturbed Zone (EDZ)

The p-adaptivity technique was applied to the underground excavations problem as will be explained in Chapter 3 and tested in Chapter 7. As mentioned earlier in section 2.5.2, the method was implemented by changing the order of shape functions, which in this thesis, is done locally in some regions of interest in the studied mesh. Those regions, referred to as the EDZ, are where a higher accuracy is required and it is defined as the

region where the underground excavation construction will lead to a percentage of disturbance of not more than 5% in the medium in respect to the initial in situ stress field (Zsaki 2005). Determining EDZ will specify which zones will be meshed using linear, quadratic or transitional elements.

2.7 Percentage of Disturbance

The percentage of disturbance is defined as the change of the model's initial conditions, such as the initial in situ stresses or model geometry, according to any disturbance in the studied medium. In this thesis, the disturbance is due to the excavation construction and the percentage is calculated with respect to the in situ stresses as follows (Zsaki 2005):

$$\Delta\sigma_i = \left| \frac{\sigma_i^{\text{in-situ}} - \sigma_i^{\text{computed}}}{\sigma_i^{\text{in-situ}}} \right| \cdot 100 \quad (8)$$

Where $i = 1, 2, 3$ denotes the major, intermediate and minor principal stresses.

It should be noted that the disturbance caused by each excavation individually in turn was found as the formulation taking into account the interaction between the two excavations is not available.

3. The Application of Partial p-Adaptive Mesh Optimization

The p-adaptive mesh optimization technique was applied throughout this research to solve stress analysis problems. The development of the procedure was started by testing a mesh of only second order elements. Then, the mesh optimization was performed by deleting selected nodes (mid-side nodes of second order elements) from the elements where the solution accuracy was the least important (being outside of the EDZ). Eventually by deleting those nodes, the number of nodes and degrees of freedom changed in the model. Also, the second order elements, where nodes were deleted, were converted to first order elements. As a result, a group of elements that connected the linear and quadratic elements was necessary. These elements were referred to as transitional elements.

As a main application of this thesis, models of a 3D linear elastic medium containing two underground excavations were analyzed. Due to the memory of the computer used to solve the models and the symmetry of boundary conditions applied to the tested problem, only one layer of elements in the out-of-plane direction was considered for testing. Although a single-element thickness is seldom practical for large models, it was accepted for the purpose of this thesis since it represents a minimum condition, which makes the problem 3D, yet more importantly, it allows direct comparison with 2D plane-strain models for the assessment of solution accuracy.

The first excavation represents a typical tunnel with a radius of 5.4 m and the second excavation is a smaller one that represents a service tunnel with a radius of 2.6 m. These tunnel dimensions represent typical sizes for a subway tunnel and its service tunnel. To simplify the scenario, the left excavation was called Excavation 1 and the right

excavation was called Excavation 2. A frontal view of the underground excavation model and a zoomed in view of the excavations are shown in Figures 3.1 and 3.2. The models' material properties are listed in Table 3.1, while the radii and centers' location of both excavations are listed in Table 3.2.

Table 3.1 Model Material Properties of Underground Excavation Model

Property	Unit	Value
γ	kN/m ³	0
E	kPa	10^6
ν	-	0.3
σ_{xx}	kPa	10
σ_{yy}	kPa	10
σ_{zz}	kPa	10
σ_{xy}	kPa	0
σ_{yz}	kPa	0
σ_{zx}	kPa	0

Table 3.2 Location, Radii and Dimensions of Underground Excavations Model

Location and Radii	Left Excavation (Excavation 1)		Right Excavation (Excavation 2)	
	X (m)	Y(m)	X(m)	Y (m)
Center Coordinates	43	18	61	13
Radius (m)	2.6		5.4	
	X (m)	Y(m)	Z (m)	
Model Dimensions	103.05		90.23	2.19

A mesh composed of only second order hexahedral elements was tested first. Afterwards, a test of an optimized mesh consisting of first order, transition and second order hexahedral elements was performed. Before applying the p-adaptive method, the

EDZ had to be determined. The EDZ zone is defined as a percentage of disturbance of 5% (Zsaki 2005) calculated as presented in section (2.7).

The change in the shape function order was applied to elements outside the zone where the two excavations had no great effect on the medium and less accuracy was acceptable in the context of inherent uncertainties in material properties.

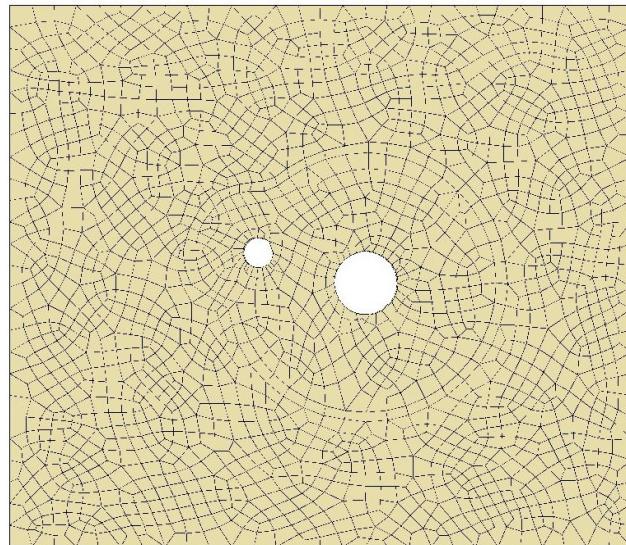


Figure 3.1 Frontal View of Underground Excavation Model

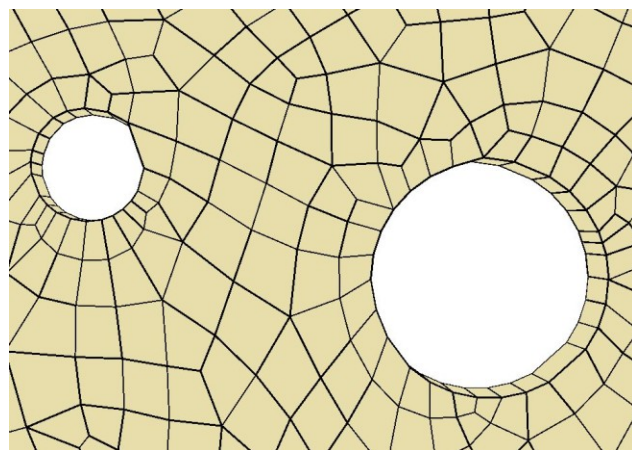


Figure 3.2 Zoomed View of Excavations 1 and 2

3.1 Determination of the Excavation Disturbed Zone (EDZ)

Calculating the displacements and stresses outside a circular hole in an infinite homogenous, isotropic and linear elastic material was first solved by the German engineer, Kirsch, in 1898 and his model setup is shown in Figure 3.3 (Jaeger et al. 2007). As the Kirsch article is written in German, the equations used in this thesis were found in the following two references; Jaeger et al. (2007) and Garcia Rosero (2011). The stress distribution caused by each of the modeled excavation was achieved by applying Kirsch's analytical solution as explained below. The results were then compared to the assumed initial field stresses, σ_H and σ_V , to find out the zone of the model that was undergoing more than a 5% disturbance, which is the EDZ zone (Zsaki 2005).

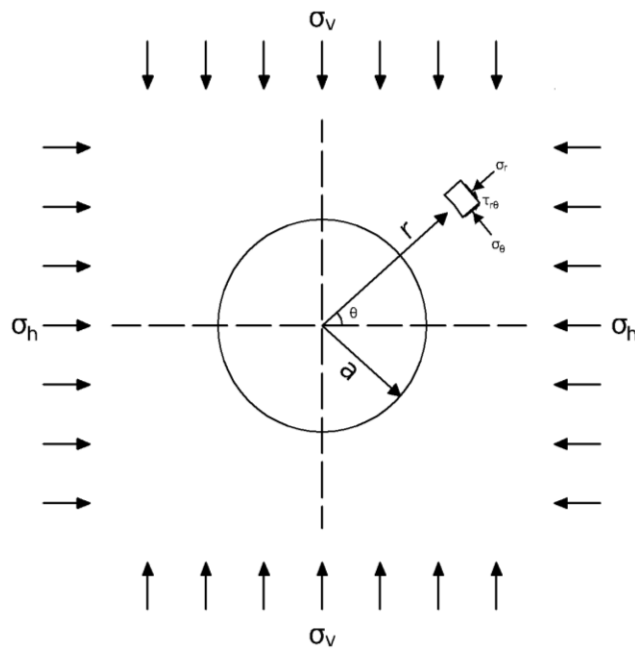


Figure 3.3 Circular hole in an infinite plate (After Kirsch, 1898) as found in (Jaeger et al. 2007)

Stresses generated around an excavation are evaluated in a polar coordinated system and governed by equations 9 to 11:

$$\sigma_r = \frac{1}{2}(\sigma_H + \sigma_V) \left(1 - \frac{a^2}{r^2}\right) + \frac{1}{2}(\sigma_H - \sigma_V) \left(1 + \frac{3a^4}{r^4} - \frac{4a^2}{r^2}\right) \cos 2\theta \quad (9)$$

$$\sigma_\theta = \frac{1}{2}(\sigma_H + \sigma_V) \left(1 + \frac{a^2}{r^2}\right) - \frac{1}{2}(\sigma_H - \sigma_V) \left(1 + \frac{3a^4}{r^4}\right) \cos 2\theta \quad (10)$$

$$\tau_{r\theta} = -\frac{1}{2}(\sigma_H - \sigma_V) \left(1 - \frac{3a^4}{r^4} + \frac{2a^2}{r^2}\right) \sin 2\theta \quad (11)$$

Where:

σ_r : The radial stress

σ_θ : The tangential stress and

$\tau_{r\theta}$: The shear stress.

σ_H and σ_V correspond to the original in situ horizontal and vertical stresses (pre-excavation) in the initial biaxial stress field.

It should be noted that the stress field applied to the underground excavations model in this thesis was assumed to be hydrostatic; meaning the initial stresses applied at any angle θ had the same value ($\sigma_H = \sigma_V = 10$ kPa) and resulted in a zero shear stress $\tau_{r\theta}$ at any point at any angle. Hence equations 9 to 11 can be simplified as follows:

$$\sigma_r = \frac{1}{2}(\sigma_H + \sigma_V) \left(1 - \frac{a^2}{r^2}\right) \quad (12)$$

$$\sigma_\theta = \frac{1}{2}(\sigma_H + \sigma_V) \left(1 + \frac{a^2}{r^2}\right) \quad (13)$$

$$\tau_{r\theta} = 0 \quad (14)$$

The previous polar stresses were calculated for a quarter of each circular excavation due to symmetry. For every 10 degrees (from 0 to 90 degrees), the r value was taken from a to $15 \cdot a$ to ensure a value large enough to find minimum disturbance in equations 12, 13 and 14 (Jaeger et al., 2007).

The polar stresses were then transformed to a Cartesian coordinate system by applying the following stress transformation equations (Garcia Rosero 2011):

$$\sigma_{xx} = \sigma_r \cos^2 \theta + \sigma_\theta \sin^2 \theta - \tau_{r\theta} \sin \theta \cos \theta \quad (15)$$

$$\sigma_{zz} = \sigma_r \sin^2 \theta + \sigma_\theta \cos^2 \theta - \tau_{r\theta} \sin \theta \cos \theta \quad (16)$$

$$\tau_{xz} = (\sigma_r - \sigma_\theta) \sin \theta \cos \theta + \tau_{r\theta} (\cos^2 \theta - \sin^2 \theta) \quad (17)$$

Considering the hydrostatic initial stress field applied to this problem, equations 15 to 17 can be rewritten as follows:

$$\sigma_{xx} = \sigma_r \cos^2 \theta + \sigma_\theta \sin^2 \theta \quad (18)$$

$$\sigma_{zz} = \sigma_r \sin^2 \theta + \sigma_\theta \cos^2 \theta \quad (19)$$

$$\tau_{xz} = (\sigma_r - \sigma_\theta) \sin \theta \cos \theta \quad (20)$$

The transition zone was determined by averaging at the nodes where the value of σ_{xx} was equal to $0.95\sigma_H$ or $1.05\sigma_H$ and the value of σ_{zz} was equal to $0.95\sigma_v$ or $1.05\sigma_v$. This +/- 5% represents the zone of disturbance deviating from the in situ stresses.

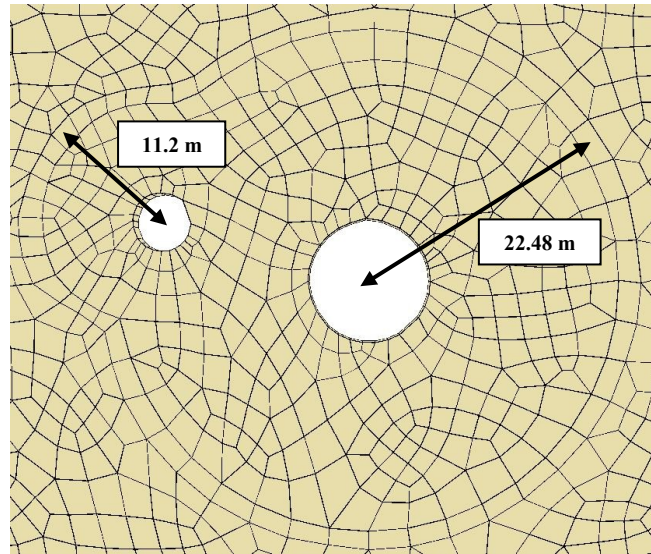


Figure 3.4 Transition Band Determination

A transitional band was created connecting the elements outside the EDZ Zone (first order elements) and the elements inside the zone (second order elements).

Figure 3.4 shows the radii at which the transition band was computed by applying equations 18-20 and determining the +/- 5 percent variation. The detailed calculations can be found in Appendixes 3 and 4.

4. Formulation of First Order, Second Order and Transition Hexahedral Elements

As the sim|FEM code (Zsaki 2010) was used to solve all models in this thesis, Chapter 4 presents the elements formulations implemented in this code. An implementation starts with the shape function formulation of a first-order (8-node) and a second-order (20-node) hexahedral elements. Then, the shape function construction of transitional hexahedral elements is explained according to Morton et al. (1995). Transition elements are defined as the elements connecting linear elements with quadratic ones. Chapter 4 finally ends by summarizing the direct stiffness assembly method for FEM analysis as implemented in sim|FEM.

4.1 Shape Functions

The solution in the FEM method is locally approximated within an element. The approximation can be done through element's shape functions, which are also called interpolation functions. They are called interpolation functions because the displacement field over the element is interpolated from the nodal displacements (Felippa 2010).

Shape functions of first order, second order and transition hexahedral elements are summarized in the following sub-sections.

4.1.1 8-Node Linear Hexahedral Elements

The linear or first-order hexahedral element shown in Figure 4.1 is the simplest element of the hexahedral family. It has 8 nodes located at the corners of the element.

The natural coordinate system is at the center of the element and the nodes' coordinates are listed in Table 4.1.

The shape functions at each node can be written in a general formula as follows (Liu and Quek 2003):

$$N_i = \frac{1}{8} (1 + \xi \xi_i)(1 + \eta \eta_i)(1 + \zeta \zeta_i) \quad (21)$$

Where (ξ_i, η_i, ζ_i) denotes the natural coordinates of the node i.

The shape functions at each node and their derivatives are listed in Table 4.2 (Morton et al. 1995).

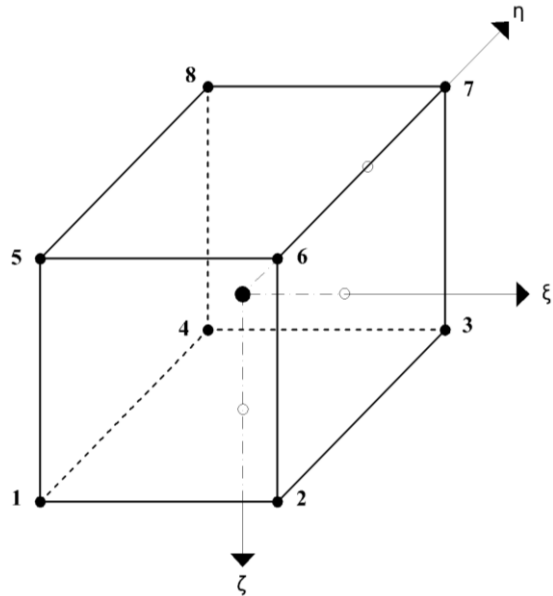


Figure 4.1 First Order Hexahedral Element

Table 4.1 Node Coordinates for the Linear Hexahedral Element in the Natural Coordinate System

Node	1	2	3	4	5	6	7	8
ξ	-1	+1	+1	-1	-1	+1	+1	-1
η	-1	-1	+1	+1	-1	-1	+1	+1
ζ	+1	+1	+1	+1	-1	-1	-1	-1

Table 4.2 Shape Functions and Their Derivatives for First Order Hexahedral Elements (Morton et al. 1995)

Shape Functions at Each Node	Shape Function Derivatives		
	$\partial N_i / \partial \xi$	$\partial N_i / \partial \eta$	$\partial N_i / \partial \zeta$
$N_1(\xi, \eta, \zeta) = \frac{1}{8}(1-\xi)(1-\eta)(1+\zeta)$	$\frac{1}{8}(\eta-1)(1+\zeta)$	$\frac{1}{8}(\xi-1)(1+\zeta)$	$\frac{1}{8}(1-\xi)(1-\eta)$
$N_2(\xi, \eta, \zeta) = \frac{1}{8}(1+\xi)(1-\eta)(1+\zeta)$	$\frac{1}{8}(1-\eta)(1+\zeta)$	$-\frac{1}{8}(1+\xi)(1+\zeta)$	$\frac{1}{8}(1+\xi)(1-\eta)$
$N_3(\xi, \eta, \zeta) = \frac{1}{8}(1+\xi)(1+\eta)(1+\zeta)$	$\frac{1}{8}(1+\eta)(1+\zeta)$	$\frac{1}{8}(1+\xi)(1+\zeta)$	$\frac{1}{8}(1+\xi)(1+\eta)$
$N_4(\xi, \eta, \zeta) = \frac{1}{8}(1-\xi)(1+\eta)(1+\zeta)$	$-\frac{1}{8}(1+\eta)(1+\zeta)$	$\frac{1}{8}(1-\xi)(1+\zeta)$	$\frac{1}{8}(1-\xi)(1+\eta)$
$N_5(\xi, \eta, \zeta) = \frac{1}{8}(1-\xi)(1-\eta)(1-\zeta)$	$\frac{1}{8}(1-\eta)(\zeta-1)$	$\frac{1}{8}(1-\xi)(\zeta-1)$	$\frac{1}{8}(\xi-1)(1-\eta)$
$N_6(\xi, \eta, \zeta) = \frac{1}{8}(1+\xi)(1-\eta)(1-\zeta)$	$\frac{1}{8}(1-\eta)(1-\zeta)$	$\frac{1}{8}(1+\xi)(\zeta-1)$	$-\frac{1}{8}(1+\xi)(1-\eta)$
$N_7(\xi, \eta, \zeta) = \frac{1}{8}(1+\xi)(1+\eta)(1-\zeta)$	$\frac{1}{8}(1+\eta)(1-\zeta)$	$\frac{1}{8}(1+\xi)(1-\zeta)$	$-\frac{1}{8}(1+\xi)(1+\eta)$
$N_8(\xi, \eta, \zeta) = \frac{1}{8}(1-\xi)(1+\eta)(1-\zeta)$	$\frac{1}{8}(1+\eta)(\zeta-1)$	$\frac{1}{8}(1-\xi)(1-\zeta)$	$\frac{1}{8}(\xi-1)(1+\eta)$

4.1.2 20-Node Quadratic Hexahedral Elements

The 20-node quadratic or second-order hexahedral element has 8 nodes at the corners and 12 nodes at the middle of the edges as shown in Figure 4.2. The coordinates for each node in the natural coordinate system, which is at the center of the element, are presented in Table 4.3.

The shape functions at each node can be condensed into four groups, as follows (Liu and Quek 2003):

- For the corner nodes: $i = 1, 2, \dots, 8$:

$$N_i = \frac{1}{8} (1 + \xi \xi_i)(1 + \eta \eta_i)(1 + \zeta \zeta_i)(\xi \xi_i + \eta \eta_i + \zeta \zeta_i - 2) \quad (22)$$

- For the mid-side nodes: $i = 9, 10, 11, 12$:

$$N_i = \frac{1}{4} (1 - \xi^2)(1 + \eta \eta_i)(1 + \zeta \zeta_i) \quad (23)$$

- For the mid-side nodes: $i = 13, 14, 15, 16$:

$$N_i = \frac{1}{4} (1 + \xi \xi_i)(1 - \eta^2)(1 + \zeta \zeta_i) \quad (24)$$

- For the mid-side nodes: $i = 17, 18, 19, 20$:

$$N_i = \frac{1}{4} (1 + \xi \xi_i)(1 + \eta \eta_i)(1 - \zeta^2) \quad (25)$$

Where (ξ_i, η_i, ζ_i) denotes the natural coordinates of the node i .

Shape functions at each node and their derivatives are listed in Table 4.4 (Dhondt 2004).

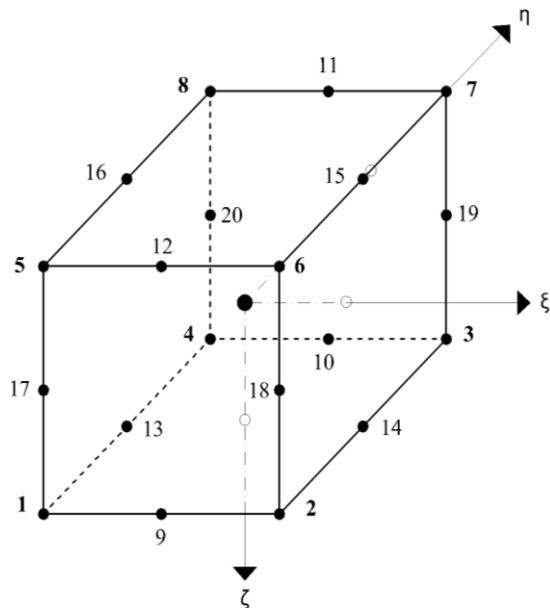


Figure 4.2 Second Order Hexahedral Element

Table 4.3 Node Coordinates for 20-Node Quadratic Hexahedral Element in the Natural Coordinate System

Corner Nodes												
Node	1	2	3	4	5	6	7	8				
ξ	-1	+1	+1	-1	-1	+1	+1	-1				
η	-1	-1	+1	+1	-1	-1	+1	+1				
ζ	+1	+1	+1	+1	-1	-1	-1	-1				
Mid-side Nodes												
Node	9	10	11	12	13	14	15	16	17	18	19	20
ξ	0	0	0	0	-1	+1	+1	-1	-1	+1	+1	-1
η	-1	+1	+1	-1	-0	0	0	0	-1	-1	+1	+1
ζ	+1	+1	-1	-1	+1	+1	-1	-1	0	0	0	0

Table 4.4 Shape Functions and Their Derivatives for the 20-Node Quadratic Hexahedral Element (Dhondt 2004)

Shape Functions And Their Derivatives		
$\partial N_i / \partial \xi$	$\partial N_i / \partial \eta$	$\partial N_i / \partial \zeta$
$N_1(\xi, \eta, \zeta) = -\frac{1}{8}(1-\xi)(1-\eta)(1+\zeta)(2+\xi+\eta-\zeta)$		
$-\frac{1}{8}(1-\eta)(1+\zeta)(-1-2\xi-\eta+\zeta)$	$-\frac{1}{8}(1-\xi)(1+\zeta)(-1-\xi-2\eta+\zeta)$	$-\frac{1}{8}(1-\xi)(1-\eta)(1+\xi+\eta-2\zeta)$
$N_2(\xi, \eta, \zeta) = -\frac{1}{8}(1+\xi)(1-\eta)(1+\zeta)(2-\xi+\eta-\zeta)$		
$-\frac{1}{8}(1-\eta)(1+\zeta)(1-2\xi+\eta-\zeta)$	$-\frac{1}{8}(1+\xi)(1+\zeta)(-1+\xi-2\eta+\zeta)$	$-\frac{1}{8}(1+\xi)(1-\eta)(1-\xi+\eta-2\zeta)$
$N_3(\xi, \eta, \zeta) = -\frac{1}{8}(1+\xi)(1+\eta)(1+\zeta)(2-\xi-\eta-\zeta)$		
$-\frac{1}{8}(1+\eta)(1+\zeta)(1-2\xi-\eta-\zeta)$	$-\frac{1}{8}(1+\xi)(1+\zeta)(1-\xi-2\eta-\zeta)$	$-\frac{1}{8}(1+\xi)(1+\eta)(1-\xi-\eta-2\zeta)$
$N_4(\xi, \eta, \zeta) = -\frac{1}{8}(1-\xi)(1+\eta)(1+\zeta)(2+\xi-\eta-\zeta)$		
$-\frac{1}{8}(1+\eta)(1+\zeta)(-1-2\xi+\eta-\zeta)$	$-\frac{1}{8}(1-\xi)(1+\zeta)(1+\xi-2\eta-\zeta)$	$-\frac{1}{8}(1-\xi)(1+\eta)(1+\xi-\eta-2\zeta)$
$N_5(\xi, \eta, \zeta) = -\frac{1}{8}(1-\xi)(1-\eta)(1-\zeta)(2+\xi+\eta+\zeta)$		
$-\frac{1}{8}(1-\eta)(1-\zeta)(-1-2\xi-\eta-\zeta)$	$-\frac{1}{8}(1-\xi)(1-\zeta)(-1-\xi-2\eta-\zeta)$	$-\frac{1}{8}(1-\xi)(1-\eta)(-1-\xi-\eta-2\zeta)$
$N_6(\xi, \eta, \zeta) = -\frac{1}{8}(1+\xi)(1-\eta)(1-\zeta)(2-\xi+\eta+\zeta)$		
$-\frac{1}{8}(1-\eta)(1-\zeta)(1-2\xi+\eta+\zeta)$	$-\frac{1}{8}(1+\xi)(1-\zeta)(-1+\xi-2\eta-\zeta)$	$-\frac{1}{8}(1+\xi)(1-\eta)(-1+\xi-\eta-2\zeta)$
$N_7(\xi, \eta, \zeta) = -\frac{1}{8}(1+\xi)(1+\eta)(1-\zeta)(2-\xi-\eta+\zeta)$		
$-\frac{1}{8}(1+\eta)(1-\zeta)(1-2\xi-\eta+\zeta)$	$-\frac{1}{8}(1+\eta)(1-\zeta)(1-2\xi-\eta+\zeta)$	$-\frac{1}{8}(1+\eta)(1-\zeta)(1-2\xi-\eta+\zeta)$
$N_8(\xi, \eta, \zeta) = -\frac{1}{8}(1-\xi)(1+\eta)(1-\zeta)(2+\xi-\eta+\zeta)$		
$-\frac{1}{8}(1+\eta)(1-\zeta)(-1-2\xi+\eta-\zeta)$	$-\frac{1}{8}(1+\eta)(1-\zeta)(-1-2\xi+\eta-\zeta)$	$-\frac{1}{8}(1+\eta)(1-\zeta)(-1-2\xi+\eta-\zeta)$

Table 4.4. (Continuing) Shape Functions and Their Derivatives for the 20-Node Quadratic Hexahedral Element (Dhondt 2004)

Shape Functions And Their Derivatives		
$\partial N_i / \partial \xi$	$\partial N_i / \partial \eta$	$\partial N_i / \partial \zeta$
	$N_9(\xi, \eta, \zeta) = \frac{1}{4} (1 - \xi^2)(1 - \eta)(1 + \zeta)$	
$-\frac{1}{2} \xi(1 - \eta)(1 + \zeta)$	$-\frac{1}{2} \xi(1 - \eta)(1 + \zeta)$	$-\frac{1}{2} \xi(1 - \eta)(1 + \zeta)$
	$N_{10}(\xi, \eta, \zeta) = \frac{1}{4} (1 - \xi^2)(1 + \eta)(1 + \zeta)$	
$-\frac{1}{2} \xi(1 + \eta)(1 + \zeta)$	$-\frac{1}{2} \xi(1 + \eta)(1 + \zeta)$	$-\frac{1}{2} \xi(1 + \eta)(1 + \zeta)$
	$N_{11}(\xi, \eta, \zeta) = \frac{1}{4} (1 - \xi^2)(1 + \eta)(1 - \zeta)$	
$-\frac{1}{2} \xi(1 + \eta)(1 - \zeta)$	$-\frac{1}{2} \xi(1 + \eta)(1 - \zeta)$	$-\frac{1}{2} \xi(1 + \eta)(1 - \zeta)$
	$N_{12}(\xi, \eta, \zeta) = \frac{1}{4} (1 - \xi^2)(1 - \eta)(1 - \zeta)$	
$-\frac{1}{4} (1 - \eta^2)(1 + \zeta)$	$-\frac{1}{4} (1 - \eta^2)(1 + \zeta)$	$-\frac{1}{4} (1 - \eta^2)(1 + \zeta)$
	$N_{13}(\xi, \eta, \zeta) = \frac{1}{4} (1 - \xi)(1 - \eta^2)(1 + \zeta)$	
$-\frac{1}{4} (1 - \eta^2)(1 + \zeta)$	$-\frac{1}{4} (1 - \eta^2)(1 + \zeta)$	$-\frac{1}{4} (1 - \eta^2)(1 + \zeta)$
	$N_{14}(\xi, \eta, \zeta) = \frac{1}{4} (1 + \xi)(1 - \eta^2)(1 + \zeta)$	
$\frac{1}{4} (1 - \eta^2)(1 + \zeta)$	$\frac{1}{4} (1 - \eta^2)(1 + \zeta)$	$\frac{1}{4} (1 - \eta^2)(1 + \zeta)$
	$N_{15}(\xi, \eta, \zeta) = \frac{1}{4} (1 + \xi)(1 - \eta^2)(1 - \zeta)$	
$\frac{1}{4} (1 - \eta^2)(1 - \zeta)$	$\frac{1}{4} (1 - \eta^2)(1 - \zeta)$	$\frac{1}{4} (1 - \eta^2)(1 - \zeta)$
	$N_{16}(\xi, \eta, \zeta) = \frac{1}{4} (1 - \xi)(1 - \eta^2)(1 - \zeta)$	
$-\frac{1}{4} (1 - \eta^2)(1 - \zeta)$	$-\frac{1}{4} (1 - \eta^2)(1 - \zeta)$	$-\frac{1}{4} (1 - \eta^2)(1 - \zeta)$
	$N_{17}(\xi, \eta, \zeta) = \frac{1}{4} (1 - \xi)(1 - \eta)(1 - \zeta^2)$	
$-\frac{1}{4} (1 - \xi)(1 - \zeta^2)$	$-\frac{1}{4} (1 - \xi)(1 - \zeta^2)$	$-\frac{1}{4} (1 - \xi)(1 - \zeta^2)$
	$N_{18}(\xi, \eta, \zeta) = \frac{1}{4} (1 + \xi)(1 - \eta)(1 - \zeta^2)$	
$-\frac{1}{4} (1 + \xi)(1 - \zeta^2)$	$-\frac{1}{4} (1 + \xi)(1 - \zeta^2)$	$-\frac{1}{4} (1 + \xi)(1 - \zeta^2)$
	$N_{19}(\xi, \eta, \zeta) = \frac{1}{4} (1 + \xi)(1 + \eta)(1 - \zeta^2)$	
$\frac{1}{4} (1 + \eta)(1 - \zeta^2)$	$\frac{1}{4} (1 + \eta)(1 - \zeta^2)$	$\frac{1}{4} (1 + \eta)(1 - \zeta^2)$
	$N_{20}(\xi, \eta, \zeta) = \frac{1}{4} (1 - \xi)(1 + \eta)(1 - \zeta^2)$	
$-\frac{1}{4} (1 + \eta)(1 - \zeta^2)$	$-\frac{1}{4} (1 + \eta)(1 - \zeta^2)$	$-\frac{1}{4} (1 + \eta)(1 - \zeta^2)$

4.1.3 Construction of Shape Functions for Transitional Hexahedral Elements

Based on Gupta's (1978) 2D transition element, Morton et al. (1995) defined the shape functions of a 3D hexahedral element to be used in 3D adaptive meshing techniques. Implementing the adaptive method allows mesh refinement or the usage of second order elements to be only in the regions where more accuracy is required. The shape functions were developed for a hexahedral element with a variable number of nodes (8 to 26 nodes) in a natural coordinate system ($-1 \leq \xi, \eta, \zeta \leq 1$) located at the center of an element (Morton et al., 1995), as shown in Figure 4.3.

In this thesis, two transition element types were chosen to be implemented: (12-node) and (16-node) hexahedral elements. More details about those elements are presented in the following sections.

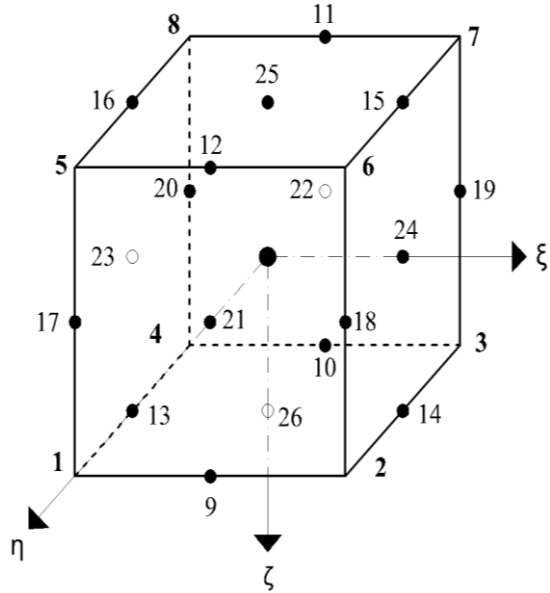


Figure 4.3 The (8 to 26)-Node Hexahedral Element

The shape function for a standard three-dimensional first order hexahedral element is presented in equations (\bar{N}_1) to (\bar{N}_8) and their derivatives were listed in Table 4.6, (Morton et al. 1995). The coordinates of nodes 1 to 8 are listed in Table 4.5.

The introduction of additional nodes will require modification of the shape functions, so they are denoted with a bar (Morton et al. 1995) while the shape functions for the transition elements in their final form will be denoted with no bar (Morton et al. 1995).

Table 4.5 The Coordinates of Nodes (1 to 8) in a Natural Coordinate System

Corner Nodes								
Node	1	2	3	4	5	6	7	8
ξ	-1	+1	+1	-1	-1	+1	+1	-1
η	-1	-1	+1	+1	-1	-1	+1	+1
ζ	+1	+1	+1	+1	-1	-1	-1	-1

Table 4.6 Shape Functions and Their Derivatives for Nodes (1 to 8) (Morton et al. 1995)

Shape Functions at Each Node	Shape Functions Derivatives		
	$\partial \bar{N}_i / \partial \xi$	$\partial \bar{N}_i / \partial \eta$	$\partial \bar{N}_i / \partial \zeta$
$\bar{N}_1(\xi, \eta, \zeta) = \frac{1}{8}(1-\xi)(1-\eta)(1+\zeta)$	$\frac{1}{8}(-1)(1+\zeta)$	$\frac{1}{8}(\eta-1)(1+\zeta)$	$\frac{1}{8}(\xi-1)(1+\zeta)$
$\bar{N}_2(\xi, \eta, \zeta) = \frac{1}{8}(1+\xi)(1-\eta)(1+\zeta)$	$\frac{1}{8}(1-\eta)(1+\zeta)$	$-\frac{1}{8}(1+\xi)(1+\zeta)$	$\frac{1}{8}(1+\xi)(1-\eta)$
$\bar{N}_3(\xi, \eta, \zeta) = \frac{1}{8}(1+\xi)(1+\eta)(1+\zeta)$	$\frac{1}{8}(1+\eta)(1+\zeta)$	$\frac{1}{8}(1+\xi)(1+\zeta)$	$\frac{1}{8}(1+\xi)(1+\eta)$
$\bar{N}_4(\xi, \eta, \zeta) = \frac{1}{8}(1-\xi)(1+\eta)(1+\zeta)$	$-\frac{1}{8}(1+\eta)(1+\zeta)$	$\frac{1}{8}(1-\xi)(1+\zeta)$	$\frac{1}{8}(1-\xi)(1+\eta)$
$\bar{N}_5(\xi, \eta, \zeta) = \frac{1}{8}(1-\xi)(1-\eta)(1-\zeta)$	$\frac{1}{8}(1-\eta)(\zeta-1)$	$\frac{1}{8}(1-\xi)(\zeta-1)$	$\frac{1}{8}(\xi-1)(1-\eta)$
$\bar{N}_6(\xi, \eta, \zeta) = \frac{1}{8}(1+\xi)(1-\eta)(1-\zeta)$	$\frac{1}{8}(1-\eta)(1-\zeta)$	$\frac{1}{8}(1+\xi)(\zeta-1)$	$-\frac{1}{8}(1+\xi)(1-\eta)$
$\bar{N}_7(\xi, \eta, \zeta) = \frac{1}{8}(1+\xi)(1+\eta)(1-\zeta)$	$\frac{1}{8}(1+\eta)(1-\zeta)$	$\frac{1}{8}(1+\xi)(1-\zeta)$	$-\frac{1}{8}(1+\xi)(1+\eta)$
$\bar{N}_8(\xi, \eta, \zeta) = \frac{1}{8}(1-\xi)(1+\eta)(1-\zeta)$	$\frac{1}{8}(1+\eta)(\zeta-1)$	$\frac{1}{8}(1-\xi)(1-\zeta)$	$\frac{1}{8}(\xi-1)(1+\eta)$

Shape functions for the hexahedral elements with nodes added only at midpoints of an edge are presented in equations (\bar{N}_9) to (\bar{N}_{20}) and their derivatives are listed in Table 4.8 (Morton et al. 1995). Again, these shape functions will need to be modified to account for other nodes that are added to the element (Morton et al. 1995). Shape functions for hexahedral elements with nodes at the center of the faces are shown in equations (N_{21}) to (N_{26}) in Table 4.9. Each of these shape functions vanish at the edges and will not need to be modified to account for the nodes introduced before. The nodal locations for nodes 9 to 26 are shown in Figure 4.4 and their coordinates are listed in Table 4.7.

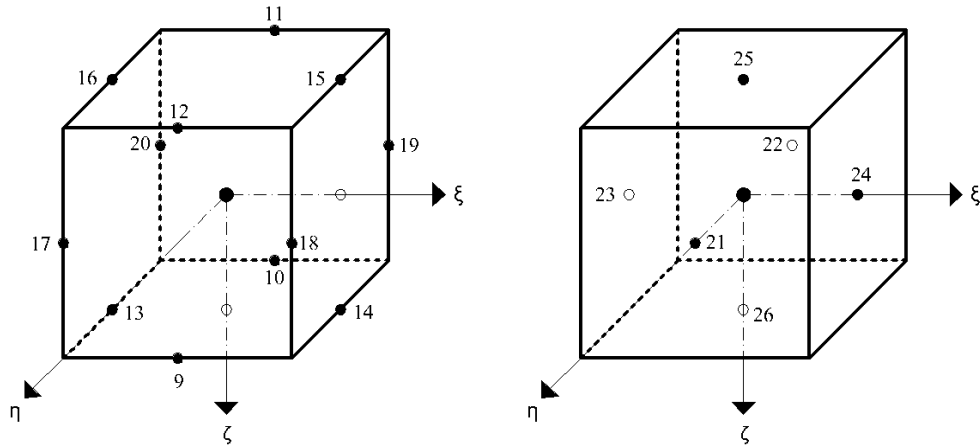


Figure 4.4 Location of Nodes 9 to 26

Table 4.7 The Coordinates of Nodes (9 to 26) in a Natural Coordinate System

Mid-side Nodes												
Node	9	10	11	12	13	14	15	16	17	18	19	20
ξ	0	0	0	0	-1	+1	+1	-1	-1	+1	+1	-1
η	-1	+1	+1	-1	-0	0	0	0	-1	-1	+1	+1
ζ	+1	+1	-1	-1	+1	+1	-1	-1	0	0	0	0
Mid-Face Nodes												
Node	21	22	23	24	25	26						
ξ	-0	0	-1	+1	0	0						
η	-1	+1	0	0	0	0						
ζ	0	0	0	0	-1	+1						

Table 4.8 Shape Functions and their Derivatives for Nodes (9 to 20)
(Morton et al., 1995)

Shape Functions And Their Derivatives		
$\partial \bar{N}_i / \partial \xi$	$\partial \bar{N}_i / \partial \eta$	$\partial \bar{N}_i / \partial \zeta$
$\xi_0 = \begin{cases} 1 & \text{for } \xi > 0 \\ -1 & \text{for } \xi < 0 \end{cases}$	$\eta_0 = \begin{cases} 1 & \text{for } \eta > 0 \\ -1 & \text{for } \eta < 0 \end{cases}$	$\zeta_0 = \begin{cases} 1 & \text{for } \zeta > 0 \\ -1 & \text{for } \zeta < 0 \end{cases}$
$\bar{N}_9(\xi, \eta, \zeta) = \frac{1}{4}(1 - \xi)(1 - \eta)(1 + \zeta)$		
$\frac{1}{4}\xi_0(\eta - 1)(1 + \zeta)$	$\frac{1}{4}(\xi - 1)(1 + \zeta)$	$\frac{1}{4}(1 - \xi)(1 - \eta)$
$\bar{N}_{10}(\xi, \eta, \zeta) = \frac{1}{4}(1 - \xi)(1 + \eta)(1 + \zeta)$		
$-\frac{1}{4}\xi_0(1 + \eta)(1 + \zeta)$	$-\frac{1}{4}(1 - \xi)(1 + \zeta)$	$\frac{1}{4}(1 - \xi)(1 + \eta)$
$\bar{N}_{11}(\xi, \eta, \zeta) = \frac{1}{4}(1 - \xi)(1 + \eta)(1 - \zeta)$		
$\frac{1}{4}\xi_0(1 + \eta)(\zeta - 1)$	$\frac{1}{4}(1 - \xi)(1 - \zeta)$	$\frac{1}{4}(\xi - 1)(1 + \eta)$
$\bar{N}_{12}(\xi, \eta, \zeta) = \frac{1}{4}(1 - \xi)(1 - \eta)(1 - \zeta)$		
$\frac{1}{4}\xi_0(1 - \eta)(\zeta - 1)$	$\frac{1}{4}(1 - \xi)(\zeta - 1)$	$\frac{1}{4}(\xi - 1)(1 - \eta)$
$\bar{N}_{13}(\xi, \eta, \zeta) = \frac{1}{4}(1 - \xi)(1 - \eta)(1 + \zeta)$		
$\frac{1}{4}(\eta - 1)(1 + \zeta)$	$-\frac{1}{4}\eta_0(1 - \xi)(1 + \zeta)$	$\frac{1}{4}(1 - \xi)(1 - \eta)$
$\bar{N}_{14}(\xi, \eta, \zeta) = \frac{1}{4}(1 + \xi)(1 - \eta)(1 + \zeta)$		
$\frac{1}{4}(1 - \eta)(1 + \zeta)$	$-\frac{1}{4}\eta_0(1 + \xi)(1 + \zeta)$	$\frac{1}{4}(1 + \xi)(1 - \eta)$
$\bar{N}_{15}(\xi, \eta, \zeta) = \frac{1}{4}(1 + \xi)(1 - \eta)(1 - \zeta)$		
$\frac{1}{4}(1 - \eta)(1 - \zeta)$	$-\frac{1}{4}\eta_0(1 + \xi)(1 - \zeta)$	$\frac{1}{4}(1 + \xi)(\eta - 1)$
$\bar{N}_{16}(\xi, \eta, \zeta) = \frac{1}{4}(1 - \xi)(1 - \eta)(1 - \zeta)$		
$\frac{1}{4}(\eta - 1)(1 - \zeta)$	$-\frac{1}{4}\eta_0(1 - \xi)(1 - \zeta)$	$\frac{1}{4}(1 - \xi)(\eta - 1)$
$\bar{N}_{17}(\xi, \eta, \zeta) = \frac{1}{4}(1 - \xi)(1 - \eta)(1 - \zeta)$		
$\frac{1}{4}(1 - \eta)(\zeta - 1)$	$\frac{1}{4}(1 - \xi)(\zeta - 1)$	$-\frac{1}{4}\zeta_0(1 - \xi)(1 - \eta)$
$\bar{N}_{18}(\xi, \eta, \zeta) = \frac{1}{4}(1 + \xi)(1 - \eta)(1 - \zeta)$		
$\frac{1}{4}(1 - \eta)(1 - \zeta)$	$\frac{1}{4}(1 + \xi)(\zeta - 1)$	$-\frac{1}{4}\zeta_0(1 + \xi)(1 - \eta)$
$\bar{N}_{19}(\xi, \eta, \zeta) = \frac{1}{4}(1 + \xi)(1 + \eta)(1 - \zeta)$		
$\frac{1}{4}(1 + \xi)(1 - \zeta)$	$\frac{1}{4}(1 + \xi)(1 - \zeta)$	$-\frac{1}{4}\zeta_0(1 + \xi)(1 + \eta)$
$\bar{N}_{20}(\xi, \eta, \zeta) = \frac{1}{4}(1 - \xi)(1 + \eta)(1 - \zeta)$		
$\frac{1}{4}(1 + \eta)(\zeta - 1)$	$\frac{1}{4}(1 - \xi)(1 - \zeta)$	$-\frac{1}{4}\zeta_0(1 - \xi)(1 + \eta)$

Table 4.9 Shape functions and their derivatives for Nodes (21 to 26)
(Morton et al. 1995)

Shape Functions at Each Node	Shape Functions Derivatives		
	$\frac{\partial \bar{N}_i}{\partial \xi}$	$\frac{\partial \bar{N}_i}{\partial \eta}$	$\frac{\partial \bar{N}_i}{\partial \zeta}$
$N_{21}(\xi, \eta, \zeta) = \frac{1}{2}(1 - \xi)(1 - \eta)(1 - \zeta)$	$\frac{1}{2}\xi_0(1 - \eta)(\zeta - 1)$	$\frac{1}{2}(1 - \xi)(\zeta - 1)$	$-\frac{1}{2}\zeta_0(1 - \xi)(1 - \eta)$
$N_{22}(\xi, \eta, \zeta) = \frac{1}{2}(1 - \xi)(1 + \eta)(1 - \zeta)$	$\frac{1}{2}\xi_0(1 + \eta)(\zeta - 1)$	$\frac{1}{2}(1 - \xi)(1 - \zeta)$	$-\frac{1}{2}\zeta_0(1 - \xi)(1 + \eta)$
$N_{23}(\xi, \eta, \zeta) = \frac{1}{2}(1 - \xi)(1 - \eta)(1 - \zeta)$	$\frac{1}{2}(1 - \eta)(\zeta - 1)$	$-\frac{1}{2}\eta_0(1 - \xi)(1 - \zeta)$	$-\frac{1}{2}\zeta_0(1 - \xi)(1 - \eta)$
$N_{24}(\xi, \eta, \zeta) = \frac{1}{2}(1 + \xi)(1 - \eta)(1 - \zeta)$	$\frac{1}{2}(1 - \eta)(1 - \zeta)$	$-\frac{1}{2}\eta_0(1 + \xi)(1 - \zeta)$	$-\frac{1}{2}\zeta_0(1 + \xi)(1 - \eta)$
$N_{25}(\xi, \eta, \zeta) = \frac{1}{2}(1 - \xi)(1 - \eta)(1 - \zeta)$	$\frac{1}{2}\xi_0(\eta - 1)(1 - \zeta)$	$-\frac{1}{2}\eta_0(1 - \xi)(1 - \zeta)$	$\frac{1}{2}(1 - \xi)(\eta - 1)$
$N_{26}(\xi, \eta, \zeta) = \frac{1}{2}(1 - \xi)(1 - \eta)(1 + \zeta)$	$\frac{1}{2}\xi_0(\eta - 1)(1 + \zeta)$	$-\frac{1}{2}\eta_0(1 - \xi)(1 + \zeta)$	$\frac{1}{2}(1 - \xi)(1 - \eta)$

4.1.4 Shape Functions for Transitional Hexahedral Elements

As mentioned earlier in this chapter, two transition elements were used throughout this thesis: (12-node) and (16-node) hexahedral elements as shown in Figure 4.5. Their shape functions were developed based on Morton et al.'s (1995) equations, as explained below and listed in Tables 4.10 and 4.11.

Nodes from 9 to 26 may or may not be present. If a node doesn't exist, its original shape function (\bar{N}_9 to \bar{N}_{20}) or (N_{21} to N_{26}) should be set to zero and then used in the following equations:

For the corner nodes:

$$N_1 = \bar{N}_1 - \frac{1}{2}(\bar{N}_9 + \bar{N}_{13} + \bar{N}_{17}) + \frac{1}{4}(N_{21} + N_{23} + N_{26}) \quad (26)$$

$$N_2 = \bar{N}_2 - \frac{1}{2}(\bar{N}_9 + \bar{N}_{14} + \bar{N}_{18}) + \frac{1}{4}(N_{21} + N_{24} + N_{26}) \quad (27)$$

$$N_3 = \bar{N}_3 - \frac{1}{2}(\bar{N}_{10} + \bar{N}_{14} + \bar{N}_{19}) + \frac{1}{4}(N_{22} + N_{24} + N_{26}) \quad (28)$$

$$N_4 = \bar{N}_4 - \frac{1}{2}(\bar{N}_{10} + \bar{N}_{13} + \bar{N}_{20}) + \frac{1}{4}(N_{22} + N_{23} + N_{26}) \quad (29)$$

$$N_5 = \bar{N}_5 - \frac{1}{2}(\bar{N}_{12} + \bar{N}_{16} + \bar{N}_{17}) + \frac{1}{4}(N_{21} + N_{23} + N_{25}) \quad (30)$$

$$N_6 = \bar{N}_6 - \frac{1}{2}(\bar{N}_{12} + \bar{N}_{15} + \bar{N}_{18}) + \frac{1}{4}(N_{21} + N_{24} + N_{25}) \quad (31)$$

$$N_7 = \bar{N}_7 - \frac{1}{2}(\bar{N}_{11} + \bar{N}_{15} + \bar{N}_{19}) + \frac{1}{4}(N_{22} + N_{24} + N_{25}) \quad (32)$$

$$N_8 = \bar{N}_8 - \frac{1}{2}(\bar{N}_{11} + \bar{N}_{16} + \bar{N}_{20}) + \frac{1}{4}(N_{22} + N_{23} + N_{25}) \quad (33)$$

For the edge mid-nodes:

$$N_9 = \bar{N}_9 - \frac{1}{2}(N_{21} + N_{26}) \quad (34)$$

$$N_{10} = \bar{N}_{10} - \frac{1}{2}(N_{22} + N_{26}) \quad (35)$$

$$N_{11} = \bar{N}_{11} - \frac{1}{2}(N_{22} + N_{25}) \quad (36)$$

$$N_{12} = \bar{N}_{12} - \frac{1}{2}(N_{21} + N_{25}) \quad (37)$$

$$N_{13} = \bar{N}_{13} - \frac{1}{2}(N_{23} + N_{26}) \quad (38)$$

$$N_{14} = \bar{N}_{14} - \frac{1}{2}(N_{24} + N_{26}) \quad (39)$$

$$N_{15} = \bar{N}_{15} - \frac{1}{2}(N_{24} + N_{25}) \quad (40)$$

$$N_{16} = \bar{N}_{16} - \frac{1}{2}(N_{23} + N_{25}) \quad (41)$$

$$N_{17} = \bar{N}_{17} - \frac{1}{2}(N_{21} + N_{23}) \quad (42)$$

$$N_{18} = \bar{N}_{18} - \frac{1}{2}(N_{21} + N_{24}) \quad (43)$$

$$N_{19} = \bar{N}_{19} - \frac{1}{2}(N_{22} + N_{24}) \quad (44)$$

$$N_{20} = \bar{N}_{20} - \frac{1}{2}(N_{22} + N_{23}) \quad (45)$$

For the face mid-nodes:

$$N_{21} = \frac{1}{2}(1 - |\xi|)(1 - \eta)(1 - |\zeta|) \quad (46)$$

$$N_{22} = \frac{1}{2}(1 - |\xi|)(1 + \eta)(1 - |\zeta|) \quad (47)$$

$$N_{23} = \frac{1}{2} (1 - \xi)(1 - |\eta|)(1 - |\zeta|) \quad (48)$$

$$N_{24} = \frac{1}{2} (1 + \xi)(1 - |\eta|)(1 - |\zeta|) \quad (49)$$

$$N_{25} = \frac{1}{2} (1 - |\xi|)(1 - |\eta|)(1 - \zeta) \quad (50)$$

$$N_{26} = \frac{1}{2} (1 - |\xi|)(1 - |\eta|)(1 + \zeta) \quad (51)$$

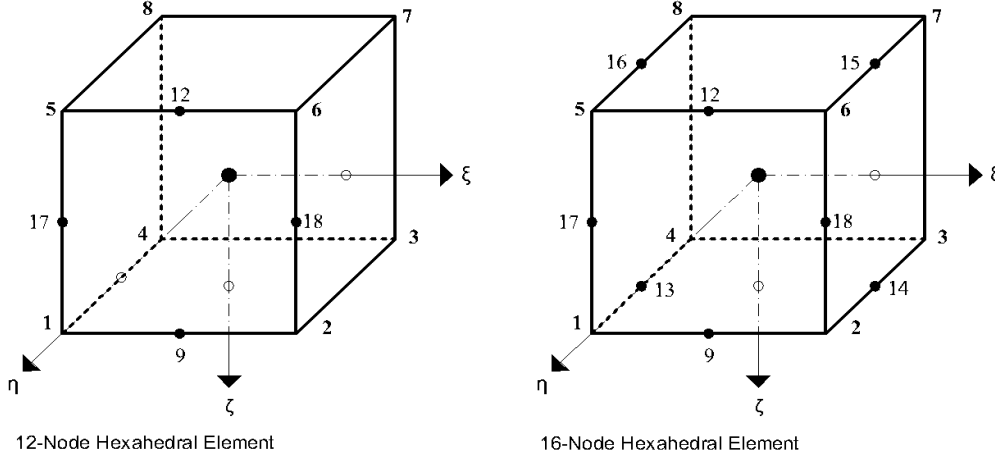


Figure 4.5 12-Node and 16-Node Transitional Elements

Table 4.10 12-Node Transitional Hexahedral Element Shape Functions

(12-Node) Transitional Hexahedral Element Shape Functions

$$N_1 = 1/8 (1 - \eta) [(1 - \xi)(1 + \zeta) - (1 - |\xi|)(1 + \zeta) - (1 - \xi)(1 - |\zeta|)]$$

$$N_2 = 1/8 (1 - \eta) [(1 + \xi)(1 + \zeta) - (1 - |\xi|)(1 + \zeta) - (1 + \xi)(1 - |\zeta|)]$$

$$N_3 = 1/8 (1 + \xi)(1 + \eta)(1 + \zeta)$$

$$N_4 = 1/8 (1 - \xi)(1 + \eta)(1 + \zeta)$$

$$N_5 = 1/8 (1 - \eta) [(1 - \xi)(1 - \zeta) - (1 - |\xi|)(1 - \zeta) - (1 - \xi)(1 - |\zeta|)]$$

$$N_6 = 1/8 (1 - \eta) [(1 + \xi)(1 - \zeta) - (1 - |\xi|)(1 - \zeta) - (1 + \xi)(1 - |\zeta|)]$$

$$N_7 = 1/8 (1 + \xi)(1 + \eta)(1 - \zeta)$$

$$N_8 = 1/8 (1 - \xi)(1 + \eta)(1 - \zeta)$$

$$N_9 = 1/4 (1 - |\xi|)(1 - \eta)(1 + \zeta)$$

$$N_{18} = 1/4 (1 + \xi)(1 - \eta)(1 - |\zeta|)$$

$$N_{12} = 1/4 (1 - |\xi|)(1 - \eta)(1 - \zeta)$$

$$N_{17} = 1/4 (1 - \xi)(1 - \eta)(1 - |\zeta|)$$

Table 4.11 16-Node Transitional Hexahedral Element Shape Functions

(16-Node) Transitional Hexahedral Element Shape Functions	
$N_1 = 1/8 [(1 - \xi)(1 - \eta)(1 + \zeta) - (1 - \xi)(1 - \eta)(1 + \zeta) - (1 - \xi)(1 - \eta)(1 + \zeta) - (1 - \xi)(1 - \eta)(1 - \zeta)]$	
$N_2 = 1/8 [(1 + \xi)(1 - \eta)(1 + \zeta) - (1 - \xi)(1 - \eta)(1 + \zeta) - (1 + \xi)(1 - \eta)(1 + \zeta) - (1 + \xi)(1 - \eta)(1 - \zeta)]$	
$N_3 = 1/8 (1 + \xi)(1 + \zeta) [(1 + \eta) - (1 - \eta)]$	
$N_4 = 1/8 (1 - \xi)(1 + \zeta) [(1 + \eta) - (1 - \eta)]$	
$N_5 = 1/8 (1 - \eta) [(1 - \xi)(1 - \zeta) - (1 - \xi)(1 - \zeta) - (1 - \xi)(1 - \zeta)]$	
$N_6 = 1/8 [(1 + \xi)(1 - \eta)(1 - \zeta) - (1 - \xi)(1 - \eta)(1 - \zeta) - (1 + \xi)(1 - \eta)(1 - \zeta)]$	
$N_7 = 1/8 (1 + \xi)(1 - \zeta) [(1 + \eta) - (1 - \eta)]$	
$N_8 = 1/8 (1 - \xi)(1 - \zeta) [(1 + \eta) - (1 - \eta)]$	
$N_9 = 1/4 (1 - \xi)(1 - \eta)(1 + \zeta)$	
$N_{10} = 1/4 (1 + \xi)(1 - \eta)(1 - \zeta)$	
$N_{11} = 1/4 (1 - \xi)(1 - \eta)(1 - \zeta)$	
$N_{12} = 1/4 (1 - \xi)(1 - \eta)(1 - \zeta)$	
$N_{13} = 1/4 (1 - \xi)(1 - \eta)(1 + \zeta)$	
$N_{14} = 1/4 (1 + \xi)(1 - \eta)(1 + \zeta)$	
$N_{15} = 1/4 (1 + \xi)(1 - \eta)(1 - \zeta)$	
$N_{16} = 1/4 (1 - \xi)(1 - \eta)(1 - \zeta)$	

4.2 Displacement, Strain and Stress for Hexahedral Elements

4.2.1 Element Equation - Displacement

There are three degrees of freedom for displacements at each node in three-dimensional elements. The displacement in a hexahedral element, as a function of the global coordinates (x, y, z), is given as follows (Liu and Quek 2003):

$$\mathbf{U}^e(x, y, z) = \mathbf{N}^e \cdot \mathbf{D}^e \quad (52)$$

where:

- $\mathbf{U}^e(x, y, z)$: The displacement vector for the element (e) in the global coordinate system.
- \mathbf{N}^e : The shape function Matrix at the element nodes:

$$\mathbf{N}^e = [N_1^e \ N_2^e \ N_3^e \ N_4^e \ \dots \ \dots \ \dots \ N_i^e] \quad (53)$$

$$\mathbf{N}_i^e = \begin{bmatrix} N_i^e & 0 & 0 \\ 0 & N_i^e & 0 \\ 0 & 0 & N_i^e \end{bmatrix} \quad (54)$$

where (i) is the number of nodes

- \mathbf{D}^e : The nodal displacement vector

$$\mathbf{D}^e = \begin{Bmatrix} D_1^e \\ D_2^e \\ D_3^e \\ \dots \\ \dots \\ D_i^e \end{Bmatrix} \quad (55)$$

where:

$$\mathbf{D}_i^e = \begin{Bmatrix} u_i^e \\ v_i^e \\ w_i^e \end{Bmatrix} \quad (56)$$

and:

u_i^e : The displacement node (i) for the element (e) in the X direction.

v_i^e : The displacement node (i) for the element (e) in the Y direction.

w_i^e : The displacement node (i) for the element (e) in the Z direction.

The nodal displacement vector can be calculated using the following equation:

$$\mathbf{K}^e \cdot \mathbf{D}^e = \mathbf{F}^e \quad (57)$$

where:

- \mathbf{K}^e : The element stiffness matrix
- \mathbf{F}^e : Element body force vector

4.2.2 Element Strain Matrix

In order to compute the stiffness matrix, the strain matrix should be obtained:

$$\mathbf{B}^e = [\mathbf{B}_1^e \quad \mathbf{B}_2^e \quad \mathbf{B}_3^e \quad \mathbf{B}_4^e \dots \dots \dots \dots \mathbf{B}_i^e] \quad (58)$$

where:

$$\mathbf{B}_i^e = \mathbf{L} \cdot \mathbf{N}_i^e = \begin{bmatrix} \frac{\partial}{\partial x} & 0 & 0 \\ 0 & \frac{\partial}{\partial y} & 0 \\ 0 & 0 & \frac{\partial}{\partial z} \\ 0 & \frac{\partial}{\partial z} & \frac{\partial}{\partial y} \\ \frac{\partial}{\partial z} & 0 & \frac{\partial}{\partial x} \\ \frac{\partial}{\partial y} & \frac{\partial}{\partial x} & 0 \end{bmatrix} \mathbf{N}_i^e = \begin{bmatrix} \frac{\partial N_i^e}{\partial x} & 0 & 0 \\ 0 & \frac{\partial N_i^e}{\partial y} & 0 \\ 0 & 0 & \frac{\partial N_i^e}{\partial z} \\ 0 & \frac{\partial N_i^e}{\partial z} & \frac{\partial N_i^e}{\partial y} \\ \frac{\partial N_i^e}{\partial z} & 0 & \frac{\partial N_i^e}{\partial x} \\ \frac{\partial N_i^e}{\partial y} & \frac{\partial N_i^e}{\partial x} & 0 \end{bmatrix} \quad (59)$$

As shape functions are defined in the natural coordinate system (ξ, η, ζ) , their derivatives with respect to the global coordinates (x, y, z) should be obtained, where:

$$\left. \begin{array}{l} x = \sum_1^i N_i^e(\xi, \eta, \zeta) \cdot x_i^e \\ y = \sum_1^i N_i^e(\xi, \eta, \zeta) \cdot y_i^e \\ z = \sum_1^i N_i^e(\xi, \eta, \zeta) \cdot z_i^e \end{array} \right\} \quad (60)$$

where:

(x_i^e, y_i^e, z_i^e) are the global coordinates for the node (i) in the element (e)

So:

$$\left. \begin{array}{l} \frac{\partial N_i^e}{\partial \xi} = \frac{\partial N_i^e}{\partial x} \frac{\partial x}{\partial \xi} + \frac{\partial N_i^e}{\partial y} \frac{\partial y}{\partial \xi} + \frac{\partial N_i^e}{\partial z} \frac{\partial z}{\partial \xi} \\ \frac{\partial N_i^e}{\partial \eta} = \frac{\partial N_i^e}{\partial x} \frac{\partial x}{\partial \eta} + \frac{\partial N_i^e}{\partial y} \frac{\partial y}{\partial \eta} + \frac{\partial N_i^e}{\partial z} \frac{\partial z}{\partial \eta} \\ \frac{\partial N_i^e}{\partial \zeta} = \frac{\partial N_i^e}{\partial x} \frac{\partial x}{\partial \zeta} + \frac{\partial N_i^e}{\partial y} \frac{\partial y}{\partial \zeta} + \frac{\partial N_i^e}{\partial z} \frac{\partial z}{\partial \zeta} \end{array} \right\} \quad (61)$$

The previous equations can be written in a matrix form:

$$\begin{aligned}
\begin{Bmatrix} \partial N_i^e / \partial \xi \\ \partial N_i^e / \partial \eta \\ \partial N_i^e / \partial \zeta \end{Bmatrix} &= \mathbf{J} \cdot \begin{Bmatrix} \partial N_i^e / \partial x \\ \partial N_i^e / \partial y \\ \partial N_i^e / \partial z \end{Bmatrix} \\
\begin{Bmatrix} \partial N_i^e / \partial x \\ \partial N_i^e / \partial y \\ \partial N_i^e / \partial z \end{Bmatrix} &= \mathbf{J}^{-1} \cdot \begin{Bmatrix} \partial N_i^e / \partial \xi \\ \partial N_i^e / \partial \eta \\ \partial N_i^e / \partial \zeta \end{Bmatrix}
\end{aligned} \tag{62}$$

where (\mathbf{J}) is the Jacobian Matrix and defined by:

$$\begin{aligned}
\mathbf{J} &= \begin{bmatrix} \partial x / \partial \xi & \partial y / \partial \xi & \partial z / \partial \xi \\ \partial x / \partial \eta & \partial y / \partial \eta & \partial z / \partial \eta \\ \partial x / \partial \zeta & \partial y / \partial \zeta & \partial z / \partial \zeta \end{bmatrix} \\
\mathbf{J} &= \begin{bmatrix} j_{11} & j_{12} & j_{13} \\ j_{21} & j_{22} & j_{23} \\ j_{31} & j_{32} & j_{33} \end{bmatrix} = \begin{bmatrix} \sum_1^8 \frac{\partial N_i^e}{\partial \xi} \cdot x_i^e & \sum_1^8 \frac{\partial N_i^e}{\partial \xi} \cdot y_i^e & \sum_1^8 \frac{\partial N_i^e}{\partial \xi} \cdot z_i^e \\ \sum_1^8 \frac{\partial N_i^e}{\partial \eta} \cdot x_i^e & \sum_1^8 \frac{\partial N_i^e}{\partial \eta} \cdot y_i^e & \sum_1^8 \frac{\partial N_i^e}{\partial \eta} \cdot z_i^e \\ \sum_1^8 \frac{\partial N_i^e}{\partial \zeta} \cdot x_i^e & \sum_1^8 \frac{\partial N_i^e}{\partial \zeta} \cdot y_i^e & \sum_1^8 \frac{\partial N_i^e}{\partial \zeta} \cdot z_i^e \end{bmatrix}
\end{aligned} \tag{63}$$

And (\mathbf{J}^{-1}) is the inverse of the Jacobian Matrix and calculated according to (Felippa 2013):

$$\mathbf{J}^{-1} = \frac{1}{|\mathbf{J}|} \cdot \begin{bmatrix} J_{11} & J_{12} & J_{13} \\ J_{21} & J_{22} & J_{23} \\ J_{31} & J_{32} & J_{33} \end{bmatrix} \tag{64}$$

where:

$$|\mathbf{J}| = j_{11} \cdot J_{11} + j_{12} \cdot J_{21} + j_{13} \cdot J_{31} \tag{65}$$

$$\begin{aligned}
J_{11} &= j_{22} \cdot j_{33} - j_{23} \cdot j_{32}, & J_{12} &= j_{23} \cdot j_{31} - j_{21} \cdot j_{33}, & J_{13} &= j_{21} \cdot j_{32} - j_{31} \cdot j_{22} \\
J_{21} &= j_{32} \cdot j_{13} - j_{12} \cdot j_{33}, & J_{22} &= j_{33} \cdot j_{11} - j_{31} \cdot j_{13}, & J_{23} &= j_{31} \cdot j_{12} - j_{32} \cdot j_{11} \\
J_{31} &= j_{12} \cdot j_{23} - j_{13} \cdot j_{22}, & J_{32} &= j_{13} \cdot j_{21} - j_{23} \cdot j_{11}, & J_{33} &= j_{11} \cdot j_{22} - j_{12} \cdot j_{21}
\end{aligned}$$

4.2.3 Element Stiffness Matrix

$$\mathbf{K}^e = \iiint \mathbf{B}^T \cdot \mathbf{C} \cdot \mathbf{B} \cdot dV^e \quad (\text{Logan 2007}) \quad (66)$$

The evaluation of the stiffness matrix is done by applying a Gauss integration scheme and it is carried out in the natural coordinate system (ξ, η, ζ) :

$$[\mathbf{K}^e] = \int_{-1}^{+1} \int_{-1}^{+1} \int_{-1}^{+1} [\mathbf{B}(\xi, \eta, \zeta)]^T \cdot \mathbf{C} \cdot \mathbf{B}(\xi, \eta, \zeta) \cdot |\mathbf{J}| \cdot d\xi \cdot d\eta \cdot d\zeta \Rightarrow \quad (67)$$

$$[\mathbf{K}^e] = \int_{-1}^{+1} \int_{-1}^{+1} \int_{-1}^{+1} f(\xi, \eta, \zeta) \cdot d\xi \cdot d\eta \cdot d\zeta = \sum_{i=1}^n \sum_{j=1}^n \sum_{k=1}^n f(\xi_i, \eta_j, \zeta_k) \cdot w_i \cdot w_j \cdot w_k$$

where:

- n: is the number of Gauss points in the directions: ξ, η and ζ respectively (usually it is the same number in all directions).
- $f(\xi, \eta, \zeta) = [\mathbf{B}(\xi, \eta, \zeta)]^T \cdot \mathbf{C} \cdot \mathbf{B}(\xi, \eta, \zeta) \cdot |\mathbf{J}|$
- C: The matrix of a linear isotropic material constant:

$$\mathbf{C} = \frac{E}{(1+\nu)(1-2\nu)} \begin{bmatrix} 1-\nu & \nu & \nu & 0 & 0 & 0 \\ \nu & 1-\nu & \nu & 0 & 0 & 0 \\ \nu & \nu & 1-\nu & 0 & 0 & 0 \\ 0 & 0 & 0 & \frac{1-2\nu}{2} & 0 & 0 \\ 0 & 0 & 0 & 0 & \frac{1-2\nu}{2} & 0 \\ 0 & 0 & 0 & 0 & 0 & \frac{1-2\nu}{2} \end{bmatrix} \quad (\text{Logan, 2007}) \quad (69)$$

- w_i, w_j, w_k : are the weights of Gauss points in the directions: ξ, η and ζ respectively.

The $1 \times 1 \times 1$ integration scheme, the $2 \times 2 \times 2$ integration scheme and the $3 \times 3 \times 3$ integration scheme are exact for a constant function, a tri-linear function and a tri-quadratic function respectively (Dhondt 2004). Therefore, the $2 \times 2 \times 2$ integration scheme represents full integration for a first order element (8-node brick) and the

$3 \times 3 \times 3$ integration scheme stands for full integration in a second order element (20-node brick) (Dhondt 2004).

The location and number of the integration points for hexahedral elements are summarized in Table 4.12 (Dhondt 2004).

Table 4.12 Locations of Integration Points in Hexahedral Elements

Scheme	Location (ξ_i, η_i, ζ_i)	Number	Weight
$1 \times 1 \times 1$	(0, 0, 0)	1	8
$2 \times 2 \times 2$	$\left(\pm \frac{1}{\sqrt{3}}, \pm \frac{1}{\sqrt{3}}, \pm \frac{1}{\sqrt{3}} \right)$	8	1
$3 \times 3 \times 3$	$\begin{cases} \left(0, 0, \pm \sqrt{\frac{3}{5}} \right) \\ (0, 0, 0) \end{cases}$	8 12 6 1	$\left(\frac{5}{9}\right)^3$ $\left(\frac{8}{9}\right)\left(\frac{5}{9}\right)^2$ $\left(\frac{8}{9}\right)^2\left(\frac{5}{9}\right)$ $\left(\frac{8}{9}\right)^3$

Strain:

$$\boldsymbol{\varepsilon}^e = \mathbf{B}^e \cdot \mathbf{U}^e \quad (\text{Logan 2007}) \quad (70)$$

Stress:

$$\boldsymbol{\sigma}^e = \boldsymbol{\varepsilon}^e \cdot \mathbf{C} \quad (\text{Logan 2007}) \quad (71)$$

4.2.4 The Direct Stiffness Assembly Method

The discrete stiffness assembly method, also known as the direct stiffness method, is the assemblage of the elements' equilibrium equations into a set of global equations. The global stiffness matrix $[K^G]$ is obtained by summing the individual element contributions taking into account the common degrees of freedom between elements (Potts & Zdravkovic 1999):

$$[K^G] \cdot \{D^G\} = \{F^G\} \quad (\text{Potts \& Zdravkovic 1999}) \quad (72)$$

where:

$[K^G]$: The global stiffness matrix

$\{D^G\}$: The global nodal displacement vector

$\{F^G\}$: The global body force vector

5. Performance Evaluation of Transition Elements

As the formulations of linear, quadratic and transition hexahedral elements were developed in sim|FEM code, a testing process was carried out to evaluate the accuracy and performance of these elements. The parameter of evaluation was set to be the nodal displacements, as it is the fundamental solution in the general matrix stiffness equation (6) (Potts & Zdravkovic 1999).

Two types of models (Type I and Type II) of 3 kinds of elements (first order, second order and transition hexahedral elements) were tested in three different programs, where the elements were available in those programs (sim|FEM, ABAQUS (HKS 2007), LISA (Sonnenhof 2012)). Type I models were aimed to test the transitional elements as single elements, while Type II models were aimed to test them as part of a simple assemblage of three-dimensional elements. The models, elements and programs used for testing are explained below:

The developed models were:

- Type I Models: Each of these models was composed of only one hexahedral element: linear, transitional or quadratic. Further description is given on the following pages.
- Type II Models: Each of these models was composed of a mesh of 27 elements (a 3 by 3 by 3 cube of elements): a mesh of only linear elements, a mesh of only quadratic elements or a mesh with transition elements. Further description is given on the following pages.

Both types of models are illustrated in Figure 5.1.

The models' and elements' naming conventions were chosen as follows: STR refers to the analysis type, which is 3D stress analysis, HEX refers to the element used that is a hexahedral element, (08, 20, 12, 16) refers to the number of nodes, (L, Q or T) refers to the kind of element tested; Linear, Quadratic or Transitional, respectively and finally (R and F) refer to the integration scheme used whether they were reduced or full, respectively.

The elements tested were:

- (8-node) linear hexahedral elements: two integration schemes (reduced and full integration) were tested; (STRHEX08LR) and (STRHEX08LF), respectively.
- (20-node) quadratic hexahedral elements: two integration schemes (reduced and full integration) were tested; (STRHEX20QR) and (STRHEX20QF), respectively.
- Transition elements where (12-node) and (16-node) elements were tested; (STRHEX12T) and (STRHEX16T), respectively. The integration scheme for these elements is explained in the following pages.

The programs used for testing were:

1. sim|FEM: a computer code developed to solve 3D models with transition elements (Zsaki 2010). The code was compiled in Microsoft Visual Studio where tests of the following elements were done:

- 8-node linear hexahedral element (STRHEX08L).
- 12-node transition hexahedral element (STRHEX12T) and 16-node transition hexahedral element (STRHEX16T).
- 20-node quadratic hexahedral element (STRHEX20Q).

2. ABAQUS: a finite element analysis software (HKS 2007) where tests of the following elements were done:

- 8-node linear hexahedral element (STRHEX08L), which is referred to in ABAQUS as C3D8.
- 20-node quadratic hexahedral element (STRHEX20Q), which is referred to in ABAQUS as C3D20.

3. LISA: a finite element analysis software (Sonnenhof 2012), where tests of the following elements were done:

- 8-node linear hexahedral element (STRHEX08L).
- 20-node quadratic hexahedral element (STRHEX20Q).

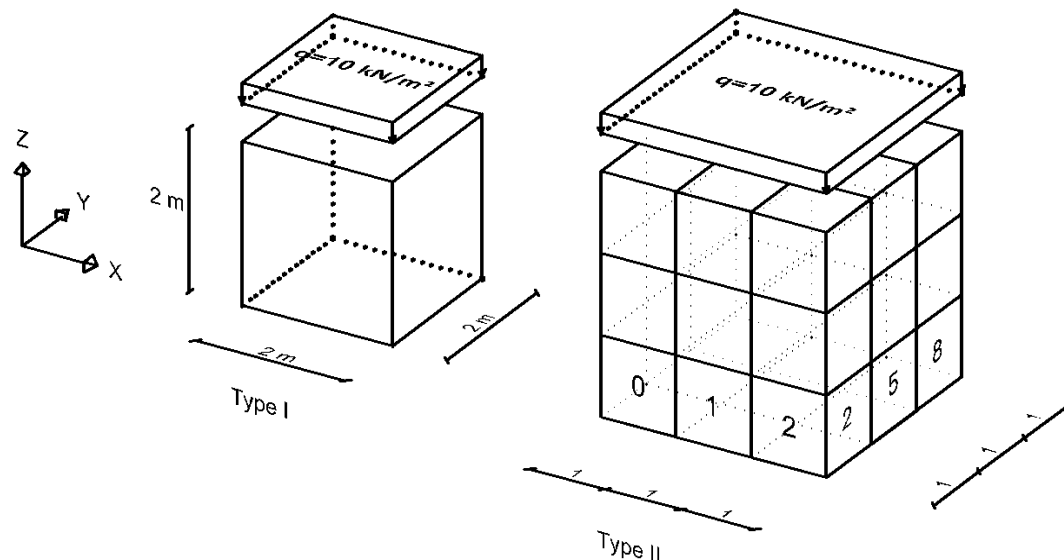


Figure 5.1 Type I and II Models

5.1 Type I Models

All models of this type consisted of one brick element of a volume of 8 m³ (2m x 2m x 2m) of a material that was assumed to be linear elastic. Its properties are shown in Table 5.1. The tested models of this type were single first and second order hexahedral elements (STRHEX08LR, STRHEX08LF, STRHEX20QR, STRHEX20QF, STRHEX12T and STRHEX16T). The first and second order elements with full integration scheme were tested in all software mentioned above, but the first and second order elements with reduced integration scheme were tested only in sim|FEM and ABAQUS since it was possible to only test fully integrated elements in the available version of LISA.

Table 5.1 Material Properties of Type I and Type II Models

Property	Unit	Value
γ	kN/m ³	0
E	kPa	1000
ν	-	0.3

After running all Type I models, in order to study the behavior of the tested elements, a comparison between the models was performed, as is explained further in the following sections.

For the boundary conditions, the elements were constrained at the base with pinned supports at the base corner nodes or base mid-side nodes depending on the element type. The upper face in each model was loaded with a (10 kPa) uniform distributed pressure load. Since the finite element method requires the forces to be applied at the nodes, the

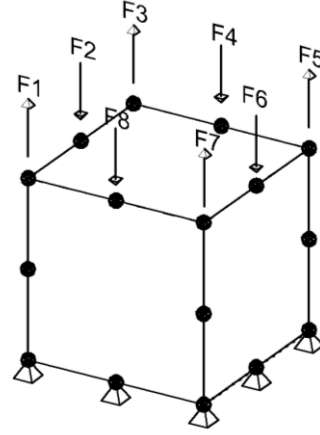
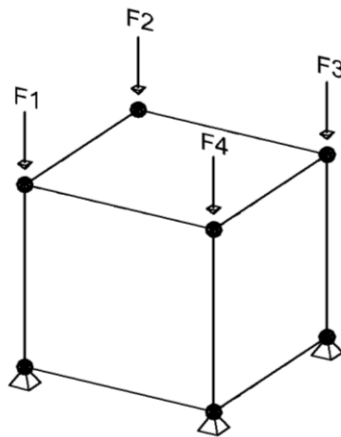
uniform distributed load was transferred to the nodes. The transformation depends on the face type (Smith & Griffiths 2004), as shown in Figure 5.2.

Performing the integration in the finite element method is done using numerical integration techniques that are approximate methods to evaluate the stiffness matrix integral, as presented in equation (61), by the sum of the products of function values at specific points over the range $[-1, +1]$. The Gaussian quadrature formula is one of these techniques that was used for carrying out numerical integration for linear and quadratic elements (Liu and Quek 2003), while what is called the modified quadrature formula (Gupta, 1978) was used for transition elements.

The quadrature formula includes two integration schemes: reduced integration scheme and full integration scheme. Reduced integration schemes were: (1x1x1) scheme that corresponds to one Gauss integration point and (2x2x2) scheme that correspond to eight Gauss integration points for (8-node) and (20-node) elements, respectively. Full integration schemes were: (2x2x2) scheme that corresponds to eight Gauss integration points and (3x3x3) scheme that corresponds to 27 Gauss integration points for (8-node) and (20-node) elements, respectively. The schemes are illustrated in Table 4.12.

Transitional elements have linear and quadratic edges where the mid-side nodes give rise to the displacement function that leads to discontinuity in the model. In 1978, Gupta developed the modified quadrature formula that is “used to numerically integrate discontinuous functions in the expression of the stiffness matrix.” The integral form in this modified formula was broken into two continuous integrals, -1.0 to 0.0 and 0.0 to +1.0. Thus, four quadrature point were used, meaning two integration points for each

sub-integral but in essence they are not really four points, they are only two points used in two discontinuous forms (Gupta 1978).



8-Node Hexahedral Element

$$F_1 = F_2 = F_3 = F_4 = q \cdot A/4$$

q : Uniform distributed load;

$$q = 10 \text{ kN/m}^2$$

A: Area of the loaded face

$$A = 4\text{m}^2$$

20-Node Hexahedral Element

$$F_1 = F_3 = F_5 = F_7 = -q \cdot A/12$$

$$F_2 = F_4 = F_6 = F_8 = q \cdot A/3$$

q : Uniform distributed load;

$$q = 10 \text{ kN/m}^2$$

A: Area of the loaded face

$$A = 4\text{m}^2$$

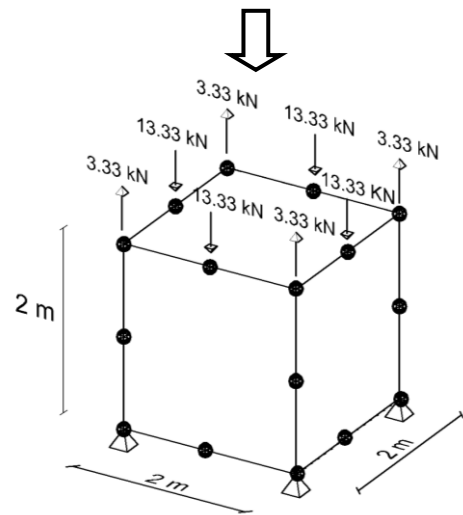
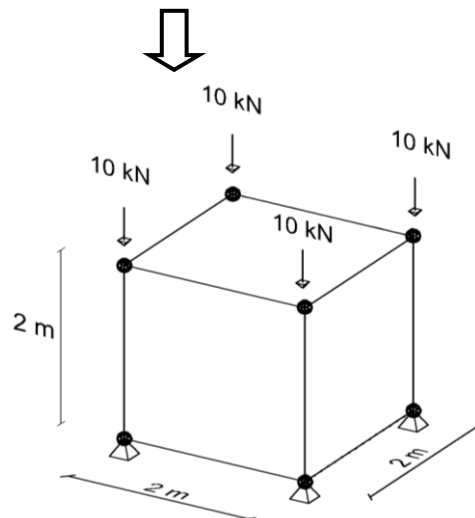


Figure 5.2 Equivalent Nodal Forces

5.1.1 Type I Models Using (STRHEX08L) - Results

The (8-node) hexahedral model (STRHEX08L) shown in Figure 5.3 was developed and tested in sim|FEM, ABAQUS and LISA. But, as mentioned before, in LISA only the full integration scheme could be tested in the available version.

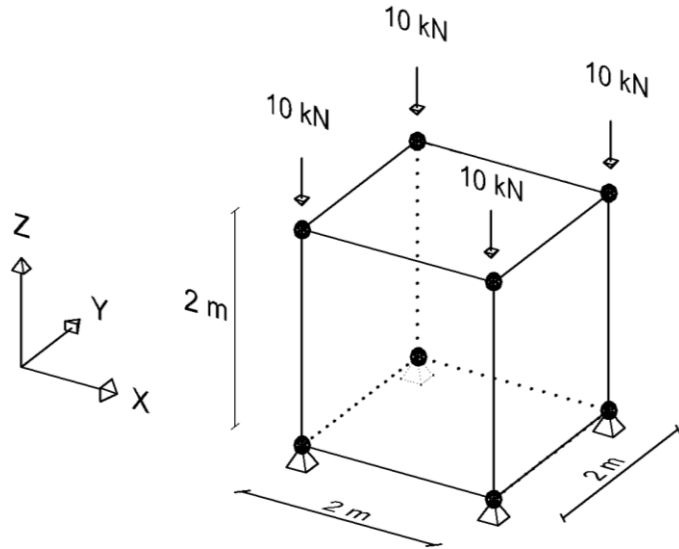


Figure 5.3 Type I Model - STRHEX08L

Since nodes at the base were all pinned supported, the displacements at them should be zero by definition. As the behavior of this simple element can be predicted, and as the test results demonstrated (refer to Appendix 1 for the full solution), the displacements at the corner nodes in Z direction (at the upper face) were equal. Also, by virtue of symmetry, $|U_x|=|U_y|$ at those nodes. Hence, to compare the element behavior in the three different programs under the same conditions, it was sufficient to plot the displacement vector magnitude at only one of the corner nodes (at the upper face) in respect to these programs, as illustrated in Figure 5.4 and 5.5. Due to the fact that the coordinate and node numbering systems were different among the three programs and in order to make the

comparison process easier, the node coordinates were used to indicate the nodes' location according to a coordinate system in which the Z axis is in the vertical direction, as shown in Figure 5.3. For a more accurate comparison, the percentage differences were calculated in the X, Y and Z directions with respect to the values obtained in sim|FEM, as shown in Table 5.2, as follows:

$$\% \text{ Difference} = \frac{(\text{Displacement Value} - \text{Benchmark Value})}{\text{Benchmark Value}} \quad (73)$$

The detailed results can be found in Appendix 1.

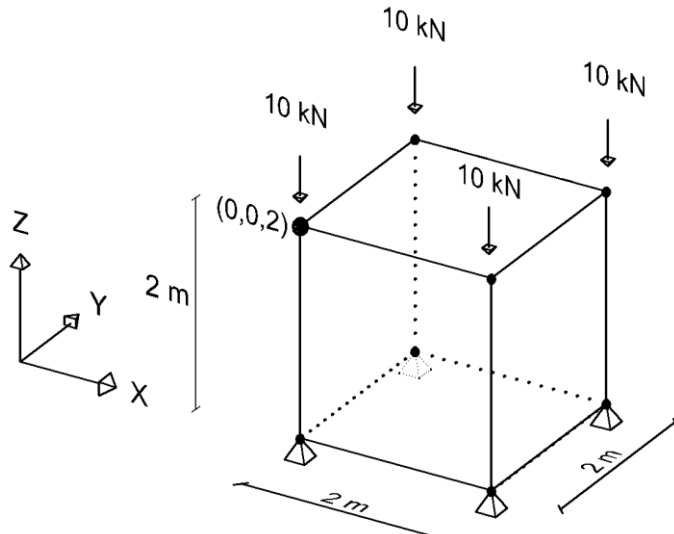


Figure 5.4 Illustration of Corner Node (0,0,2) location for the STRHEX08L Model

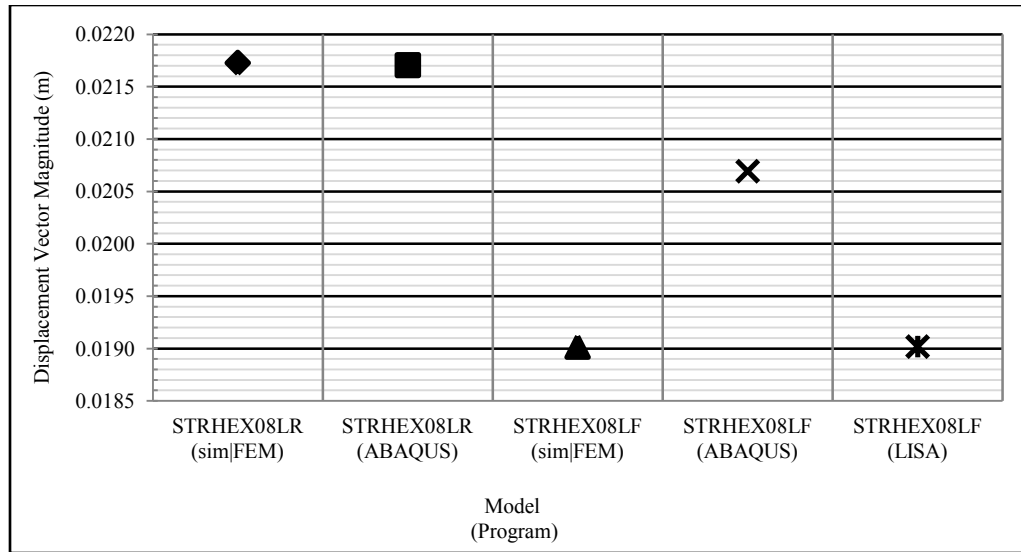


Figure 5.5 Displacement Vector Magnitude at Corner Node (0,0,2)
Model STRHEX08L

Table 5.2 Displacement Percentage Difference at the Corner Node (0,0,2) for the STRHEX08L Element

Displacement Difference @ Node (0,0,2) in %/ Model: STRHEX08LR			
Software	Ux (m)	Uy (m)	Uz (m)
ABAQUS	-5.98481E-03	-5.98481E-03	-1.99870E-02
With Respect to			
sim FEM	-6.00E-03	-6.00E-03	-2.00E-02
% Difference in Ux % Difference in Uy % Difference in Uz			
ABAQUS vs. sim FEM	0.25	0.25	0.06
Displacement Difference @ Node (0,0,2) in %/ Model: STRHEX08LF			
Software	Ux (m)	Uy (m)	Uz (m)
ABAQUS	-5.21933E-03	-5.21933E-03	-1.93309E-02
LISA	-3.90000E-03	-3.90000E-03	-1.82000E-02
With Respect to			
sim FEM	-3.90000E-03	-3.90000E-03	-1.82000E-02
% Difference in Ux % Difference in Uy % Difference in Uz			
ABAQUS vs. sim FEM	33.83	33.83	6.21
LISA vs. sim FEM	0.00	0.00	0.00

As can be observed, using the reduced integrated elements in both sim|FEM and ABAQUS resulted in almost identical values, where the maximum difference was (0.25%) in X and Y directions, but that was not the case when the full integrated element was used, where the results obtained in ABAQUS showed a considerable difference [(33.83%) in the X and Y directions and (6.21%) in the Z direction] in respect to those obtained in sim|FEM and LISA. It should be noted that the results of the fully integrated elements obtained from sim|FEM and LISA were identical.

Choosing the integration scheme that gives acceptable results in respect to the examined problem is important in finite element analysis. A general discussion in ABAQUS' documentations can be found regarding this point. It is mentioned that the reduced integration accuracy depends on the nature of the problem and fully integrated elements should be avoided in problems with large distortions or bending. These conditions don't apply for this test. Additionally, there is no indication in LISA's manual about which scheme tends to give more accurate results. Thus, for one 8-node element and linear elastic analysis, the best way to adapt certain results obtained using a specific scheme is to compare the test results with the ones obtained from 3D Hooke's Law (Stress-Strain Relationship) for which an analytical solution exists (Davis and Selvadurai 1996).

3D Hooke's Law (Stress-Strain Relationship):

$$\left. \begin{aligned} \varepsilon_x &= \frac{1}{E} \cdot [\sigma_{xx} - v(\sigma_{yy} + \sigma_{zz})] \\ \varepsilon_y &= \frac{1}{E} \cdot [\sigma_{yy} - v(\sigma_{xx} + \sigma_{zz})] \\ \varepsilon_z &= \frac{1}{E} \cdot [\sigma_{zz} - v(\sigma_{xx} + \sigma_{yy})] \end{aligned} \right\} \quad (74)$$

Where:

$$E=1000 \text{ kPa}, \nu = 0.3, \sigma_{xx} = \sigma_{yy} = 0, \sigma_{zz} = 10 \text{ kPa} \Rightarrow$$

$$\varepsilon_x = \left| \frac{0.3(10)}{1000} \right| = 0.003 \Rightarrow \Delta x = 0.003(L=2 \text{ m}) = 0.006 \text{ m}$$

$$\varepsilon_y = \left| \frac{0.3(10)}{1000} \right| = 0.003 \Rightarrow \Delta y = 0.003(L=2 \text{ m}) = 0.006 \text{ m}$$

$$\varepsilon_z = \left| \frac{10}{1000} \right| = 0.001 \Rightarrow \Delta z = 0.001(L=2 \text{ m}) = 0.002 \text{ m}$$

According to the simple manual calculations for a single linear hexahedral element following Hooke's Law, the displacements were 0.006 m in both of the X and Y directions and 0.002 m in the Z direction. Comparing those with the values obtained using each of sim|FEM, ABAQUS and LISA, reduced integrated element results were adapted as they were closer to Hooke's Law results than the fully integrated ones.

5.1.2 Type I Models Using (STRHEX20Q) - Results

The (20-node) hexahedral model (STRHEX20Q) shown in Figure 5.6 was developed in sim|FEM, ABAQUS and LISA but, in LISA only the fully integrated scheme could be tested in the available version.

The results were summarized in three plots and as in the STRHEX08L model, the nodes' coordinates were used to indicate the nodes' locations according to coordinate system in which the Z axis is in the vertical direction, as shown in Figure 5.6. Following the same discussion for the displacement results at corner nodes in the STRHEX08L model, the displacement vectors magnitudes at only one corner node (0,0,2) were plotted, as shown in Figure 5.8. Node (0,0,2)'s location is shown in Figure 5.7.

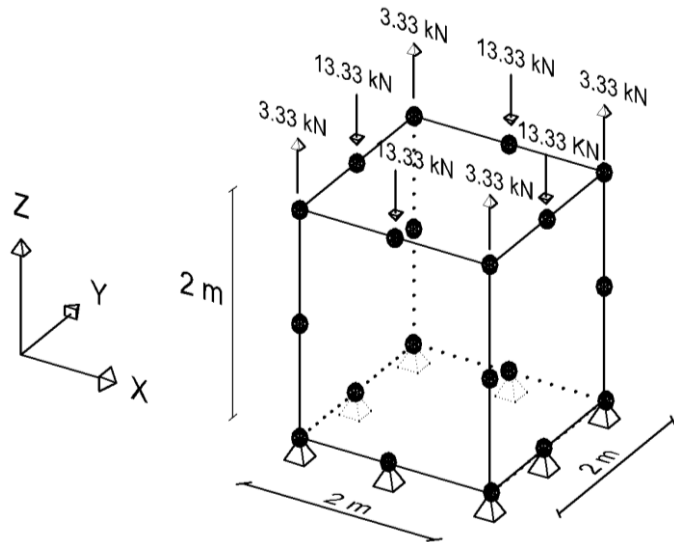


Figure 5.6 Type I Model - STRHEX20Q

The vector magnitudes at the mid-side nodes at the upper face were equal (refer to Appendix 1), so only one plot was necessary and the same applied for the mid-side nodes at the side faces, as shown in Figures 5.9 and 5.10. Mid-side nodes' locations are shown in Figure 5.9.

For more accurate comparisons, the percent difference was calculated in the X, Y and Z directions in respect to the values obtained in sim|FEM as shown in Tables 5.3, 5.4 and 5.5. The detailed results can be found in Appendix 1.

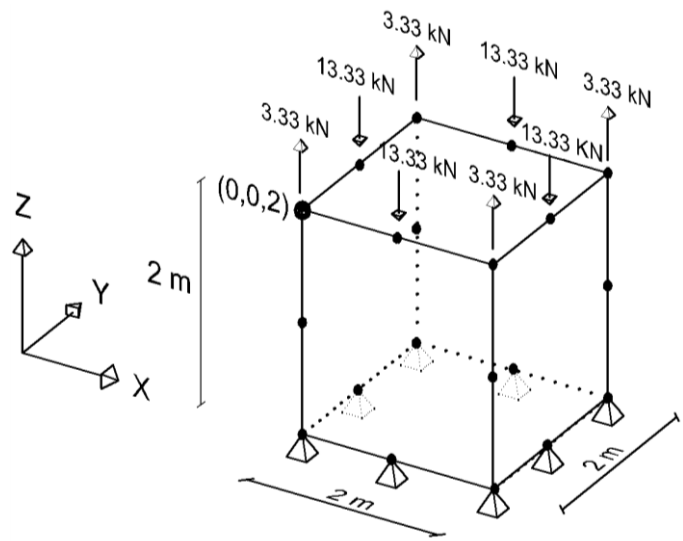


Figure 5.7 Illustration of Corner Node (0,0,2) location for the STRHEX20Q Model

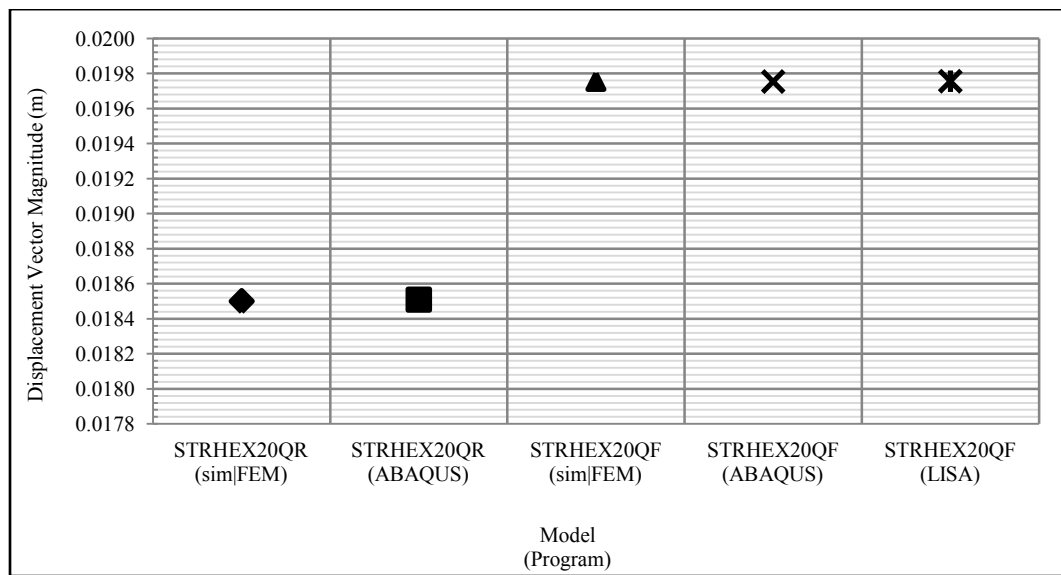


Figure 5.8 Displacement Vector Magnitude at the Corner Node (0,0,2) Model STRHEX20

Table 5.3 Displacement Percentage Difference at Corner Node (0,0,2) for STRHEX20Q Element

Displacement Difference @ Node (0,0,2) in %/ Model: STRHEX20QR			
Software	Ux (m)	Uy (m)	Uz (m)
ABAQUS	-2.0542500E-03	-1.2398700E-03	-1.8352900E-02
With Respect to			
sim FEM	-1.6470588E-03	-1.6470588E-03	-1.8352941E-02
	% Difference in Ux	% Difference in Uy	% Difference in Uz
ABAQUS vs. sim FEM	24.72232	24.72218	0.0002
Displacement Difference @ Node (0,0,2) in %/ Model: STRHEX20QF			
Software	Ux (m)	Uy (m)	Uz (m)
ABAQUS	-2.8239800E-03	-2.8239800E-03	-1.9346300E-02
LISA	-2.8242240E-03	-2.8242240E-03	-1.9347060E-02
With Respect to			
sim FEM	-2.8239842E-03	-2.8239842E-03	-1.9346317E-02
	% Difference in Ux	% Difference in Uy	% Difference in Uz
ABAQUS vs. sim FEM	0.00	0.00	0.00
LISA vs. sim FEM	0.01	0.01	0.00

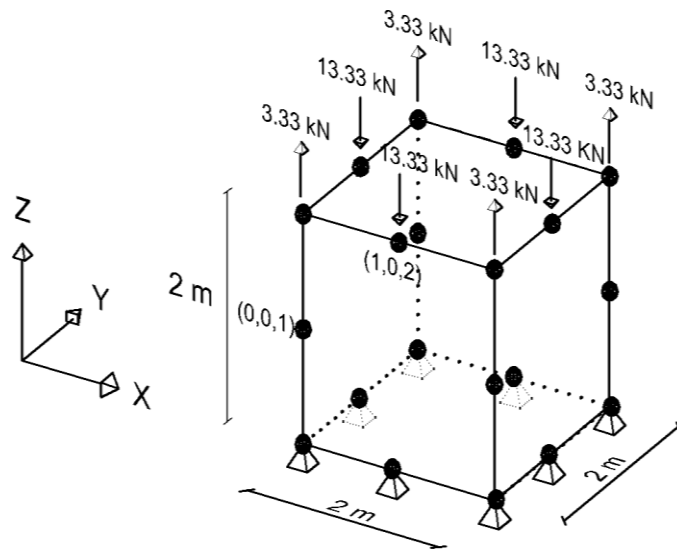


Figure 5.9 Illustration of Mid-Side Nodes (1,0,2) and (0,0,1) location for STRHEX20Q Model

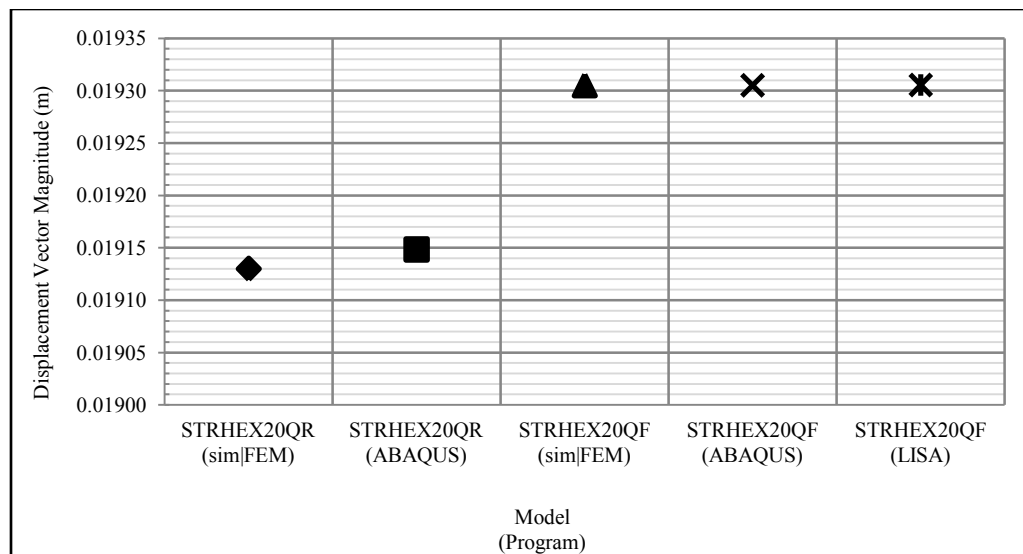


Figure 5.10 Displacement Vector Magnitude at the Mid-Side Node (1,0,2) Model STRHEX20Q

Table 5.4 Displacement Percentage Difference at Mid-Side Node (1,0,2) for the STRHEX20Q Element

Displacement Difference @ Node (1,0,2) in %/ Model: STRHEX20QR			
Software	Ux (m)	Uy (m)	Uz (m)
ABAQUS	0.0000000E+00	-1.8506500E-03	-1.9058800E-02
with Respect to			
sim FEM	0.0000000E+00	-1.6470588E-03	-1.9058824E-02
% Difference in			
	Ux	Uy	Uz
ABAQUS vs.	0.00	12.36	0.00
sim FEM			
Displacement Difference @ Node (1,0,2) in %/ Model: STRHEX20QF			
Software	Ux (m)	Uy (m)	Uz (m)
ABAQUS	0.0000000E+00	-2.8038700E-03	-1.9100500E-02
LISA	0.0000000E+00	-2.8040690E-03	-1.9100720E-02
with Respect to			
sim FEM	0.0000000E+00	-2.8038739E-03	-1.9100525E-02
% Difference in			
	Ux	Uy	Uz
ABAQUS vs.	0.00	0.00	0.00
sim FEM			
LISA vs. sim FEM	0.00	0.01	0.00

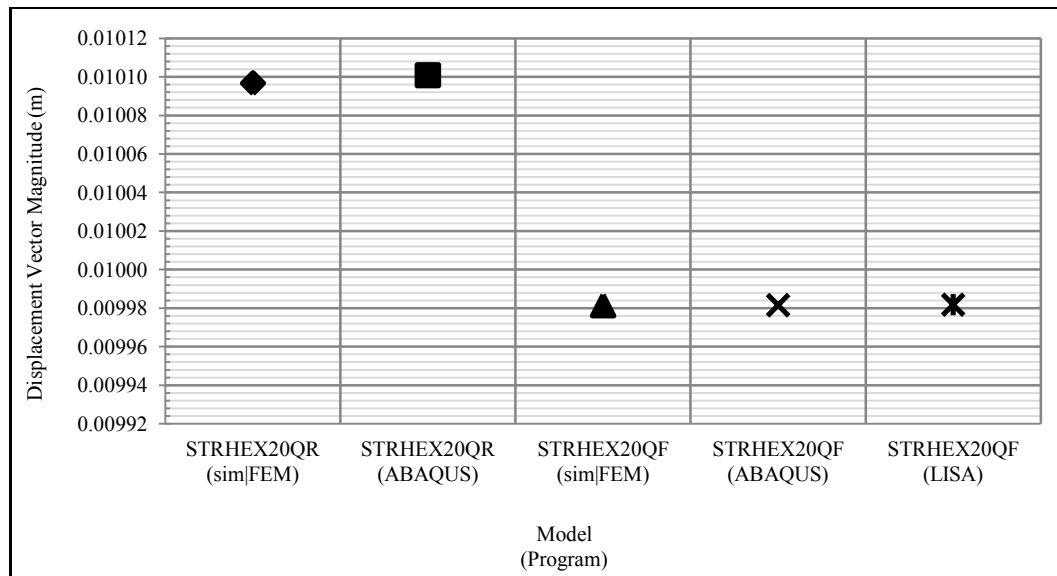


Figure 5.11 Displacement Vector Magnitude at the Mid-Side Node (0,0,1) Model STRHEX20Q

Table 5.5 Displacement Percentage Difference at the Mid-Side Node (0,0,1) for the STRHEX20Q Element

Displacement Difference @ Node (0,0,1) in %/ Model: STRHEX20QR			
Software	Ux (m)	Uy (m)	Uz (m)
ABAQUS	-3.6741800E-03	-3.2669900E-03	-8.8235300E-03
with Respect to			
sim FEM	-3.4705882E-03	-3.4705882E-03	-8.8235294E-03
	% Difference in Ux	% Difference in Uy	% Difference in Uz
ABAQUS vs. sim FEM	0.00	5.87	0.00
Displacement Difference @ Node (0,0,1) in %/ Model: STRHEX20QF			
Software	Ux (m)	Uy (m)	Uz (m)
ABAQUS	-2.9453300E-03	-2.9453300E-03	-9.0708900E-03
LISA	-2.9452980E-03	-2.9452980E-03	-9.0712170E-03
with Respect to			
sim FEM	-2.9453288E-03	-2.9453288E-03	-9.0708922E-03
	% Difference in Ux	% Difference in Uy	% Difference in Uz
ABAQUS vs. sim FEM	0.00	0.00	0.00
LISA vs. sim FEM	0.00	0.00	0.00

The reduced integrated element in ABAQUS resulted in a relatively considerable difference in both of the X and Y directions in respect to sim|FEM, as shown in Tables 5.3, 5.4 and 5.5. Yet, it should be noted that this difference was not clear in the figures, since the vector magnitude only was plotted. Almost identical values were obtained from sim|FEM, ABAQUS and LISA when the fully integrated element was used.

According to ABAQUS' documentations, reduced integrated elements are generally more accurate than the fully integrated ones. That might be true for a mesh of elements in certain conditions, but it doesn't seem to be the case for the element tested in this section. Also, as mentioned before, there is no indication about integration schemes accuracy in LISA's manual, so depending on the test results for STRHEX20Q model, fully integrated element results were adapted to be considered acceptable for the studied case.

5.1.3 Type I Models Using (STRHEX12T) and (STRHEX16T) – Results

In this section, two kinds of transitional elements were tested: (12-node) and (16-node) hexahedral elements, where transition elements are those that connect first order elements with second order ones. The models were tested in sim|FEM and illustrated in Figures 5.12 and 5.13.

The modified quadrature formula was used as explained earlier in this chapter. The same geometry and material properties assumed for STRHEX08L and STRHEX20Q models were used as well. The material properties were as shown in Table 5.1.

For the boundary conditions, the element base was constrained with pinned supports at the corner nodes in the STRHEX12T and STRHEX16T models, while the upper face in

each was loaded with a (10 kPa) uniformly distributed pressure that had to be transferred to the nodes, as illustrated earlier in Figure 5.2.

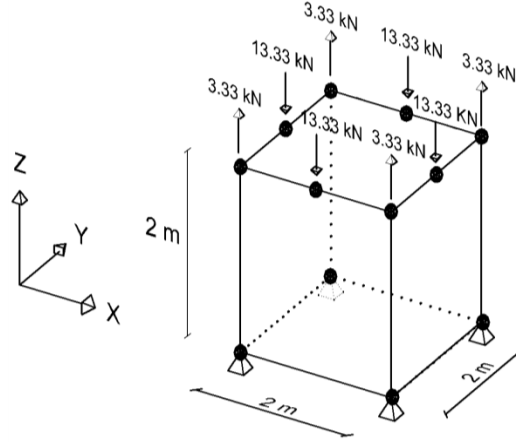


Figure 5.12 Type I Model - STRHEX12T

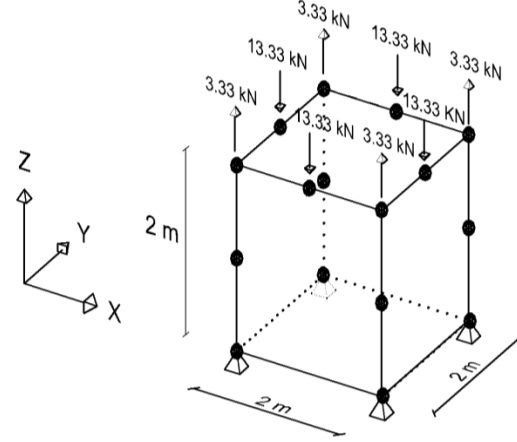


Figure 5.13 Type I Model - STRHEX16T

The results of both models were compared to STRHEX08LR and STRHEX20QF models' results that were tested in sim|FEM and presented in the previous two sections. The comparison was summarized in three plots, as illustrated in Figures 5.14, 5.15 and 5.16. One plot was for corner nodes, where the results of STRHEX08LR, STRHEX20QF, STRHEX12T and STRHEX16T were compared, as shown in Figure 5.14. The other two plots were for mid-side points at both the upper face and side faces. Based on the mid-side node location, Figure 5.15 compared the results of STRHEX20QF, STRHEX12T and STRHEX16T models, while Figure 5.16 compared only the results of STRHEX20QF and STRHEX16T models, since STRHEX12T does not have nodes at that location. It should be noted that the comparison was done at the nodes of the same locations chosen for previous models; STRHEX08L and STRHEX20Q where the location of these nodes is illustrated in Figures 5.4, 5.7 and 5.9.

The detailed results can be found in Appendix 1.

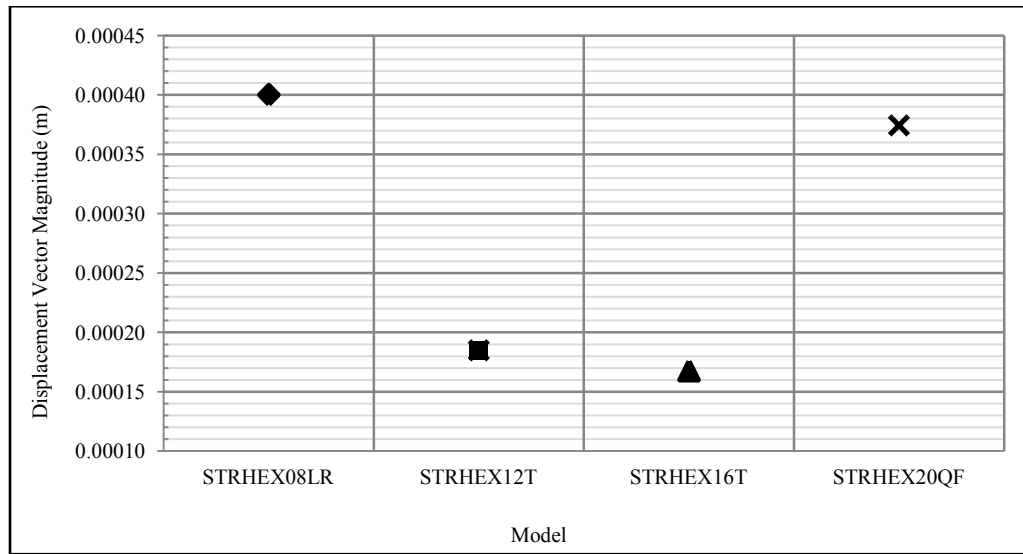


Figure 5.14 Displacement Vector Magnitude at the Corner Node (0,0,2) with respect to sim|FEM Models: STRHEX08LR, STRHEX12T, STRHEX16T, STRHEX20QF

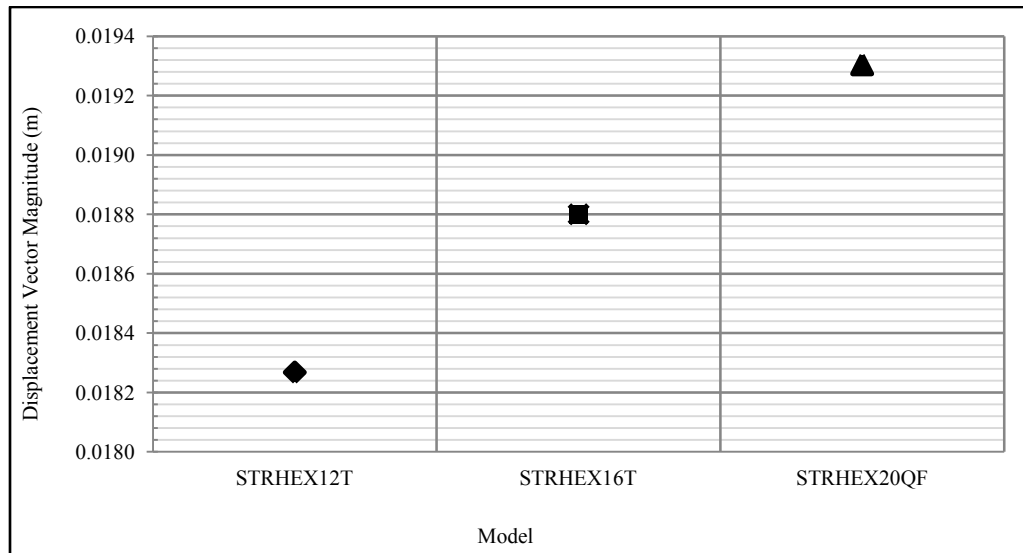


Figure 5.15 Displacement Vector Magnitude at the Mid-Side Node (1,0,2) with respect to sim|FEM Models: STRHEX12T, STRHEX16T, STRHEX20QF

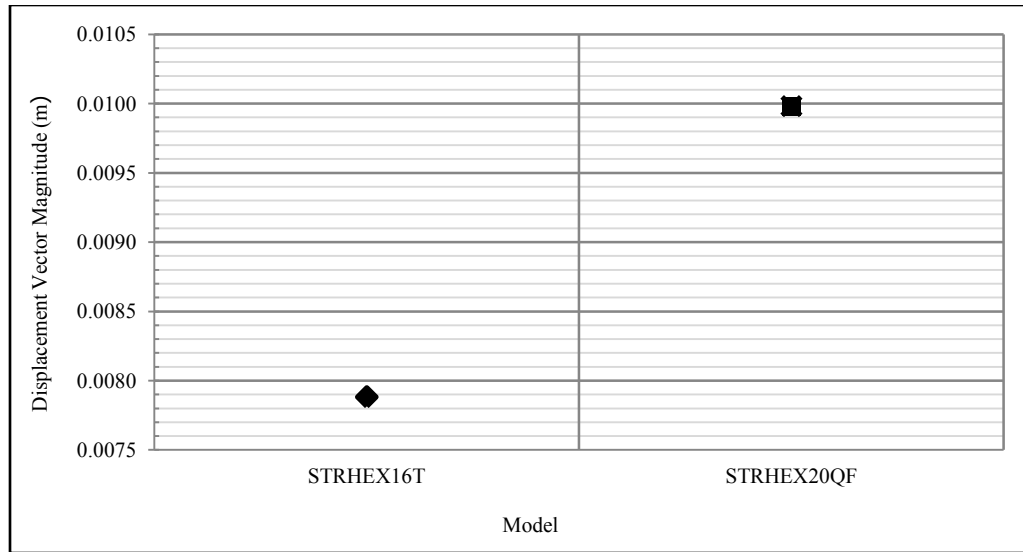


Figure 5.16 Displacement Vector Magnitude at Node (0,0,1) with respect to sim|FEM Models: STRHEX16T, STRHEX20QF

It should be noted that the displacement values in all directions at the corner node (0,0,2) obtained from the STRHEX12T, STRHEX16T and STRHEX20F models were greater than the ones obtained from the STRHEX08LR model. Also, the displacement values in all directions obtained from the STRHEX12T and STRHEX16T models were closer to the ones obtained from the STRHEX20F model.

The nodal displacements for STRHEX12T and STRHEX16T elements were ideally expected to fall in between the results of STRHEX08L and STRHEX20Q, but as can be observed from the figures above, that was not the case where a single hexahedral element was tested. That can be justified by the fact that in transition elements some edges are linear and the others are quadratic, and for a single element model the results might not have been approximated accurately enough. But, this approximation was expected to be noticeably reduced in case of a mesh of elements with the increasing of the number of both the nodes and the integration points, as the test of Type II Models indicated.

Analysing the results of all Type I models obtained in three different programs demonstrated an acceptable performance of these elements as implemented in the sim|FEM code. To further ensure the performance of the transitional hexahedral elements, new tests of larger models were carried out.

5.2 Type II Models

The previous test was done for Type I models that consisted of only a single element. To ensure the performance of transition elements, tests of a mesh of only linear elements, a mesh of only quadratic elements and a mesh with transition elements were performed. Each of these models consisted of 27 elements (3 elements in each direction of volume of 1 m^3 ($1\text{m} \times 1\text{m} \times 1\text{m}$)). The models had the same material properties used for Type I models, as listed in Table 5.1. Regarding the boundary conditions, the nodes at the base were constrained in all directions and a load of 10 kN/m^2 was applied at the top face of the model. Figures 5.17, 5.18, 5.20 and 5.21 show a summary of the loading scheme, geometry and boundary conditions of the models.

The models' and elements' naming convention was chosen to be as follows: M refers to mesh, HEX refers to the element used that is hexahedral element, (08, 20, 12, 16) refer to the number of nodes, (L, Q or T) refer to what kind of element was tested; Linear, quadratic or transitional, respectively, and finally the name of the program used to carry out the test.

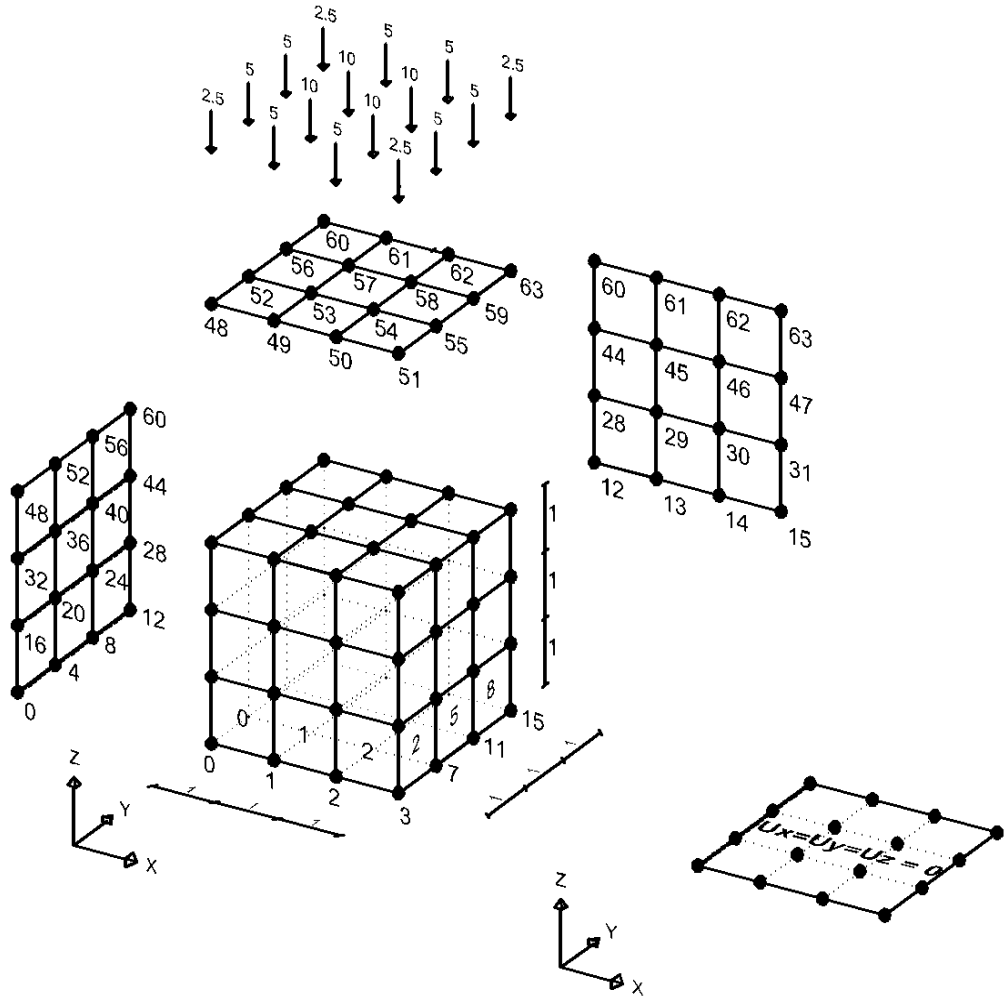
A total of six models were developed. Two of them were tested in ABAQUS and the remaining four were tested in sim|FEM:

- MHex08L_sim|FEM: a mesh composed of only linear hexahedral elements tested in sim|FEM.
- MHex08L_ABAQUS: a mesh composed of only linear hexahedral elements tested in ABAQUS.
- MHex20Q_sim|FEM: a mesh composed of only quadratic elements tested in sim|FEM.
- MHex20Q_ABAQUS: a mesh composed of only quadratic elements tested in ABAQUS.
- MHex12T_sim|FEM: a mesh of linear, 12-node transition hexahedral, quadratic elements tested in sim|FEM.
- MHex16T_sim|FEM: a mesh of linear, 16-node transition hexahedral, quadratic elements tested in sim|FEM.

5.2.1 Type II Models Using (MHex08L) and (MHex20Q) - Results

Both integration schemes (reduced and full) were checked for MHex08L_sim|FEM, MHex08L_ABAQUS, MHex20Q_sim|FEM and MHex20Q_ABAQUS models that are shown in Figures 5.17 and 5.18. To determine which integration scheme's results were more accurate for the studied cases, the displacements' values of each scheme in sim|FEM and ABAQUS were compared.

Due to the large number of results to be plotted, the comparison was done at only some of the corner nodes with the following coordinates: (0,0,3), (3,0,3), (3,3,3), (0,3,3), (2,0,3), (2,3,3), (0,1,3) and (3,1,3). The locations of these nodes are illustrated in Figure 5.19 and the detailed displacement values at these nodes can be found in Appendix 2.



Loads (kN)

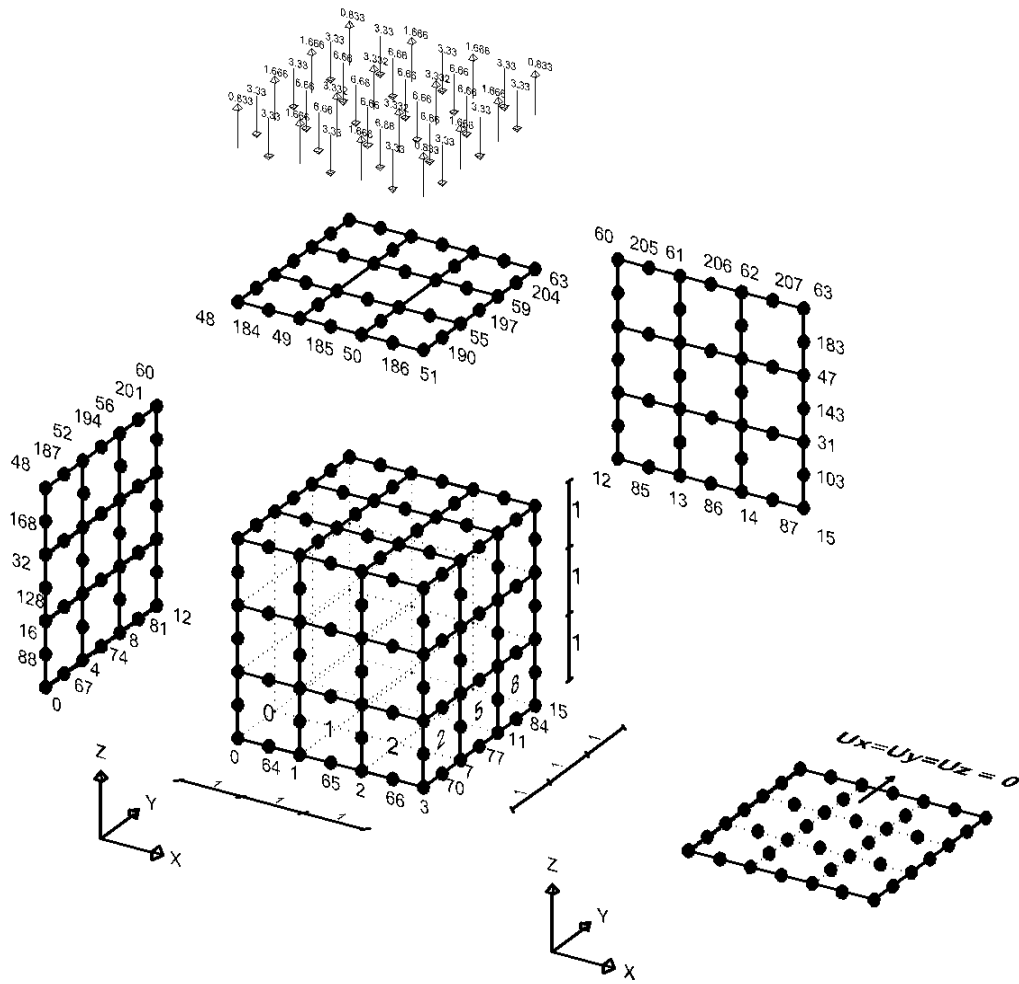
$F_{48} = F_{51} = F_{60} = F_{63} = -2.5$

$F_{49} = F_{50} = F_{52} = F_{55} = F_{56} = F_{59} = F_{61} = F_{62} = -5$

$F_{53} = F_{54} = F_{58} = F_{57} = -10$

All dimensions are in units of meters

Figure 5.17 Mesh With Only Linear Hexahedral Elements - MHex08L



Loads (kN)

$F_{168} = F_{174} = F_{201} = F_{207} = 0.833$

$F_{169} = F_{171} = F_{173} = F_{175} = F_{178} = F_{186} = F_{189} = F_{197} = F_{200} = F_{202} = F_{204} = F_{206} = -3.33$

$F_{170} = F_{172} = F_{179} = F_{185} = F_{190} = F_{196} = F_{203} = F_{205} = 1.666$

$F_{176} = F_{177} = F_{180} = F_{182} = F_{184} = F_{187} = F_{188} = F_{191} = F_{193} = F_{195} = F_{198} = F_{199} = -6.66$

$F_{181} = F_{183} = F_{192} = F_{194} = 3.332$

All dimensions are in units of meters

Figure 5.18 Mesh With Only Quadratic Hexahedral Elements - MHex20

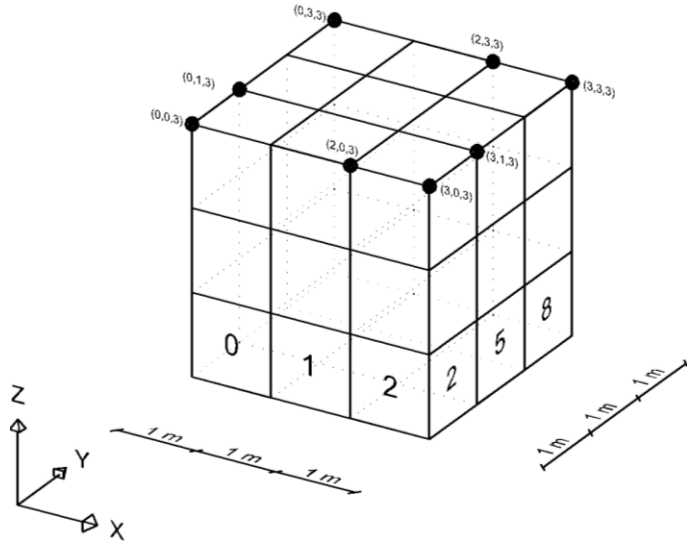


Figure 5.19 Illustration of Nodes (0,0,3), (3,0,3), (3,3,3), (0,3,3), (2,0,3), (2,3,3), (0,1,3) and (3,1,3) location

Table 5.6 Percentage Difference of Reduced Integrated Models in Respect to Fully Integrated Models

**Percent Difference of Reduced Integrated Model in Respect to Fully Integrated Model in %
Mesh of (3x3x3) Elements**

MHex08L_sim|FEM

Nodes	% Difference in Ux	% Difference in Uy	% Difference in Uz
(0,0,3)	11.18	11.18	1.44
(2,0,3)	69.78	9.68	0.88
(0,1,3)	9.68	69.78	0.88

MHex08L_ABAQUS

Nodes	% Difference in Ux	% Difference in Uy	% Difference in Uz
(0,0,3)	8.83%	8.83%	1.52%
(2,0,3)	64.17	9.84	0.2
(0,1,3)	9.84	64.17	0.2

Table 5.6 (Continuing) Percentage Difference of Reduced Integrated Models in Respect to Fully Integrated Models

MHex20Q_sim FEM			
Nodes	% Difference in Ux	% Difference in Uy	% Difference in Uz
(0,0,3)	0.3	0.3	0.19
(2,0,3)	0.31	0.09	0.23
(0,1,3)	0.09	0.31	0.23

MHex20Q_ABAQUS			
Nodes	% Difference in Ux	% Difference in Uy	% Difference in Uz
(0,0,3)	0.29	0.29	0.19
(2,0,3)	0.30	0.10	0.23
(0,1,3)	0.10	0.30	0.23

As the tests' results showed and as the nodes at the base of these models are constrained in all directions, the displacements at them are zero by definition. It can also be noted that the displacements vector magnitudes at the nodes (0,0,3), (3,0,3), (3,3,3) and (0,3,3) are the same due to the symmetry of the boundary conditions applied to the models. The same applies for nodes (2,0,3) and (2,3,3) and nodes (0,1,3) and (3,1,3). Therefore, for simplifying, the percentage difference of the reduced integrated models in respect to the fully integrated ones within each program were calculated at the nodes with the following coordinates (0,0,3), (2,0,3) and (0,1,3).

It can be noticed from Table 5.6 that there were considerable percentage differences between the reduced integrated models with only linear hexahedral elements in comparison to the fully integrated ones (69.78% in sim|FEM and 64.17% in ABAQUS). While, the reduced integrated models with only quadratic hexahedral elements yielded very close results to the fully integrated ones with small percentage differences in both sim|FEM and ABAQUS (maximum of 0.31%).

The considerable percentage differences were expected in the studied mesh of linear elements with reduced integration scheme, because in this case the results were approximated at only one integration point for each linear element in the linear mesh. For the studied meshes, that was not sufficient to reach accurate results. But, in a fully integrated mesh of only linear elements, the results were approximated at eight integration points for each linear element.

On the other hand, using quadratic elements did not yield such large differences because of many facts, such as, the increase of number of the nodes and that the results were approximated at eight integration points in the reduced integrated models and at twenty seven integration points in the fully integrated models which seemed to be sufficient to reach acceptable solution accuracy, beside the fact that the second-degree edge is more flexible (since it can assume the shape of a quadratic function over the three nodes) than a first degree edge.

According to the tests' results, the full integration scheme of both linear and quadratic models was adapted to be used for the models tested in the next sections and chapters.

5.2.2 Type II Models Using (MHex12T) and (MHex16T) - Results

After choosing the integration scheme to be used, a comparison between the results of MHex08L_sim|FEM and MHex20Q_sim|FEM models and the results obtained from the two meshes with transition elements; MHex12T_sim|FEM and MHex16T_sim|FEM was performed in order to evaluate the transition element performance. The transition elements were placed at the middle layer in Z direction in between a bottom layer of

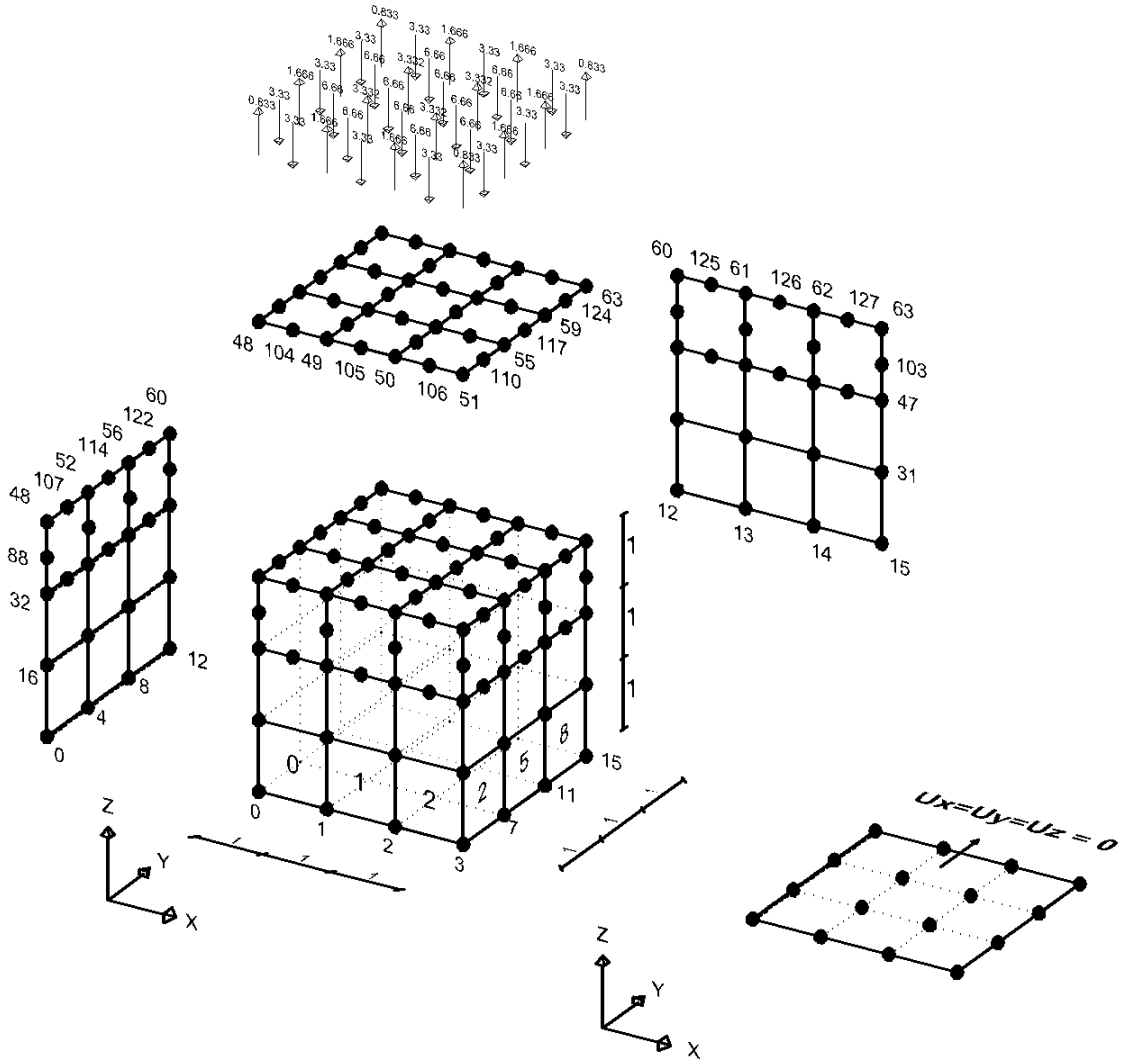
linear elements and a top layer of quadratic elements. MHex12T_sim|FEM and MHex16T_sim|FEM models are illustrated in Figures 5.20 and 5.21.

Due to the large number of results to be plotted, the comparison was done at only some of the corner nodes with the following coordinates: (0,0,3), (3,0,3), (3,3,3), (0,3,3), (2,0,3), (2,3,3), (0,1,3) and (3,1,3). The locations of these nodes are illustrated in Figure 5.19 and the detailed displacement values at these nodes can be found in Appendix 2.

As the tests' results indicated and as the nodes at the base of these models are constrained in all directions, the displacements at them are zero by definition. On the other hand, the displacements vector magnitudes at the nodes (0,0,3), (3,0,3), (3,3,3) and (0,3,3) were the same due to the symmetry of the boundary conditions applied to the models. The same applies for nodes (2,0,3) and (2,3,3) and nodes (0,1,3) and (3,1,3). Therefore, for simplifying, the percentage difference of both meshes with 12-node and 16-node transition elements in respect to quadratic and linear meshes analysed in sim|FEM were calculated at the nodes with the following coordinates (0,0,3), (2,0,3) and (0,1,3).

Finally, the results of sim|FEM are summarized in three plots; one for each corner nodes as shown in Figures 5.22, 5.23 and 5.24. The detailed results are shown in Appendix 2.

As can be noticed from Table 5.7 and Figures 5.22, 5.23 and 5.24, the differences between the results from meshes with transitional elements in comparison to meshes with quadratic elements decreased from what they were in Type I models.



Loads (kN)

$$F_{48} = F_{51} = F_{60} = F_{63} = 0.833$$

$$F_{104} = F_{105} = F_{106} = F_{110} = F_{114} = F_{117} = F_{121} = F_{124} = F_{125} = F_{126} = F_{127} = -3.33$$

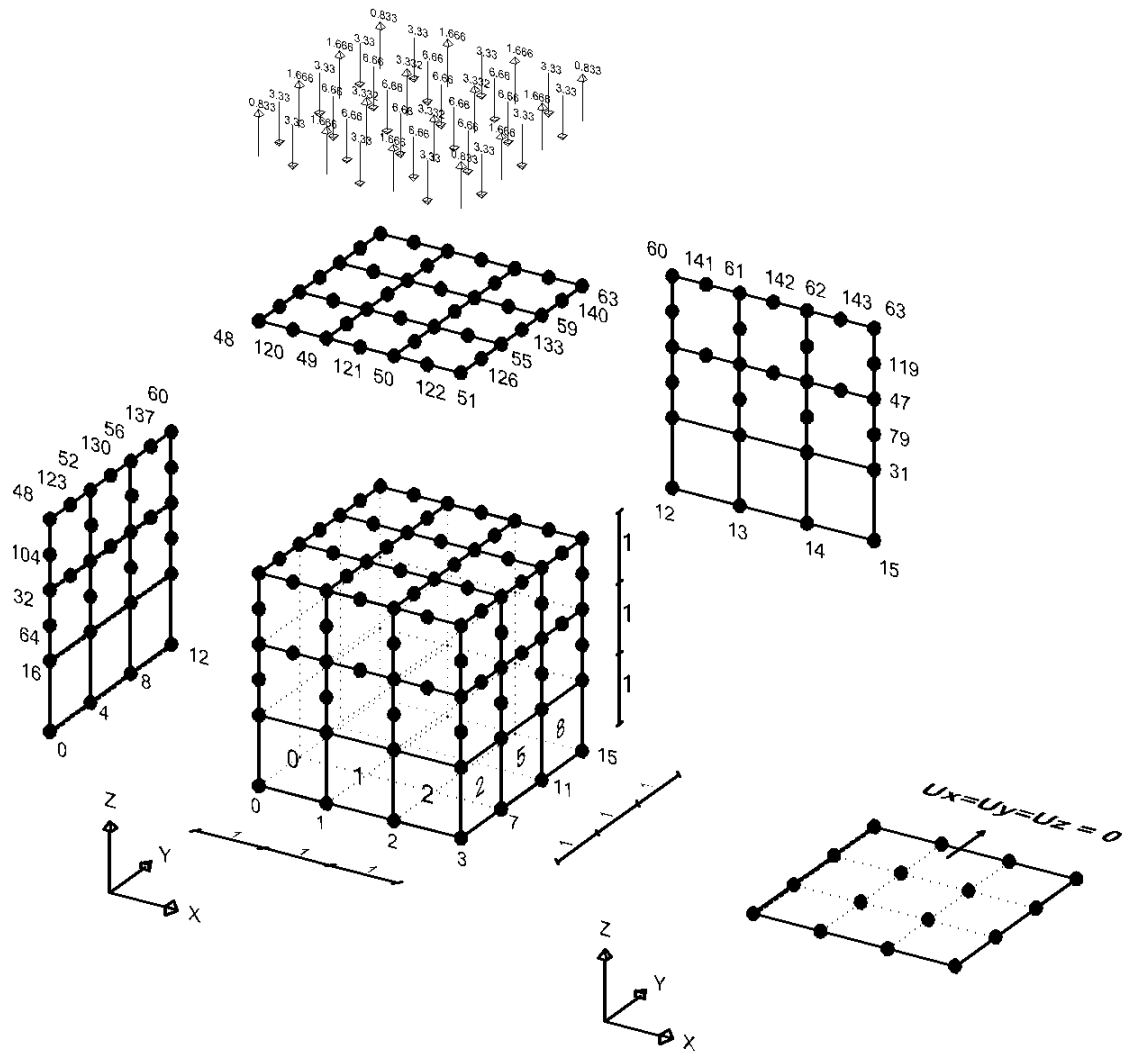
$$F_{49} = F_{50} = F_{52} = F_{55} = F_{56} = F_{59} = F_{61} = F_{62} = 1.666$$

$$F_{108} = F_{109} = F_{111} = F_{112} = F_{113} = F_{115} = F_{116} = F_{118} = F_{119} = F_{120} = F_{122} = F_{123} = -6.66$$

$$F_{53} = F_{54} = F_{57} = F_{58} = 3.332$$

All dimensions are in units of meters

Figure 5.20 Mesh With (12) Transition Hexahedral Elements - MHex12T



Loads (kN)
$F_{104} = F_{110} = F_{137} = F_{143} = 0.833$
$F_{105} = F_{107} = F_{109} = F_{111} = F_{114} = F_{122} = F_{125} = F_{133} = F_{136} = F_{138} = F_{140} = F_{142} = -3.33$
$F_{106} = F_{108} = F_{115} = F_{121} = F_{126} = F_{132} = F_{139} = F_{141} = 1.666$
$F_{112} = F_{113} = F_{116} = F_{118} = F_{120} = F_{123} = F_{124} = F_{127} = F_{129} = F_{131} = F_{134} = F_{135} = -6.66$
$F_{117} = F_{119} = F_{128} = F_{130} = 3.332$
All dimensions are in units of meters

Figure 5.21 Mesh With (16) Transition Hexahedral Elements - MHex16

Table 5.7 Percentage Differences of Models with Transition Elements in Respect to Linear and Quadratic Models

Percent Differences of MHex12T_sim FEM Model in Respect to MHex08L_sim FEM Model in %			
Nodes	% Difference in Ux	% Difference in Uy	% Difference in Uz
(0,0,3)	0.08	0.08	3.18
(2,0,3)	5.54	0.16	3.06
(0,1,3)	0.16	5.54	3.06
Percent Differences of MHex12T_sim FEM Model in Respect to MHex20Q_sim FEM Model in %			
Nodes	% Difference in Ux	% Difference in Uy	% Difference in Uz
(0,0,3)	0.32	0.32	2.19
(2,0,3)	6.14	0.77	2.04
(0,1,3)	0.77	6.14	2.04
Percent Differences of MHex16T_sim FEM Model in Respect to MHex08L_sim FEM Model in %			
Nodes	% Difference in Ux	% Difference in Uy	% Difference in Uz
(0,0,3)	0.49	0.49	3.15
(2,0,3)	6.39	0.41	3.11
(0,1,3)	0.41	6.39	3.11
Percent Differences of MHex16T_sim FEM Model in Respect to MHex20Q_sim FEM Model in %			
Nodes	% Difference in Ux	% Difference in Uy	% Difference in Uz
(0,0,3)	0.09	0.09	2.16
(2,0,3)	6.99	0.52	2.09
(0,1,3)	0.52	6.99	2.09

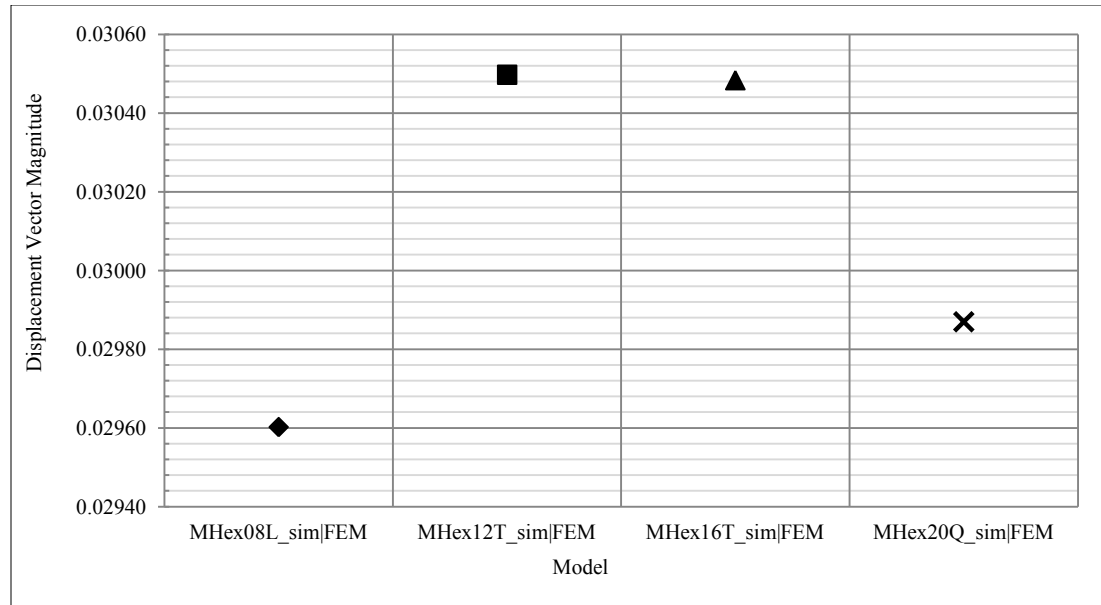


Figure 5.22 Displacement Vector Magnitude at Node (0, 0,3)

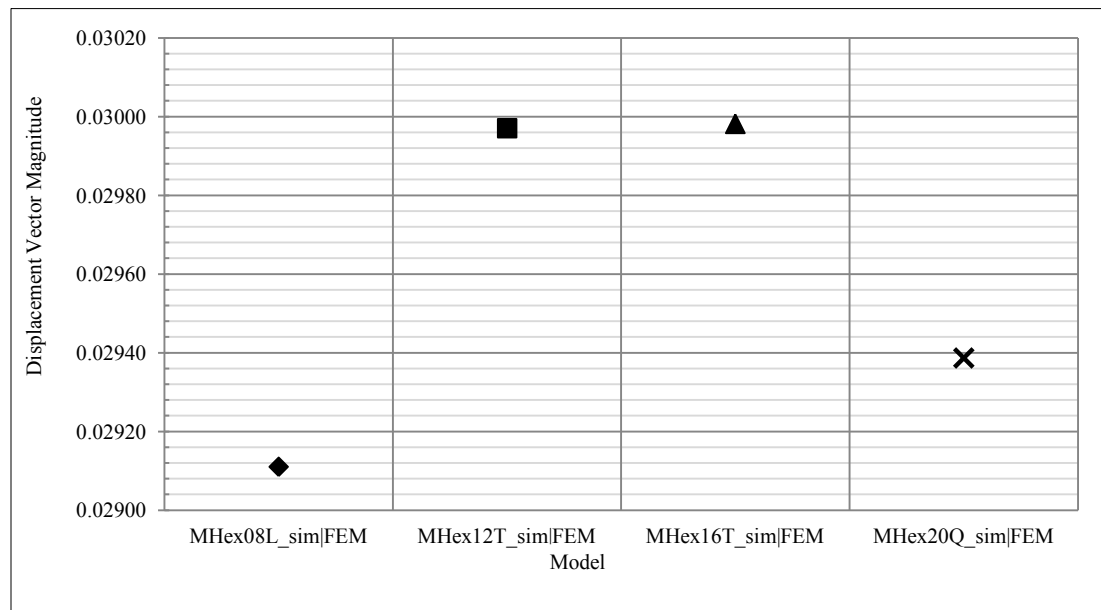


Figure 5.23 Displacement Vector Magnitude at Node (2, 0, 3)

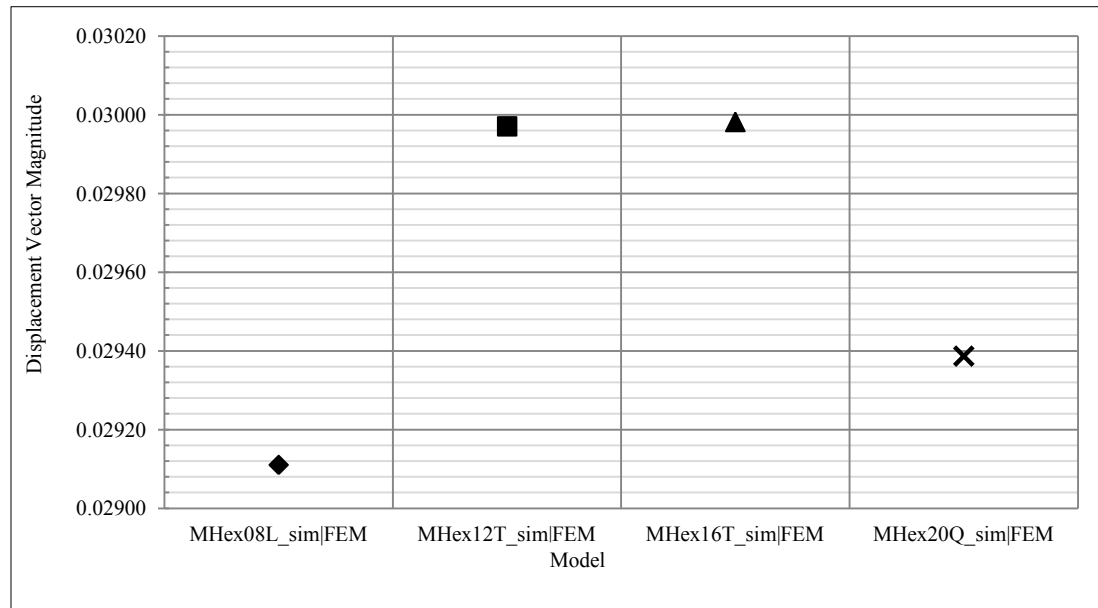


Figure 5.24 Displacement Vector Magnitude at Node (0, 1, 3)

6 Verification of Practical Performance of Transitional Elements – Pressurized Cavity Problem

Models in the previous chapter have verified the accuracy and performance of transitional elements both as single elements and as part of a simple assemblage of 3-dimensional elements. Although the transitional elements performed well, their intended application is to serve as connections between the first order and second order hexahedral elements in analyzing large and complex problems in dimensions.

As a relatively simple, yet practical problem, a pressurized circular tunnel in an elastic isotropic medium was selected as the next model in the real-world application of p-type mesh optimization using transitional elements. The model represents a typical scenario of an underground water conveyance tunnel under pressure, often found in hydro-electric or pumped storage facilities as tailrace tunnels or tunnels feeding the turbines (Hoek 2007). The stability of these tunnels is often governed by the adequacy of the in situ confining rock pressure to balance the internal pressure of water running through a tunnel. If the internal pressure exceeds the confining pressure, a blowout can occur, leading to the failure of a tunnel, jeopardizing the operation of a facility (Hoek 2007). Due to the symmetry in both loading conditions and geometry of the problem, only one quarter of the tunnel needs to be modeled using appropriate boundary conditions, as subsequently discussed. The physical domain representing the problem was modeled using a rock mass of 20 m by 20 m perpendicular to the 10 m diameter tunnel as seen in Figure 6.1. These dimensions were selected to provide enough rock mass around a tunnel to avoid the boundaries affecting the solution via stress reflection if they were placed too close to the tunnel. The thickness (Z dimension) of the rock mass along the

axis of the tunnel was selected to be 26.32 m. This number was arrived at by finding the average finite element edge length of quadrilaterals in the XY plane and using it to generate an even number of elements in the Z direction. For this problem 12 layers of elements were used, resulting in the depth of 26.32m. The choice of 12 layers can be justified because it results in a more-or-less cubic volume of rock to be analyzed, as shown in Figure 6.2. To assess the performance of transitional elements, three different bands of transitional zones were considered yielding three separate problems. The transition bands were selected to be located at distances of 7.5 m, 10 m and 12.5 m from the tunnel center as shown in Figure 5.1. These distances could represent possible zones of yielding and failure of the rock mass around the tunnel if plastic analysis was to be performed. Elements within the transition zones were kept at the second-order (quadratic) while elements beyond the transition zone were modeled using first-order (linear) hexahedral elements. The transition band was discretized using either 12 or 16-noded transitional hexahedral elements. The rock mass properties are summarized in Table 6.1. Note that the unit weight of the rock was not considered, effectively set to zero, since the internal pressure supplied by the water can easily exceed the pressure from the weight of the rock at close to ground surface problems. This decision does not affect the validity of the model to represent the tunnels. Other rock mass properties such as E and Poisson's ratio were selected to represent a typical intact rock. The water pressure was applied to the tunnel boundary as a distributed load of 1.2785 kN/m per meter thickness of tunnel. This value represents a relatively low value of pressure, however, since the rock mass was considered weightless, nevertheless it exerts pressure and causes deformation within the rock mass. The distributed load was transformed into nodal loads and applied to the

element nodes comprising the tunnel boundary. The boundary conditions of the model were such that movement of rock, due to the pressurized tunnel, was allowed, as seen in Figure 6.1 for the simple 2D case of showing only the front face of the model. By setting the upper and right boundaries fixed and having the left and bottom boundaries on rollers, the initial simplifying assumption of using one quarter of a problem was maintained. It is expected that displacements along the bottom and left side of the model will be equal to each other due to the symmetry in both loading and geometry of the problem. The complete set of boundary conditions in 3D are summarized in Figure 6.2, noting that displacements along the Z direction were restrained for the front and back faces, in essence creating a model that will not deform in that direction at all and imitate a plane strain case in 3D.

Table 6.1 Material Properties

Property	Units	Value
γ	kN/m ³	0
E	kPa	10^6
v	-	0.3

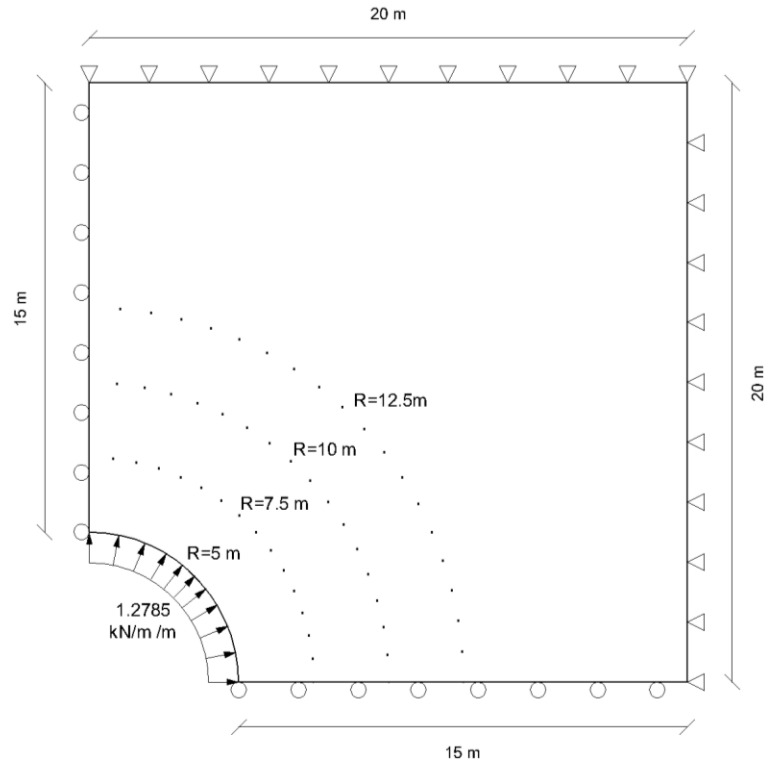


Figure 6.1 Frontal View of Boundary Conditions and Transition Bands Used in the Pressurized Cavity Problem

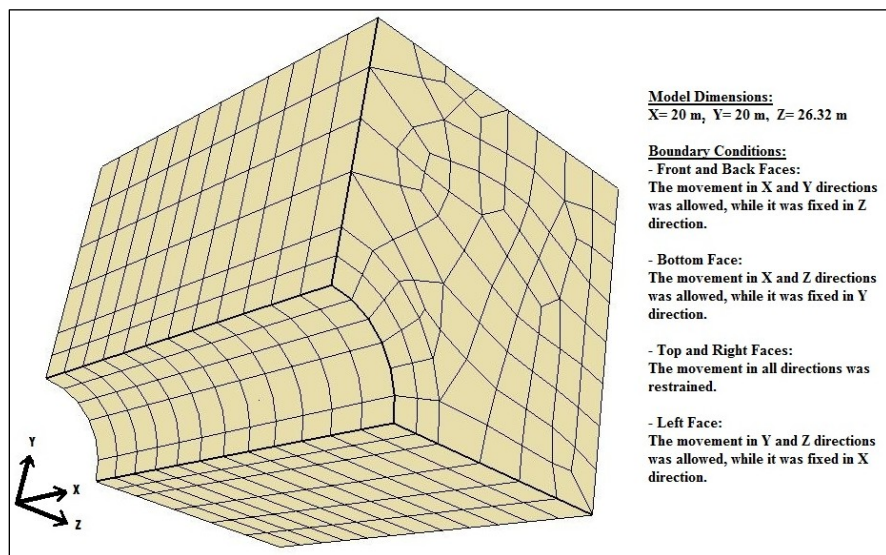


Figure 6.2 3D View of the Pressurized Cavity Problem Summarizing the Boundary Conditions

The pressurized cavity problem was modeled using both ABAQUS and sim|FEM. The models used in ABAQUS served as benchmark problems for the cases with either all first-order or all second-order elements. No models with transitional elements were done in ABAQUS since it does not include that type of element, while all models were analyzed using sim|FEM. In total ten models were analyzed, as summarized in the matrix below.

Table 6.2 Summary of Models for Pressurized Cavity Analysis

Case	Model – element type	Analysis tool
1	HEX8L	sim FEM
2	HEX8L	ABAQUS
3	HEX20Q	sim FEM
4	HEX20Q	ABAQUS
5	HEX_TRANS1 (12T)	sim FEM
6	HEX_TRANS1 (16T)	sim FEM
7	HEX_TRANS2 (12T)	sim FEM
8	HEX_TRANS2 (16T)	sim FEM
9	HEX_TRANS3 (12T)	sim FEM
10	HEX_TRANS3 (16T)	sim FEM

Where:

- HEX8L is a mesh of first-order, linear 8-noded hexahedral elements.
- HEX20Q is a mesh of second-order, quadratic 20-noded hexahedral elements.
- HEX_TRANS1 is a mesh with a band of transitional hexahedral elements (12-noded and 16-noded) located at a radius of 7.5 m.
- HEX_TRANS2 is a mesh with a band of transitional hexahedral elements (12-noded and 16-noded) located at a radius of 10 m.
- HEX_TRANS3 is a mesh with a band of transitional hexahedral elements (12-noded and 16-noded) located at a radius of 12.5 m.

The ABAQUS models (cases 2 and 4) were modeled using C3D8 (linear hexahedral) and C3D20 (quadratic hexahedral) elements. The location of nodes, elements, loadings, boundary conditions and material properties correspond to the models done in sim|FEM to serve as a basis of comparison. The purpose of this testing regime was to assess the performance of the transition elements in sim|FEM and not to validate either ABAQUS or sim|FEM against analytical solutions since both ABAQUS and sim|FEM are thoroughly tested and verified finite element codes.

The evaluation of the results was done by comparing the stress and displacement contours of all models for a visual check and the displacement values along both the lower boundary and the left boundary at the middle cross section (half-way through the Z thickness) of the model. For the purpose of visualizing results generated with sim|FEM, a set of TCL scripts were written to use the Visualization Toolkit (VTK) (Kitware Inc. 2010) to render the results in 3D. The following sub-sections assess the results obtained from models for each case.

6.2 Cases 1 through 4 – Baseline cases

The models comprised purely of 8-noded and 20-noded hexahedral elements (HEX8L and HEX20Q) were developed and tested in both sim|FEM and ABAQUS. The meshes used in the models are shown in Figures 6.3 and 6.4 for 8-noded and 20-noded elements, respectively. These four cases show the extremes of what a typical analysis would entail; discretizing the problem geometry by either all 8-noded first-order elements and saving on computation time while perhaps sacrificing solution quality or going for 20-noded

second-order elements and bearing the cost of increased time to solution and computer hardware requirements.

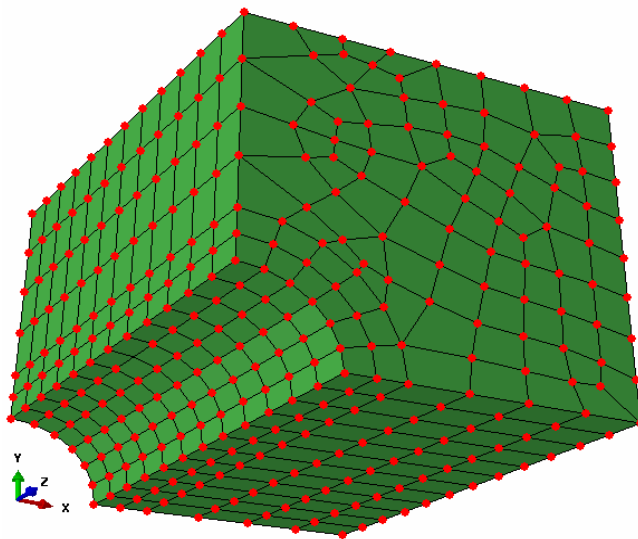


Figure 6.3 Model with HEX08L Elements - Undeformed Mesh

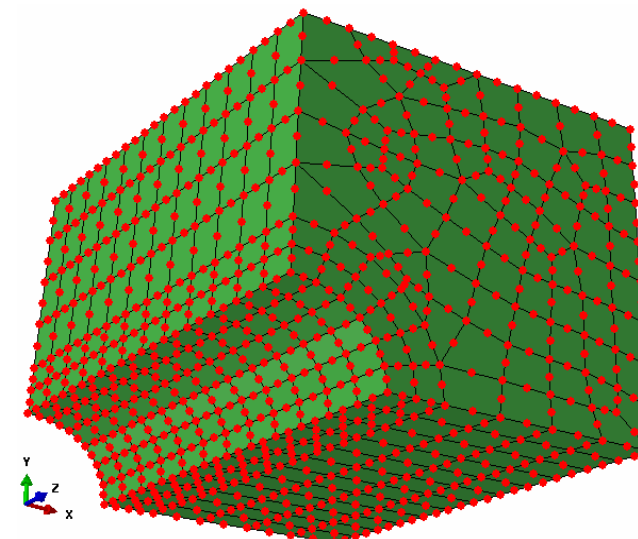


Figure 6.4 Model with HEX20Q Elements - Undeformed Mesh

As previously discussed, the comparison between Cases 1 and 2 and 3 and 4 was performed only at the lower and left boundaries of the problem due to symmetry in both loading and boundary conditions. Even for these cases the solution was expected to be the same due to symmetry. The following comparison of results, summarised in Table 6.3 and 6.4 was based on a percentage difference computed for all displacement directions (X, Y and Z) based on the sim|FEM results.

As is evident from Table 6.3, the results for Cases 1 and 2 between ABAQUS and sim|FEM yielded a maximum difference of 0.81% at the lower boundary. Since the documentation of ABAQUS does not reason how the results were computed with respect to the number of Gauss points or the interpolation from the Gauss points to the nodes, it was assumed that the discrepancy was attributable to implementation differences given such a low number for maximum difference. Using similar reasoning, the maximum difference in the solution at the left boundary was 1.84%, still very reasonable. The summary for all of the nodes is given in Table 6.4. As a quick visual comparison, the magnitude of computed displacements for both Cases 1 and 2 was plotted as shown in Figures 6.5 and 6.6 for sim|FEM and ABAQUS, respectively. While the normal stresses in the X direction (σ_{xx}) are shown for both models in Figures 6.7 and 6.8. The pattern of displacements and stresses appears to be uniform around the circular excavation in both models, further confirming the validity of the solution.

For Cases 3 and 4, modeled with second-order hexahedral elements, the assessment of the solution accuracy was summarized in Tables 6.5 and 6.6 for lower and left boundaries, respectively. Table 6.5 reveals a maximum difference in solution of 10% at the lower boundary and 4.48% on the left boundary. Again, most likely due to the

uncertainty in solution schemes in ABAQUS the two solutions differ, yet not in a significant way. Plots of displacements for the two cases, similar to Case 1 and 2, were plotted using the VTK scripts. Figures 6.9 and 6.10 show the plots of displacement magnitudes for both the sim|FEM and ABAQUS models. The plots reveal the rings of equal displacement around the periphery of the circular tunnel. Both models have captured the correct physical behaviour. Stress contours for the normal stresses in the Y direction (σ_{yy}) were plotted for Case 3 and 4 as shown in Figure 6.11 and 6.12, respectively. The uniformity of stresses correlates well between the two cases.

Table 6.3 Comparison of Displacement Results for Cases 1 and 2 – Lower Boundary

Node Coordinates (m)			Software	Displacements (m)			Difference (%)		
x	y	z		Ux	Uy	Uz	Ux	Uy	Uz
5	0	13.16	sim FEM	6.86E-06	0.0	0.0	0.81	0.00	0.00
			ABAQUS	6.91E-06	0.0	0.0			
6.5	0	13.16	sim FEM	5.07E-06	0.0	0.0	0.57	0.00	0.00
			ABAQUS	5.10E-06	0.0	0.0			
8	0	13.16	sim FEM	3.92E-06	0.0	0.0	0.55	0.00	0.00
			ABAQUS	3.94E-06	0.0	0.0			
11	0	13.16	sim FEM	2.36E-06	0.0	0.0	0.38	0.00	0.00
			ABAQUS	2.35E-06	0.0	0.0			
14	0	13.16	sim FEM	1.37E-06	0.0	0.0	0.13	0.00	0.00
			ABAQUS	1.37E-06	0.0	0.0			
17	0	13.16	sim FEM	6.10E-07	0.0	0.0	0.37	0.00	0.00
			ABAQUS	6.08E-07	0.0	0.0			
20	0	13.16	sim FEM	0.00E+00	0.0	0.0	0.00	0.00	0.00
			ABAQUS	0.00E+00	0.0	0.0			

Table 6.4 Comparison of Displacement Results for Cases 1 and 2 – Left Boundary

Node Coordinates (m)			Software	Displacements (m)			Difference (%)		
x	y	z		Ux	Uy	Uz	Ux	Uy	Uz
0	5	13.16	sim FEM	0.0	6.87E-06	0.0	0.00	0.43	0.00
			ABAQUS	0.0	6.901E-06	0.0			
0	6.5	13.16	sim FEM	0.0	5.07E-06	0.0	0.00	0.06	0.00
			ABAQUS	0.0	5.07E-06	0.0			
0	8	13.16	sim FEM	0.0	3.90E-06	0.0	0.00	0.96	0.00
			ABAQUS	0.0	3.86E-06	0.0			
0	11	13.16	sim FEM	0.0	2.42E-06	0.0	0.00	0.35	0.00
			ABAQUS	0.0	2.41E-06	0.0			
0	14	13.16	sim FEM	0.0	1.39E-06	0.0	0.00	1.84	0.00
			ABAQUS	0.0	1.36E-06	0.0			
0	17	13.16	sim FEM	0.0	6.11E-07	0.0	0.00	0.14	0.00
			ABAQUS	0.0	6.12E-07	0.0			
0	20	13.16	sim FEM	0.0	0.00E+00	0.0	0.00	0.00	0.00
			ABAQUS	0.0	0.00E+00	0.0			

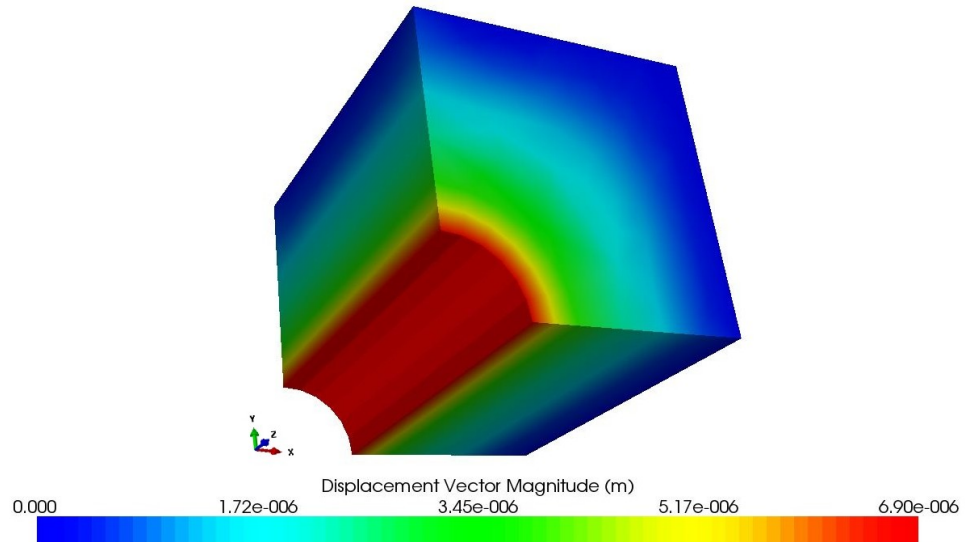


Figure 6.5 Plot of Displacement Magnitude (m) – Case 1 (sim|FEM)

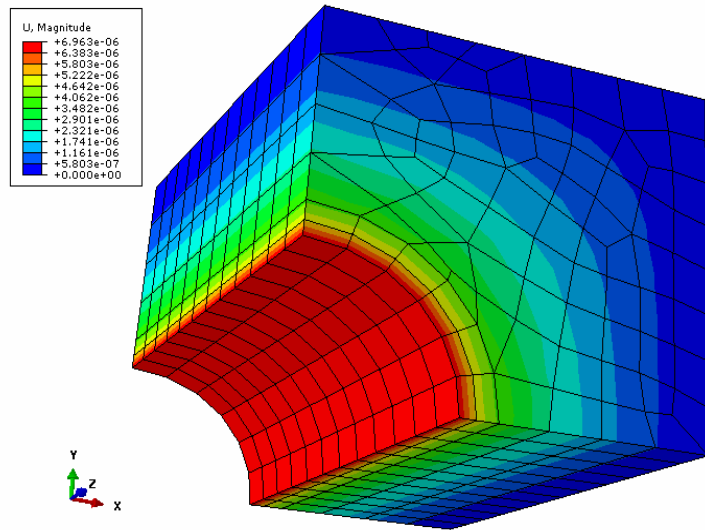


Figure 6.6 Plot of Displacement Magnitude (m) – Case 2 (ABAQUS)

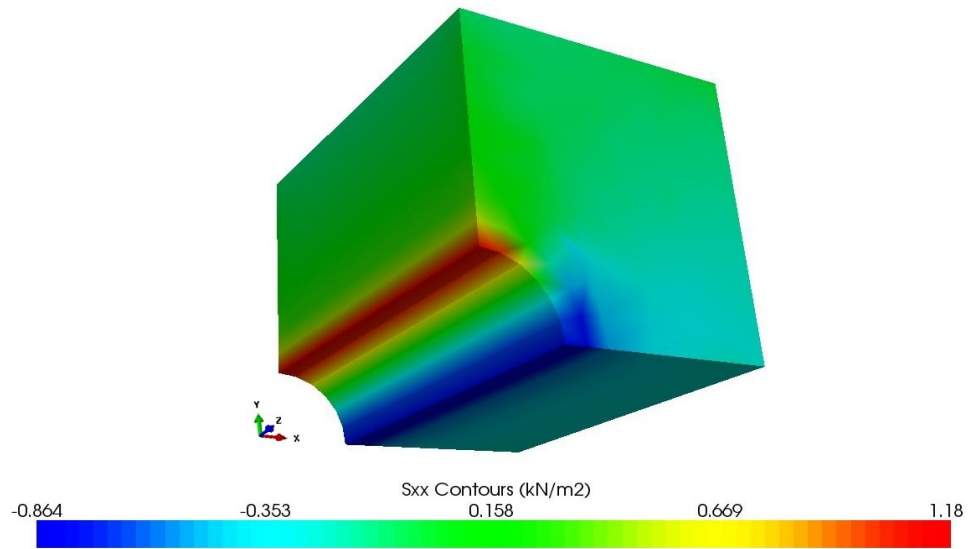


Figure 6.7 Plot of σ_{xx} Stress Contours (kPa) – Case 1 (sim|FEM)

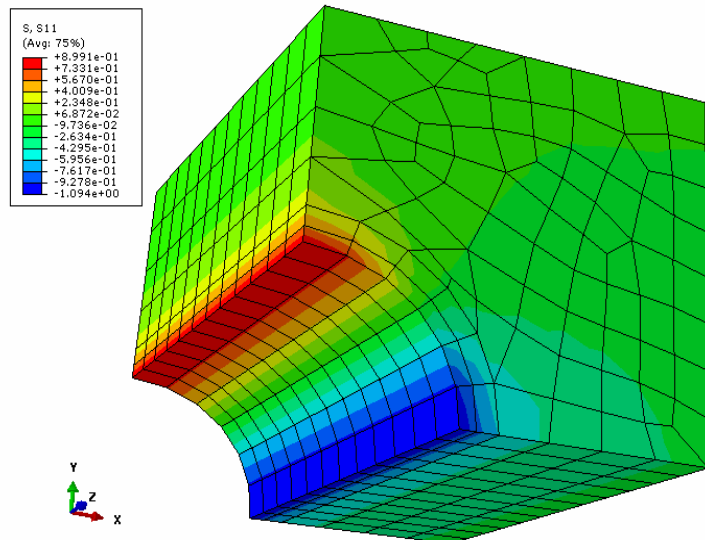


Figure 6.8 Plot of σ_{xx} (or S11 in ABAQUS) Stress Contours (kPa) – Case 2 (ABAQUS)

Table 6.5 Comparison of Displacement Results for Cases 3 and 4 – Lower Boundary

Node Coordinates (m)			Software	Displacements (m)			Difference (%)		
x	y	z		Ux	Uy	Uz	Ux	Uy	Uz
5	0	13.16	sim FEM	1.32E-05	0.0	0.0	1.07	0.00	0.00
			ABAQUS	1.33E-05	0.0	0.0			
5.75	0	13.16	sim FEM	1.05E-05	0.0	0.0	1.35	0.00	0.00
			ABAQUS	1.07E-05	0.0	0.0			
6.5	0	13.16	sim FEM	8.23E-06	0.0	0.0	1.73	0.00	0.00
			ABAQUS	8.37E-06	0.0	0.0			
7.25	0	13.16	sim FEM	7.24E-06	0.0	0.0	1.95	0.00	0.00
			ABAQUS	7.38E-06	0.0	0.0			
8	0	13.16	sim FEM	6.43E-06	0.0	0.0	2.16	0.00	0.00
			ABAQUS	6.56E-06	0.0	0.0			
9.5	0	13.16	sim FEM	4.99E-06	0.0	0.0	2.65	0.00	0.00
			ABAQUS	5.12E-06	0.0	0.0			
11	0	13.16	sim FEM	3.92E-06	0.0	0.0	3.12	0.00	0.00
			ABAQUS	4.04E-06	0.0	0.0			
12.5	0	13.16	sim FEM	3.02E-06	0.0	0.0	3.66	0.00	0.00
			ABAQUS	3.13E-06	0.0	0.0			
14	0	13.16	sim FEM	2.26E-06	0.0	0.0	4.35	0.00	0.00
			ABAQUS	2.36E-06	0.0	0.0			
15.5	0	13.16	sim FEM	1.60E-06	0.0	0.0	6.16	0.00	0.00
			ABAQUS	1.69E-06	0.0	0.0			
17	0	13.16	sim FEM	1.00E-06	0.0	0.0	10.01	0.00	0.00
			ABAQUS	1.10E-06	0.0	0.0			
18.5	0	13.16	sim FEM	4.75E-07	0.0	0.0	0.65	0.00	0.00
			ABAQUS	4.78E-07	0.0	0.0			
20	0	13.16	sim FEM	0.00E+00	0.0	0.0	0.00	0.00	0.00
			ABAQUS	0.00E+00	0.0	0.0			

Table 6.6 Comparison of Displacement Results for Cases 3 and 4 – Left Boundary

Node			Software	Displacements (m)			Difference (%)		
x	y	z		Ux	Uy	Uz	Ux	Uy	Uz
0	5	13.16	sim FEM	0.0	1.27E-05	0.0	0.00	4.38	0.00
			ABAQUS	0.0	1.33E-05	0.0			
0	5.75	13.16	sim FEM	0.0	1.02E-05	0.0	0.00	4.48	0.00
			ABAQUS	0.0	1.06E-05	0.0			
0	6.5	13.16	sim FEM	0.0	8.28E-06	0.0	0.00	0.44	0.00
			ABAQUS	0.0	8.32E-06	0.0			
0	7.25	13.16	sim FEM	0.0	7.58 E-06	0.0	0.00	3.49	0.00
			ABAQUS	0.0	7.32E-06	0.0			
0	8	13.16	sim FEM	0.0	6.76E-06	0.0	0.00	3.68	0.00
			ABAQUS	0.0	6.51E-06	0.0			
0	9.5	13.16	sim FEM	0.0	4.04E-06	0.0	0.00	2.50	0.00
			ABAQUS	0.0	5.10E-06	0.0			
0	11	13.16	sim FEM	0.0	3.12E-06	0.0	0.00	1.69	0.00
			ABAQUS	0.0	3.98E-06	0.0			
0	12.5	13.16	sim FEM	0.0	2.34E-06	0.0	0.00	1.80	0.00
			ABAQUS	0.0	3.07E-06	0.0			
0	14	13.16	sim FEM	0.0	2.34E-06	0.0	0.00	1.95	0.00
			ABAQUS	0.0	2.30E-06	0.0			
0	15.5	13.16	sim FEM	0.0	1.66E-06	0.0	0.00	1.74	0.00
			ABAQUS	0.0	1.63E-06	0.0			
0	17	13.16	sim FEM	0.0	1.04E-06	0.0	0.00	1.31	0.00
			ABAQUS	0.0	1.02E-06	0.0			
0	18.5	13.16	sim FEM	0.0	4.82E-07	0.0	0.00	0.38	0.00
			ABAQUS	0.0	4.84E-07	0.0			
0	20	13.16	sim FEM	0.0	0.00E+00	0.0	0.00	0.00	0.00
			ABAQUS	0.0	0.00E+00	0.0			

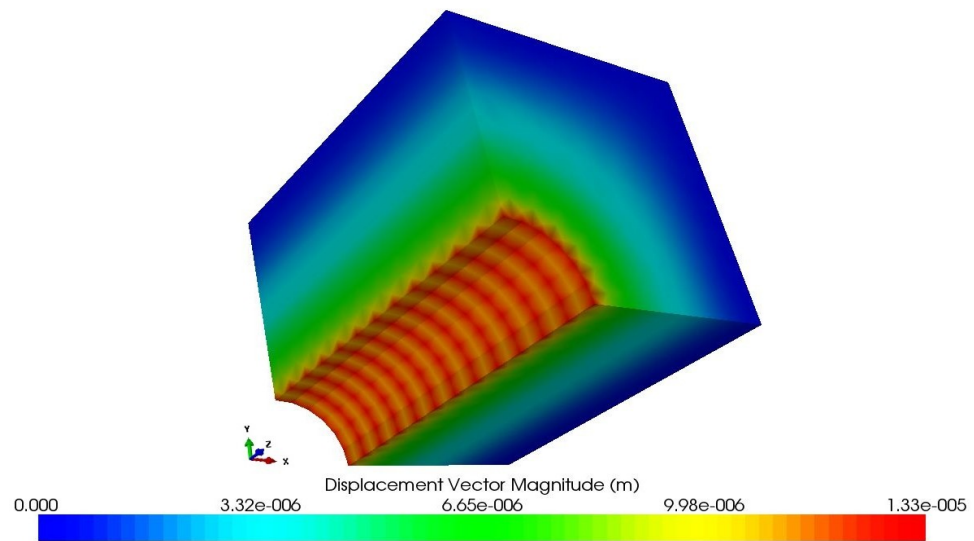


Figure 6.9 Plot of Displacement Magnitude (m) – Case 3 (sim|FEM)

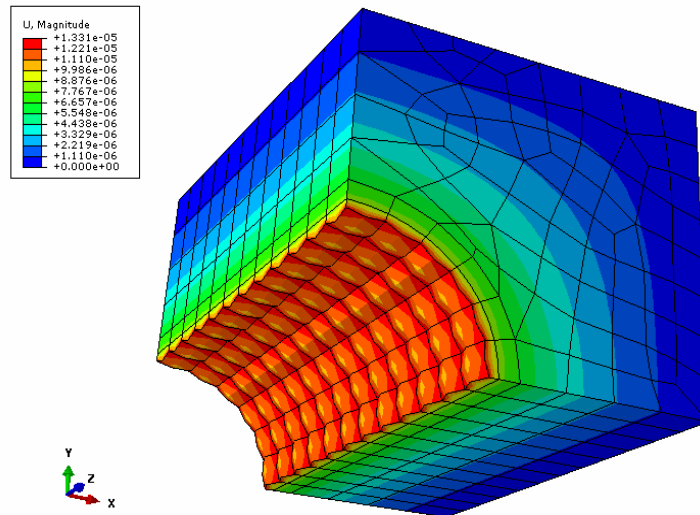


Figure 6.10 Plot of Displacement Magnitude (m) – Case 4 (ABAQUS)

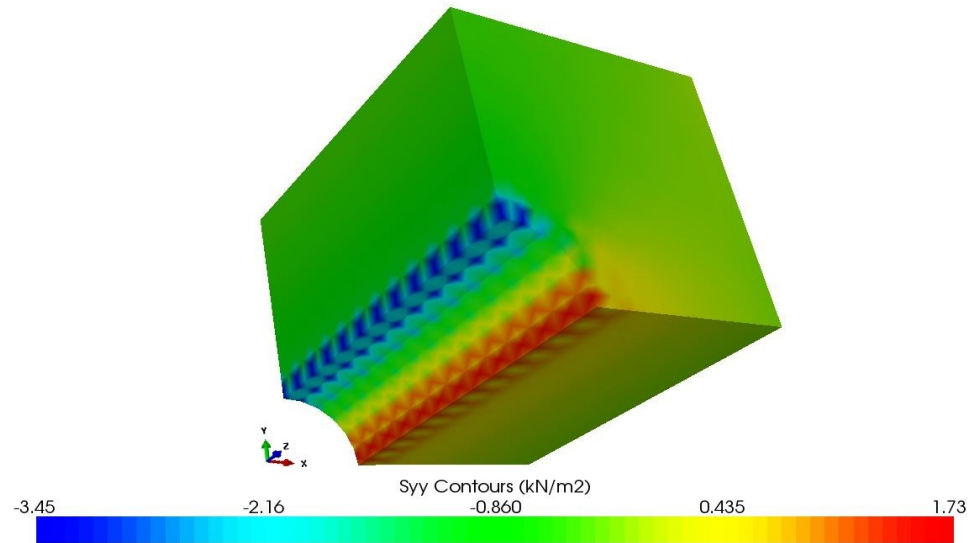


Figure 6.11 Plot of σ_{yy} Stress Contours (kPa) – Case 3 (sim|FEM)

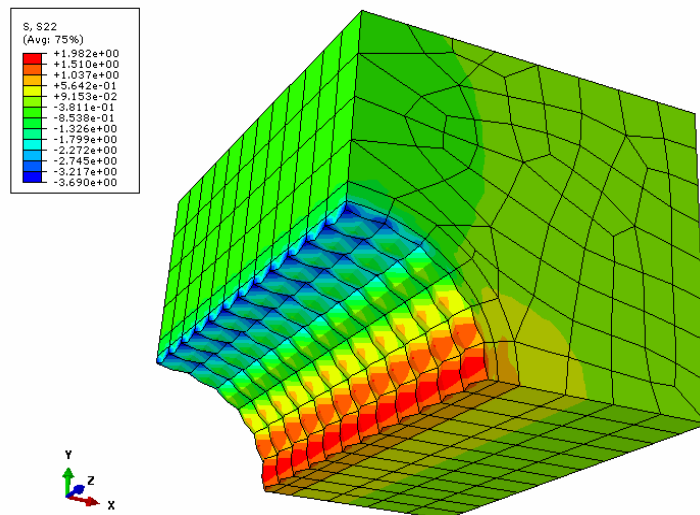


Figure 6.12 Plot of σ_{yy} Stress Contours (kPa) – Case 4 (ABAQUS)

Having established that the solution correlates well between sim|FEM and ABAQUS, our attention turned towards comparing the behavior of first-order and second-order hexahedral elements. Since the second-order elements have mid-side nodes, they can

conform to the shape of the circular excavation more readily. Similarly, if the resulting displacement field is non-linear, the second-order elements should be able to capture it better. Generally, first-order elements exhibit a stiffer response. This is evident from Figures 6.13 and 6.14, where displacements for the lower and left boundary were plotted resulting from the use of both first-order and second-order elements. The first-order elements, due to their relative higher stiffness, resulted in consistently under-estimating the amount of displacement. On average, the Cases 1 and 2 resulted in 50% smaller displacements at the tunnel boundary than Cases 3 and 4 modeled using second-order elements. This difference in values obtained is even throughout the analysis domain, starting from the far field at the model boundary. This finding re-iterates the need to use higher-order elements to obtain a better estimate of the displacement field at the cost of increased computation time and memory requirements. However, using the p-type mesh refinement put forward in this thesis, the best of both worlds can be achieved by using higher-order elements where they count the most, near the excavation. The next section will summarize the models employing transitional elements.

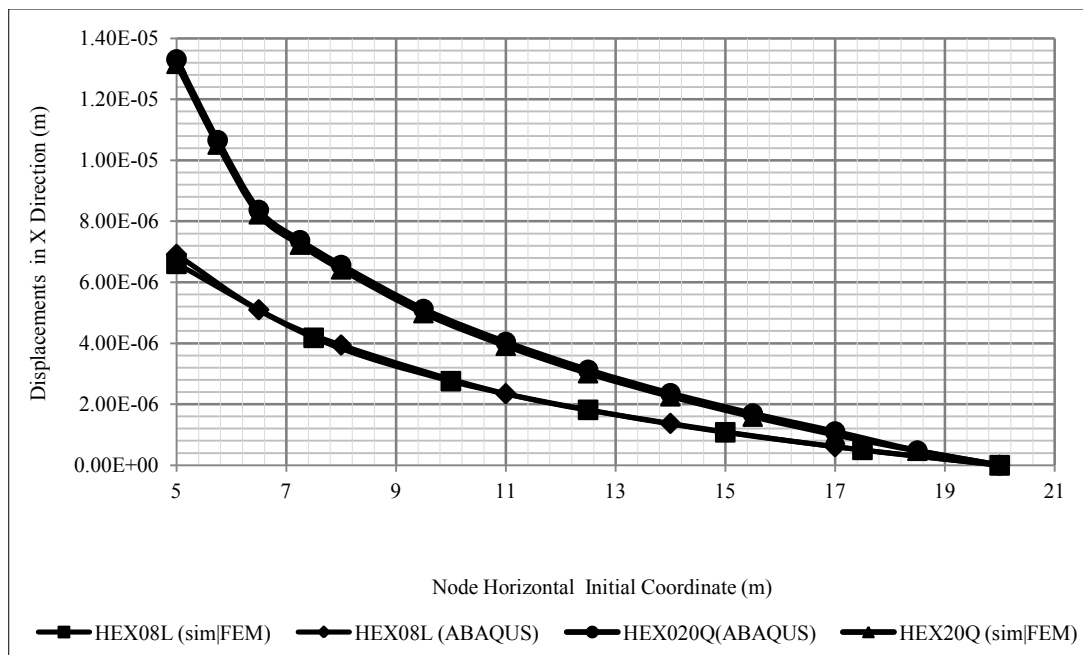


Figure 6.13 Plot of Displacement Magnitude at Lower Boundary – Cases 1 through 4

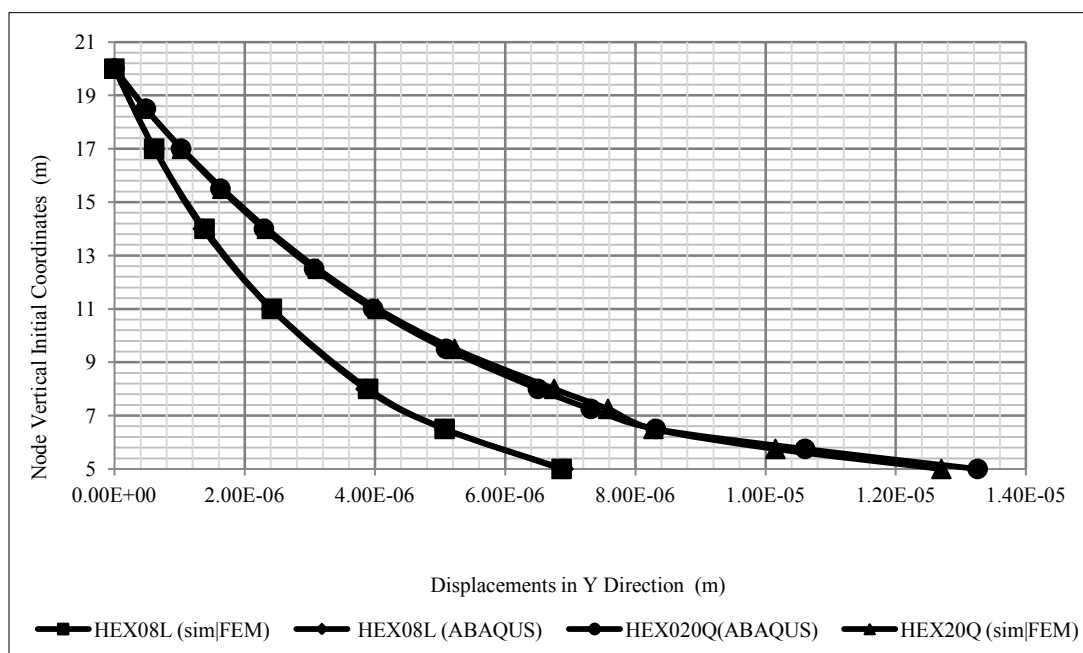


Figure 6.14 Plot of displacement magnitude at the Left Boundary – Cases 1 through 4

6.3 Cases 5 through 10: The use of transitional elements

It is anticipated that the use of transitional elements will retain the solution qualities of second-order elements, which will result in considerable savings in computation time and utilization of resources. Three sets of models were developed using transitional elements for the three locations of the transition zone using the two types of elements (12 and 16-noded hexahedra). As shown in Figure 6.1 the transition zones were located 7.5 m, 10 m and 12.5 m from the centre of the tunnel. All of the elements inside the transition zone were second-order hexahedral elements, while all of the elements outside of the transition zone were first-order elements. Figure 6.15 shows a typical mesh of the front face using a transitional zone. The models employ the same loads and boundary conditions as Cases 1 – 4. The results of analysis, summarized in Figures 6.16 and 6.17, reveal that all models using transitional elements behaved more like Cases 3 and 4, comprised of all second-order hexahedral elements. Plots of displacements along the lower and left boundary were investigated to be able to draw a direct comparison to Cases 1 though 4. Although surprising, the location of the transition band did not affect the behaviour of the model. The implication of this is that multiple stages of yielding, where the yield envelope can be quite close or far from the excavation, can be captured using the hybrid models of first-order, second-order and transitional elements. Although not tabulated but plotted in Figure 6.17, the values along the left boundary, by virtue of symmetry, are close to those tabulated in Table 6.7 with the exception of Case 5. In this case, the displacement obtained at the excavation boundary was 20% greater.

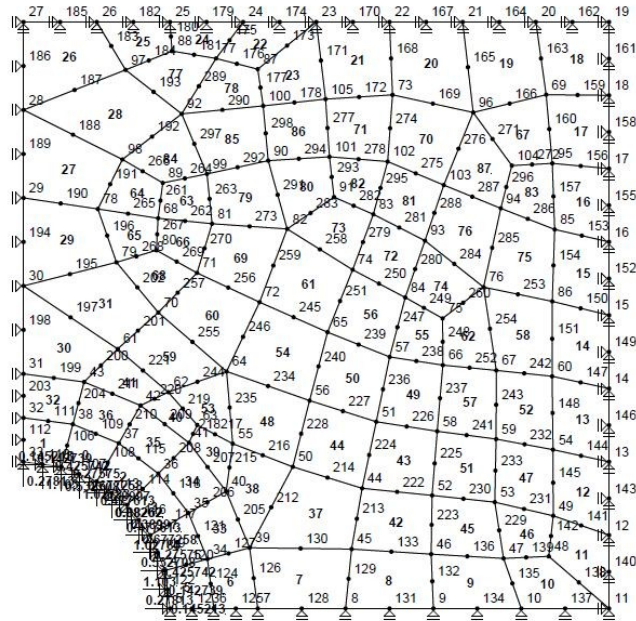


Figure 6.15 Frontal View of Typical Mesh Using Transition Zone

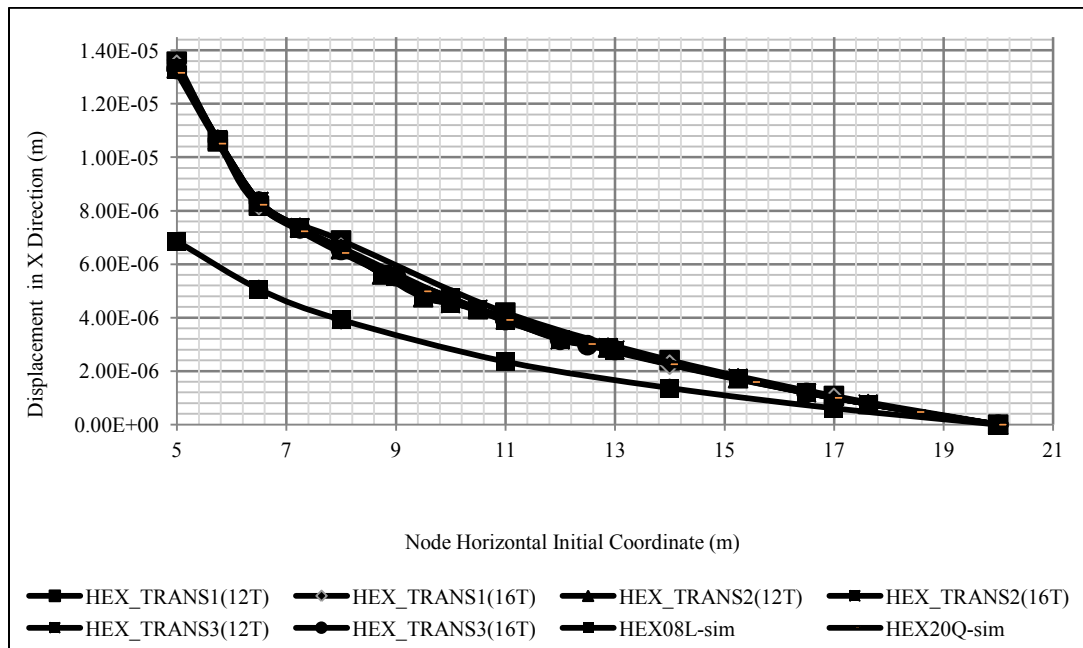


Figure 6.16 Plot of Displacement Magnitude at the Lower Boundary for Cases 5-10

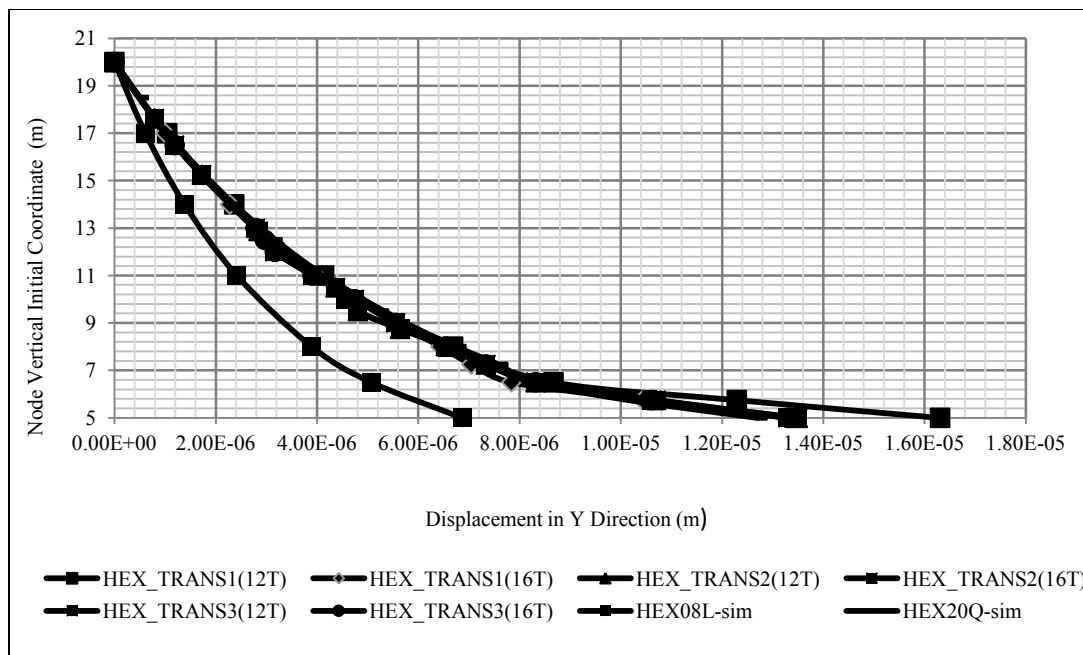


Figure 6.17 Plot of Displacement Magnitude at the Left Boundary for Cases 5-10

6.4 Benefits of mesh optimization

Although the previous section established that the models with transition elements generated results superior to ones with first-order elements, the real motivation for using these special types of elements was to reduce computation time and resource requirements. The cost of computation will be assessed using three relevant metrics: the memory footprint of the global stiffness matrix, the number of iterations to solution and the time to solution. The model characteristics such as the number of nodes or elements and the number of degrees of freedom were condensed in the metric for the global stiffness matrix. The analysis of all models was conducted using a computer with 6.00 GB RAM, 2.4 GHz Intel Core Processor and Windows 7 (Professional-64 bit) as the operating system. Tables 6.7 and 6.8 summarize the effect of p-type mesh optimization on computational resources. Table 6.7 list the raw numbers for the matrix size in bytes,

the number of iterations to convergence using a conjugate gradient solver and the solution time in seconds. The first entry is Case 1, discretized with first-order hexahedral elements. It required uncompressed matrix storage of 76.5 MB and needed 87 iterations and 89 seconds. Although quite fast, its shortcomings were discussed in the previous section. At the other end of the list, Case 3 with all second-order elements needed 1.15GB of memory for matrix storage and 280 iterations totalling in 4999 seconds of solution time. The models with transition elements, even with the farthest location of the transition zone from the excavation center, needed less than half as much memory and solution time as Case 3 with all second-order hexahedral elements.

A more illustrative summary of requirements and solution times is shown in Table 6.8, where all quantities were made relative to Case 1. Models with transition zones possess the benefits of relatively fast solution times, like models with first-order elements, and solution accuracy of second-order elements translating into savings in memory usage of at least 57% (Case 10 compared to Case 3) to as high as 90% (Case 5 compared to Case 3) while solution times were reduced by 65 percent (Case 10 compared to Case 3) and up to 95% (Case 5 compared to Case 3) as shown in Figure 6.18.

Table 6.7 Use of Computational Resources Comparison for Pressurized Cavity Models

Model	No. of Nodes	No. of Elements	No. of Degrees of Freedom	Size of Global Stiffness Matrix (Bytes)	Iterations Required for Convergence	Solution Time (CPU) (sec)
Case 1	1378	1056	3093	76,533,192	87	89
Case 5	1793	1056	3887	120,870,152	167	268
Case 6	1884	1056	4098	134,348,832	194	334
Case 7	2715	1416	6249	312,400,008	230	1031
Case 8	2806	1416	6460	333,852,800	262	1131
Case 9	3179	1296	7553	456,382,472	242	1484
Case 10	3322	1296	7912	500,797,952	257	1759
Case 3	5159	1056	12001	1,152,192,008	280	4999

Table 6.8 Ratio of Computational Resource Requirements for Pressurized Cavity Models

Model	Size of Global Stiffness Matrix Ratio	Iteration Steps Required for Convergence Ratio	Solution Time (CPU) Ratio
Case 1	1.00	1.00	1.00
Case 5	1.58	1.92	3.01
Case 6	1.76	2.23	3.75
Case 7	4.08	2.64	11.58
Case 8	4.36	3.01	12.71
Case 9	5.96	2.78	16.67
Case 10	6.54	2.95	19.76
Case 3	15.05	3.22	56.17

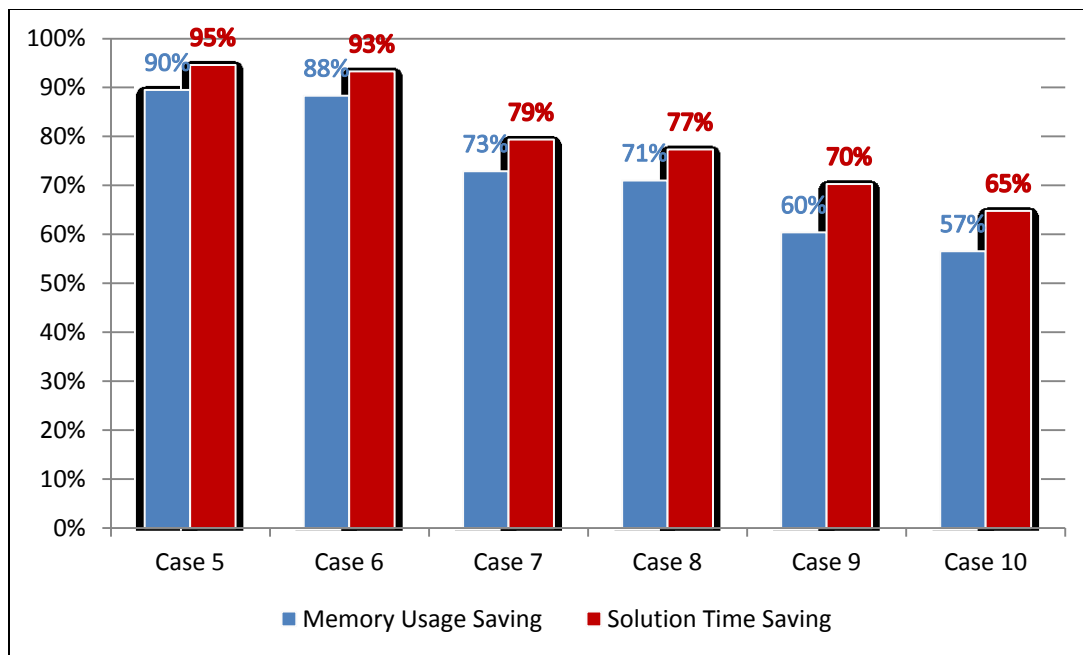


Figure 0.18 Memory Usage and Solution Time Savings for Cases 5 through 10 in Comparison to Case 3

7. Application of Partial p-Adaptive Mesh Optimization to Underground Excavations with Prismatic Cross-sections

The main application of p-adaptive mesh optimization in this research is studying the benefits of using transition elements in modeling underground excavations that are constant in cross-section (prismatic).

As explained in Chapter 3, two underground excavations were analyzed, as illustrated in Figures 3.1 and 3.2. The model material properties were listed in Table 3.1. The radii and locations of excavation centers of both excavations were listed in Table 3.2. The 3D underground excavation model is shown in Figure 7.1.

In this model both tunnels were excavated using the Tunnel Boring Machine technology (TBM). TBM is a machine for excavating tunnels with a circular profile and was chosen because it can be applied to varying rock types (Maidl et al. 2008).

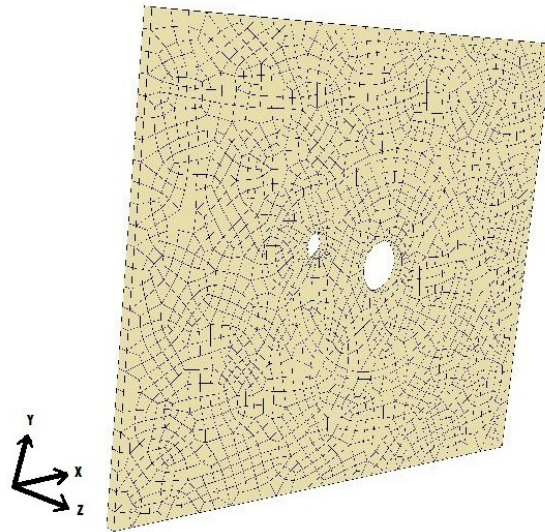


Figure 7.1 Underground Excavation Model

As explained earlier, the transition band could be found by determining the EDZ. In addition, Zsaki (2005) presented an algorithm based on an object-aligned minimum-volume bounding box to approximate the shape of an excavation to a (circular or elliptical) shape in 2D or to a spherical or ellipsoidal shape in 3D, as shown in Figure 7.2.

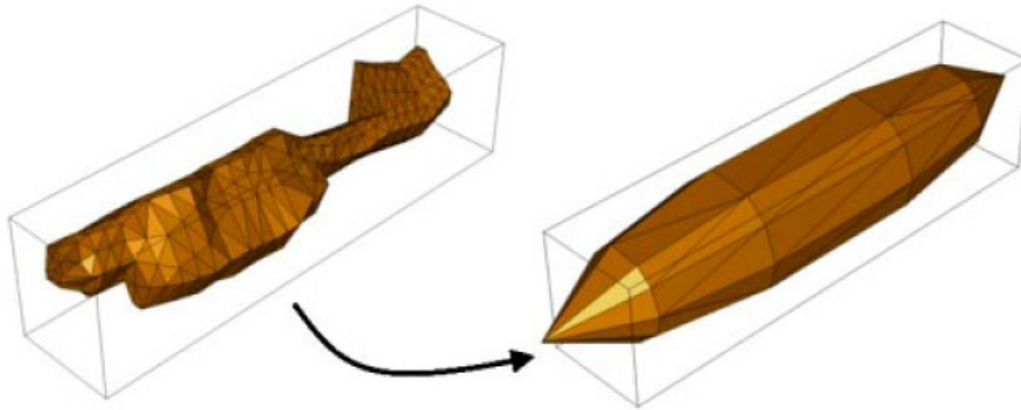


Figure 7.2 Ellipsoidal Approximation of an Excavation (Zsaki 2005)

Three models were tested; the first model was non-optimized mesh consisting of quadratic hexahedral elements, while the other two models were optimized models using transitional elements to connect the linear and quadratic elements. Two kinds of transitional elements were used in the optimization; 12-node and 16-node transition hexahedral elements.

7.1 Results of the Non-optimized Model

The non-optimized model is entirely meshed with 20-node quadratic hexahedral elements, with a total of 2005 elements and 29861 degrees of freedom. The model's

material was assumed to be linear elastic and its properties are listed in Table 3.1, while the geometry and boundary conditions are summarized in Figure 7.3.

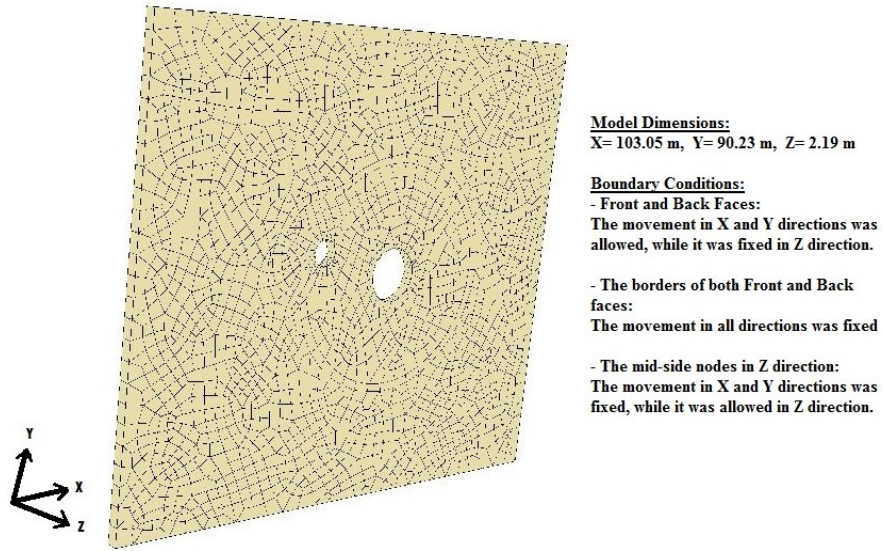


Figure 7.3 Summary of the Boundary Conditions of the Non-optimized Model

The displacement magnitude and stress results were plotted as shown in Figures 7.4 to 7.15. The displacements' detailed results are listed in Tables 7.1 and 7.2 and those results were compared with the results of the optimized models as illustrated later on this chapter in Tables 7.7, 7.8, 7.9 and 7.10. The comparison was done at the nodes located at the borders of both excavations.

Table 7.1 Non-optimized Model Displacement Results at the Border of Excavation 1

Corner Nodes						
Node Coordinates (m)			Displacements (m)			
x	y	z	Ux	Uy	Uz	Vector Magnitude
47.54	17.85	0.00	7.50E-06	9.44E-06	0.00E+00	1.21E-05
46.83	19.88	0.00	4.12E-06	3.08E-05	0.00E+00	3.11E-05
45.94	20.35	0.00	-3.86E-06	3.96E-05	0.00E+00	3.98E-05
44.90	20.52	0.00	-1.33E-05	4.02E-05	0.00E+00	4.24E-05
44.13	20.40	0.00	-2.16E-05	3.65E-05	0.00E+00	4.24E-05
43.51	20.10	0.00	-2.92E-05	3.06E-05	0.00E+00	4.23E-05
42.86	19.40	0.00	-3.74E-05	2.02E-05	0.00E+00	4.25E-05
42.58	18.66	0.00	-4.19E-05	1.00E-05	0.00E+00	4.31E-05
42.50	18.14	0.00	-4.34E-05	2.74E-06	0.00E+00	4.35E-05
42.52	17.61	0.00	-4.39E-05	-5.02E-06	0.00E+00	4.42E-05
42.89	16.63	0.00	-4.12E-05	-1.73E-05	0.00E+00	4.47E-05
43.22	16.22	0.00	-3.78E-05	-2.32E-05	0.00E+00	4.43E-05
43.63	15.88	0.00	-3.36E-05	-2.80E-05	0.00E+00	4.37E-05
44.28	15.60	0.00	-2.77E-05	-3.19E-05	0.00E+00	4.23E-05
44.97	15.48	0.00	-2.13E-05	-3.28E-05	0.00E+00	3.91E-05
45.66	15.55	0.00	-1.46E-05	-3.07E-05	0.00E+00	3.40E-05
46.16	15.74	0.00	-9.59E-06	-2.71E-05	0.00E+00	2.88E-05
46.60	16.02	0.00	-4.99E-06	-2.21E-05	0.00E+00	2.26E-05
46.98	16.40	0.00	-9.71E-07	-1.54E-05	0.00E+00	1.55E-05
47.27	16.84	0.00	2.75E-06	-7.38E-06	0.00E+00	7.87E-06

Table 7.1. (Continuing) Non-optimized Model Displacement Results at the Border of Excavation 1

Mid-Side Nodes			Displacements (m)			
Node Coordinates (m)						Vector Magnitude
x	y	z	Ux	Uy	Uz	
47.19	18.87	0.00	1.07E-05	2.22E-05	0.00E+00	2.46E-05
46.38	20.12	0.00	7.35E-07	3.68E-05	0.00E+00	3.68E-05
45.42	20.44	0.00	-8.47E-06	4.14E-05	0.00E+00	4.22E-05
44.51	20.46	0.00	-1.74E-05	3.91E-05	0.00E+00	4.28E-05
43.82	20.25	0.00	-2.55E-05	3.41E-05	0.00E+00	4.26E-05
43.19	19.75	0.00	-3.40E-05	2.61E-05	0.00E+00	4.29E-05
42.72	19.03	0.00	-4.04E-05	1.52E-05	0.00E+00	4.32E-05
42.54	18.40	0.00	-4.30E-05	6.48E-06	0.00E+00	4.35E-05
42.51	17.88	0.00	-4.40E-05	-1.24E-06	0.00E+00	4.40E-05
42.47	15.99	0.00	-4.36E-05	-1.15E-05	0.00E+00	4.51E-05
43.06	16.42	0.00	-3.98E-05	-2.04E-05	0.00E+00	4.47E-05
43.43	16.05	0.00	-3.58E-05	-2.59E-05	0.00E+00	4.41E-05
43.95	15.74	0.00	-3.08E-05	-3.06E-05	0.00E+00	4.34E-05
44.62	15.54	0.00	-2.46E-05	-3.30E-05	0.00E+00	4.12E-05
45.31	15.51	0.00	-1.79E-05	-3.24E-05	0.00E+00	3.70E-05
45.91	15.64	0.00	-1.21E-05	-2.93E-05	0.00E+00	3.17E-05
46.38	15.88	0.00	-7.20E-06	-2.50E-05	0.00E+00	2.60E-05
46.79	16.21	0.00	-2.86E-06	-1.91E-05	0.00E+00	1.93E-05
47.12	16.62	0.00	1.12E-06	-1.16E-05	0.00E+00	1.16E-05
47.40	17.35	0.00	6.14E-06	7.15E-07	0.00E+00	6.18E-06

Table 7.2 Non-optimized Model Displacement Results at the Border of Excavation 2

Corner Nodes						
Node Coordinates (m)			Displacements (m)			
x	y	z	Ux	Uy	Uz	Vector Magnitude
68.20	12.89	0.00	6.54E-05	6.09E-07	0.00E+00	6.54E-05
68.09	13.99	0.00	6.47E-05	1.46E-05	0.00E+00	6.63E-05
67.91	14.53	0.00	6.32E-05	2.17E-05	0.00E+00	6.68E-05
67.75	15.04	0.00	6.07E-05	2.79E-05	0.00E+00	6.68E-05
67.20	16.00	0.00	5.44E-05	4.00E-05	0.00E+00	6.75E-05
66.46	16.82	0.00	4.57E-05	5.04E-05	0.00E+00	6.80E-05
65.56	17.47	0.00	3.53E-05	5.86E-05	0.00E+00	6.84E-05
64.00	18.14	0.00	1.77E-05	6.50E-05	0.00E+00	6.74E-05
62.63	18.33	0.00	-1.25E-06	6.49E-05	0.00E+00	6.49E-05
61.28	17.93	0.00	-1.86E-05	6.36E-05	0.00E+00	6.63E-05
60.27	17.48	0.00	-2.95E-05	5.81E-05	0.00E+00	6.52E-05
59.37	16.83	0.00	-3.98E-05	4.95E-05	0.00E+00	6.35E-05
58.63	16.01	0.00	-4.84E-05	3.84E-05	0.00E+00	6.18E-05
58.08	15.06	0.00	-5.52E-05	2.55E-05	0.00E+00	6.08E-05
57.73	14.00	0.00	-5.96E-05	1.11E-05	0.00E+00	6.06E-05
57.62	12.90	0.00	-6.17E-05	-4.19E-06	0.00E+00	6.18E-05
57.86	11.56	0.00	-6.14E-05	-2.14E-05	0.00E+00	6.50E-05
58.36	10.33	0.00	-5.65E-05	-3.56E-05	0.00E+00	6.68E-05
59.36	8.97	0.00	-4.44E-05	-5.00E-05	0.00E+00	6.69E-05
60.26	8.32	0.00	-3.31E-05	-5.83E-05	0.00E+00	6.70E-05
61.27	7.86	0.00	-2.06E-05	-6.36E-05	0.00E+00	6.69E-05
62.35	7.63	0.00	-7.26E-06	-6.61E-05	0.00E+00	6.65E-05
63.45	7.63	0.00	6.48E-06	-6.57E-05	0.00E+00	6.60E-05
64.54	7.86	0.00	2.00E-05	-6.23E-05	0.00E+00	6.55E-05
65.55	8.31	0.00	3.36E-05	-5.61E-05	0.00E+00	6.54E-05
67.19	9.78	0.00	5.19E-05	-3.95E-05	0.00E+00	6.52E-05
67.74	10.73	0.00	5.93E-05	-2.64E-05	0.00E+00	6.49E-05
68.08	11.79	0.00	6.41E-05	-1.30E-05	0.00E+00	6.54E-05

Table 7.2. (Continuing) Non-optimized Model Displacement Results at the Border of Excavation 2

Mid-Side Nodes						
Node Coordinates (m)			Displacements (m)			
x	y	z	Ux	Uy	Uz	Vector Magnitude
68.14	13.44	0.00	6.58E-05	7.62E-06	0.00E+00	6.62E-05
68.14	12.34	0.00	6.42E-05	1.83E-05	0.00E+00	6.67E-05
68.00	14.26	0.00	6.21E-05	2.47E-05	0.00E+00	6.69E-05
67.83	14.78	0.00	5.81E-05	3.44E-05	0.00E+00	6.75E-05
67.47	15.52	0.00	5.06E-05	4.57E-05	0.00E+00	6.81E-05
66.83	16.41	0.00	4.09E-05	5.51E-05	0.00E+00	6.86E-05
66.01	17.15	0.00	2.73E-05	6.33E-05	0.00E+00	6.90E-05
64.78	17.81	0.00	8.82E-06	6.61E-05	0.00E+00	6.67E-05
63.31	18.23	0.00	-1.06E-05	6.54E-05	0.00E+00	6.63E-05
61.96	18.13	0.00	-2.43E-05	6.17E-05	0.00E+00	6.63E-05
60.78	17.71	0.00	-3.49E-05	5.45E-05	0.00E+00	6.47E-05
59.82	17.16	0.00	-4.47E-05	4.44E-05	0.00E+00	6.30E-05
59.00	16.42	0.00	-5.24E-05	3.23E-05	0.00E+00	6.15E-05
58.36	15.53	0.00	-5.80E-05	1.85E-05	0.00E+00	6.09E-05
57.91	14.53	0.00	-6.12E-05	3.55E-06	0.00E+00	6.13E-05
57.68	13.45	0.00	-6.26E-05	-1.33E-05	0.00E+00	6.40E-05
57.74	12.23	0.00	-5.99E-05	-2.89E-05	0.00E+00	6.65E-05
58.11	10.94	0.00	-5.19E-05	-4.37E-05	0.00E+00	6.78E-05
58.86	9.65	0.00	-3.92E-05	-5.48E-05	0.00E+00	6.73E-05
59.81	8.64	0.00	-2.72E-05	-6.16E-05	0.00E+00	6.74E-05
60.76	8.09	0.00	-1.41E-05	-6.56E-05	0.00E+00	6.71E-05
61.81	7.75	0.00	-3.60E-07	-6.66E-05	0.00E+00	6.66E-05
62.90	7.63	0.00	1.35E-05	-6.48E-05	0.00E+00	6.62E-05
63.99	7.74	0.00	2.70E-05	-5.98E-05	0.00E+00	6.56E-05
65.04	8.08	0.00	4.46E-05	-4.99E-05	0.00E+00	6.69E-05
66.37	9.04	0.00	5.61E-05	-3.32E-05	0.00E+00	6.52E-05
67.46	10.26	0.00	6.24E-05	-1.99E-05	0.00E+00	6.55E-05
67.91	11.26	0.00	6.56E-05	-6.13E-06	0.00E+00	6.59E-05

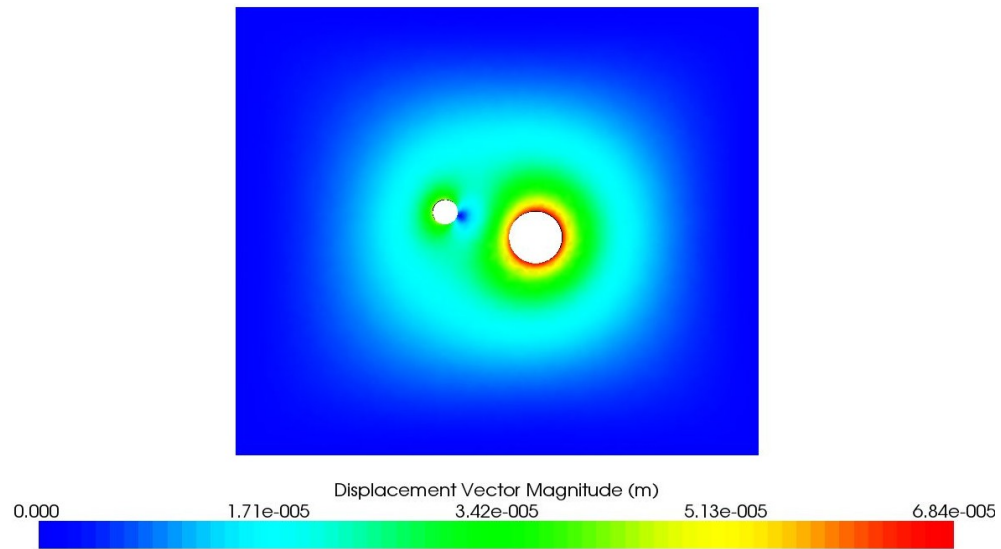


Figure 7.4 Frontal Plot of Displacement Magnitude (m) of the Non-optimized Model

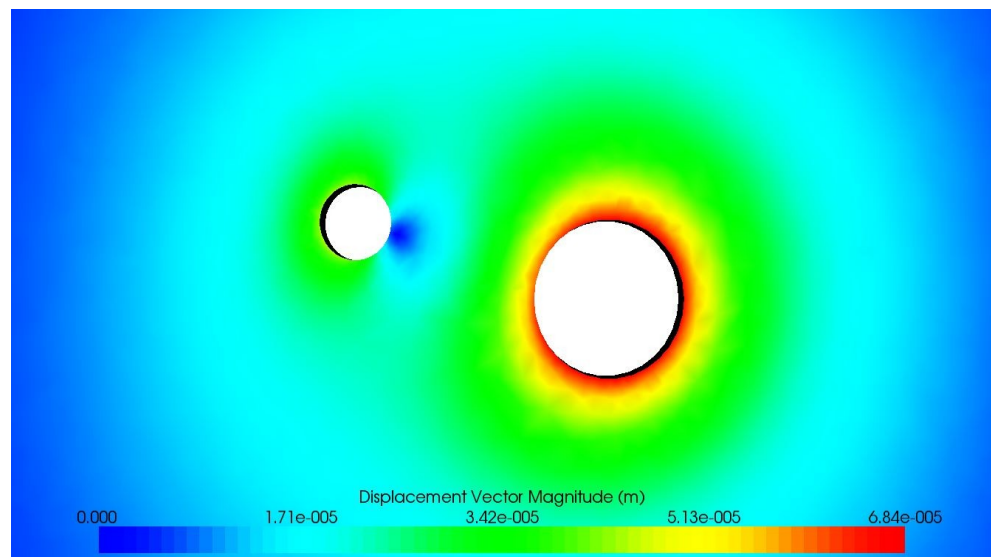


Figure 7.5 Zoomed View of Frontal Plot of Displacement Magnitude (m) of the Non-optimized Model

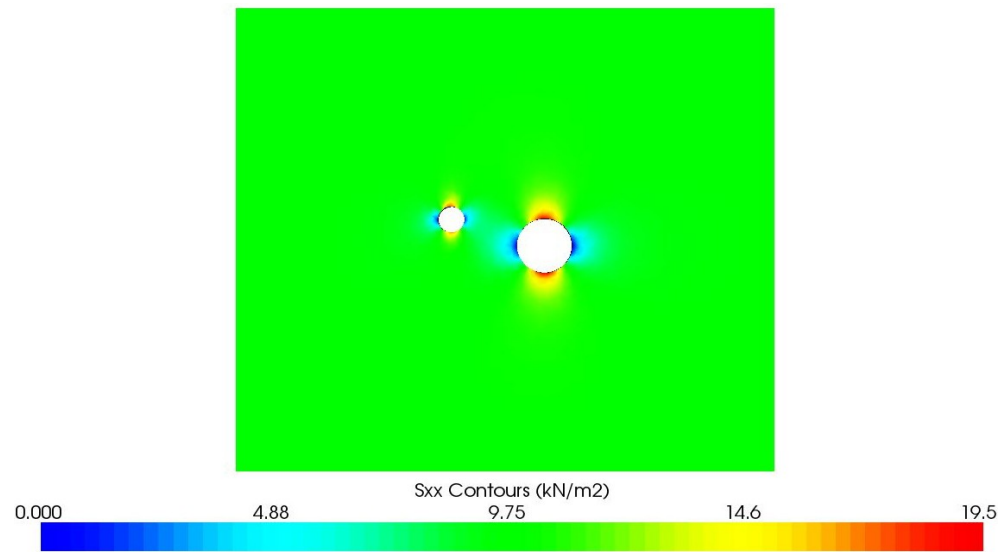


Figure 7.6 Frontal Plot of σ_{xx} (kPa) of the Non-optimized Model

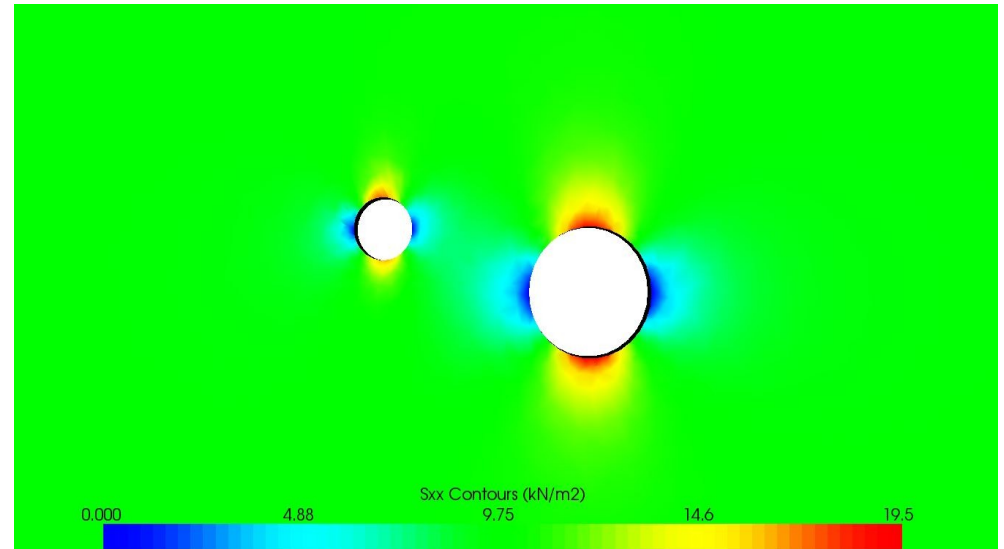


Figure 7.7 Zoomed View of Frontal Plot of σ_{xx} (kPa) of the Non-optimized Model

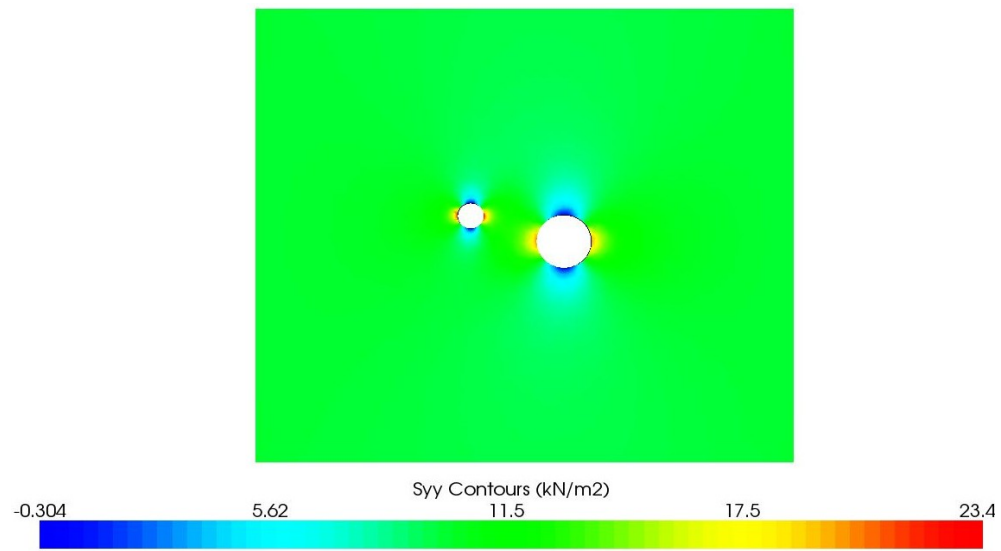


Figure 7.8 Frontal Plot of σ_{yy} (kPa) of the Non-optimized Model

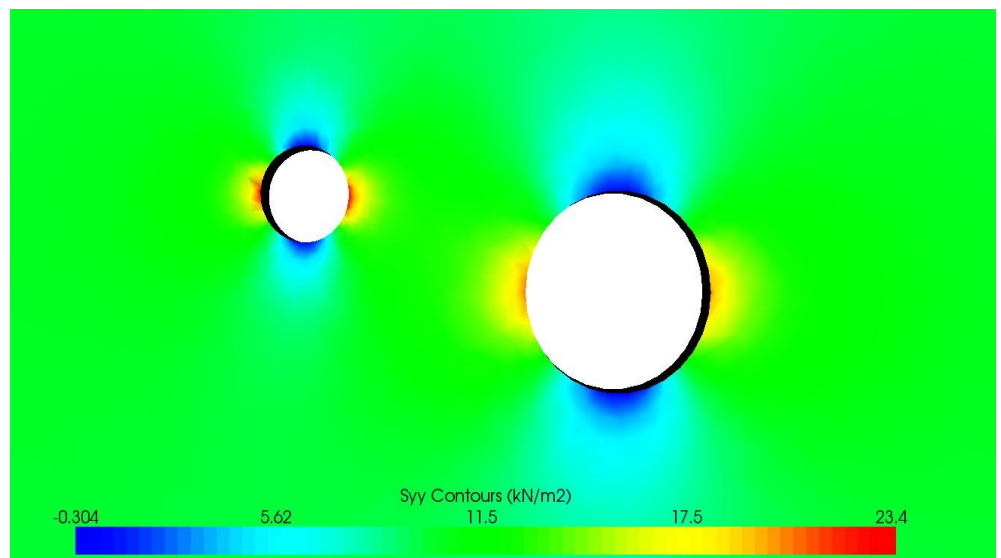


Figure 7.9 Zoomed View of Frontal Plot of σ_{yy} (kPa) of the Non-optimized Model

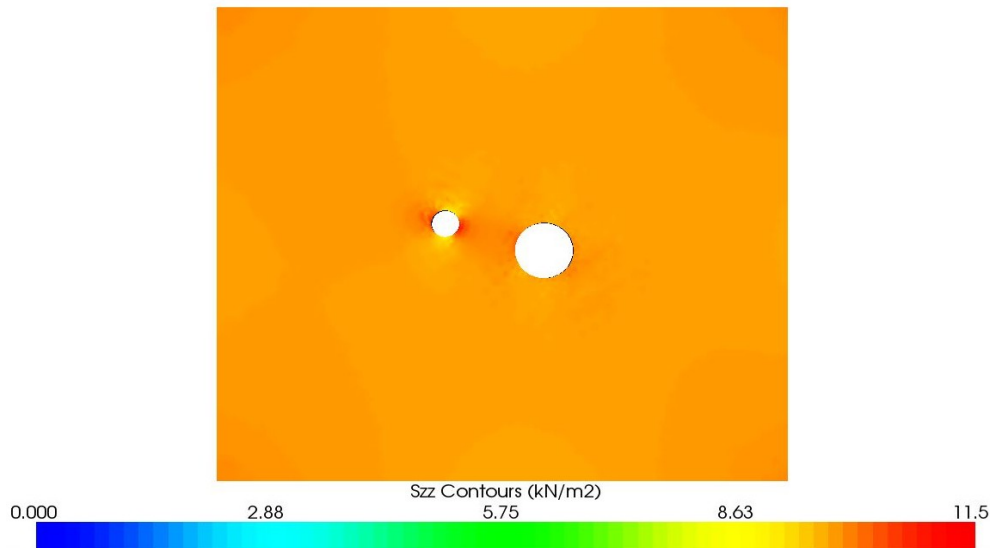


Figure 7.10 Frontal Plot of σ_{zz} (kPa) of the Non-optimized Model

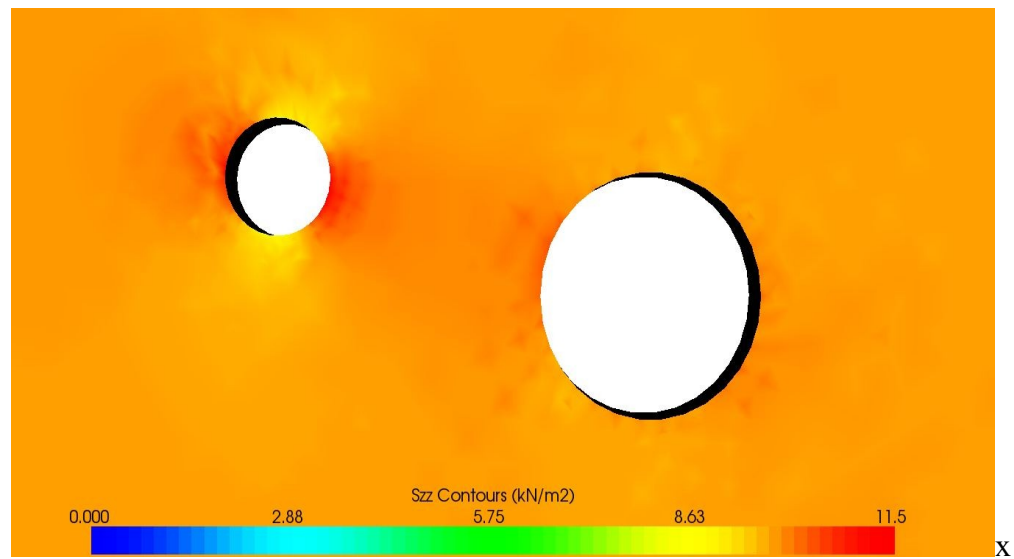


Figure 7.4 Zoomed View of Frontal Plot of σ_{zz} (kPa) of the Non-optimized Model

7.2 Results of the Optimized Models

The optimized models consisted of three kinds of elements; second order, first order and transitional hexahedral elements. The continuum's material was assumed to be linear elastic and its properties are listed in Table 3.1, while the geometry and boundary conditions are summarized in Figure 7.16. The determination of the transition zone was accomplished as explained in Chapter 3. In this thesis, two kinds of transitional elements were chosen to be tested: 12-node and 16-node transitional elements. For these elements, two cases were tested; Case 1 was an optimized mesh of 20-node quadratic elements, 12-node transitional elements and 8-node linear elements; while Case 2 was an optimized mesh of 20-node quadratic elements, 16-node transitional elements and 8-node linear elements.

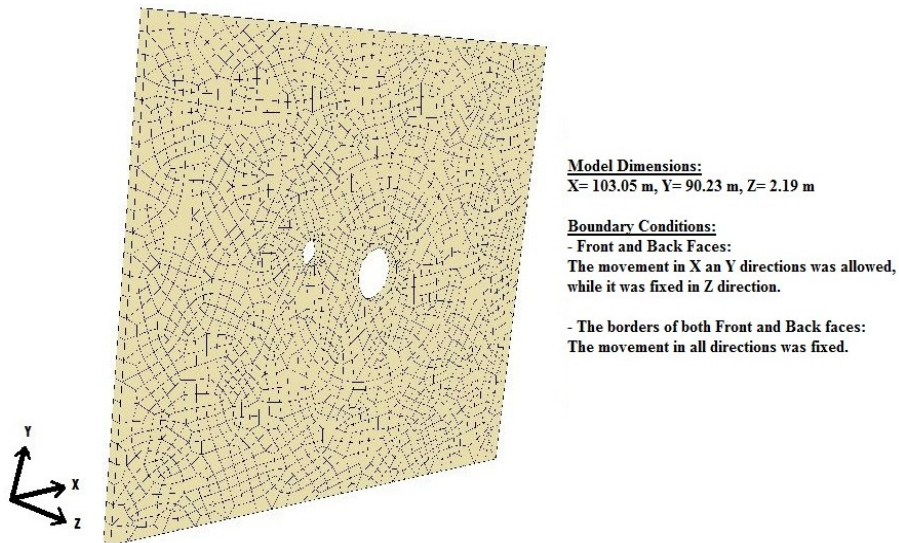


Figure 7.5 The Boundary Conditions of Optimized Models

7.2.1 Case 1 Results

The mesh using 12-node transitional hexahedral elements as the connection between the 20-noded and 8-noded elements consisted of 2005 elements with a total of 12622 degrees of freedom. The displacement results at both excavations borders are listed in Tables 7.3 and 7.4.

Table 7.3 Optimized Model Displacement Results at the Border of Excavation 1- Case 1

Corner Nodes						
Node Coordinates (m)			Displacements (m)			Vector Magnitude
x	y	z	Ux	Uy	Uz	
47.54	17.85	0.00	7.57E-06	9.23E-06	0.00E+00	1.19E-05
46.83	19.88	0.00	4.24E-06	3.06E-05	0.00E+00	3.09E-05
45.94	20.35	0.00	-3.68E-06	3.94E-05	0.00E+00	3.95E-05
44.90	20.52	0.00	-1.31E-05	4.00E-05	0.00E+00	4.20E-05
44.13	20.40	0.00	-2.13E-05	3.63E-05	0.00E+00	4.20E-05
43.51	20.10	0.00	-2.88E-05	3.04E-05	0.00E+00	4.19E-05
42.86	19.40	0.00	-3.70E-05	1.99E-05	0.00E+00	4.20E-05
42.58	18.66	0.00	-4.15E-05	9.76E-06	0.00E+00	4.26E-05
42.50	18.14	0.00	-4.30E-05	2.50E-06	0.00E+00	4.31E-05
42.52	17.61	0.00	-4.34E-05	-5.25E-06	0.00E+00	4.38E-05
42.89	16.63	0.00	-4.09E-05	-1.75E-05	0.00E+00	4.44E-05
43.22	16.22	0.00	-3.75E-05	-2.34E-05	0.00E+00	4.42E-05
43.63	15.88	0.00	-3.33E-05	-2.82E-05	0.00E+00	4.36E-05
44.28	15.60	0.00	-2.75E-05	-3.22E-05	0.00E+00	4.23E-05
44.97	15.48	0.00	-2.11E-05	-3.30E-05	0.00E+00	3.92E-05
45.66	15.55	0.00	-1.45E-05	-3.09E-05	0.00E+00	3.41E-05
46.16	15.74	0.00	-9.46E-06	-2.73E-05	0.00E+00	2.89E-05
46.60	16.02	0.00	-4.87E-06	-2.23E-05	0.00E+00	2.28E-05
46.98	16.40	0.00	-8.71E-07	-1.56E-05	0.00E+00	1.56E-05
47.27	16.84	0.00	2.84E-06	-7.57E-06	0.00E+00	8.08E-06

Table 7.3. (Continuing) Optimized Model Displacement Results at the Border of Excavation 1- Case 1

Mid-Side Nodes			Displacements (m)			
Node Coordinates (m)						Vector Magnitude
x	y	z	Ux	Uy	Uz	
47.19	18.87	0.00	1.07E-05	2.19E-05	0.00E+00	2.44E-05
46.38	20.12	0.00	8.85E-07	3.65E-05	0.00E+00	3.66E-05
45.42	20.44	0.00	-8.25E-06	4.11E-05	0.00E+00	4.19E-05
44.51	20.46	0.00	-1.72E-05	3.89E-05	0.00E+00	4.25E-05
43.82	20.25	0.00	-2.52E-05	3.38E-05	0.00E+00	4.22E-05
43.19	19.75	0.00	-3.37E-05	2.58E-05	0.00E+00	4.24E-05
42.72	19.03	0.00	-4.00E-05	1.50E-05	0.00E+00	4.27E-05
42.54	18.40	0.00	-4.25E-05	6.24E-06	0.00E+00	4.30E-05
42.51	17.88	0.00	-4.36E-05	-1.47E-06	0.00E+00	4.36E-05
42.47	15.99	0.00	-4.32E-05	-1.18E-05	0.00E+00	4.48E-05
43.06	16.42	0.00	-3.94E-05	-2.06E-05	0.00E+00	4.45E-05
43.43	16.05	0.00	-3.55E-05	-2.61E-05	0.00E+00	4.41E-05
43.95	15.74	0.00	-3.06E-05	-3.08E-05	0.00E+00	4.34E-05
44.62	15.54	0.00	-2.44E-05	-3.33E-05	0.00E+00	4.13E-05
45.31	15.51	0.00	-1.78E-05	-3.26E-05	0.00E+00	3.71E-05
45.91	15.64	0.00	-1.19E-05	-2.95E-05	0.00E+00	3.18E-05
46.38	15.88	0.00	-7.08E-06	-2.52E-05	0.00E+00	2.61E-05
46.79	16.21	0.00	-2.75E-06	-1.93E-05	0.00E+00	1.95E-05
47.12	16.62	0.00	1.22E-06	-1.18E-05	0.00E+00	1.18E-05
47.40	17.35	0.00	6.22E-06	5.12E-07	0.00E+00	6.24E-06

Table 7.4 Optimized Model Displacement Results at the Border of Excavation 2 - Case 1

Corner Nodes						
Node Coordinates (m)			Displacements (m)			Vector Magnitude
x	y	z	Ux	Uy	Uz	
68.20	12.89	0.00	6.51E-05	1.82E-08	0.00E+00	6.51E-05
68.09	13.99	0.00	6.43E-05	1.39E-05	0.00E+00	6.58E-05
67.91	14.53	0.00	6.29E-05	2.10E-05	0.00E+00	6.63E-05
67.75	15.04	0.00	6.04E-05	2.72E-05	0.00E+00	6.62E-05
67.20	16.00	0.00	5.40E-05	3.93E-05	0.00E+00	6.68E-05
66.46	16.82	0.00	4.54E-05	4.97E-05	0.00E+00	6.73E-05
65.56	17.47	0.00	3.50E-05	5.79E-05	0.00E+00	6.76E-05
64.00	18.14	0.00	1.75E-05	6.43E-05	0.00E+00	6.66E-05
62.63	18.33	0.00	-1.39E-06	6.42E-05	0.00E+00	6.42E-05
61.28	17.93	0.00	-1.87E-05	6.30E-05	0.00E+00	6.57E-05
60.27	17.48	0.00	-2.95E-05	5.76E-05	0.00E+00	6.47E-05
59.37	16.83	0.00	-3.98E-05	4.90E-05	0.00E+00	6.31E-05
58.63	16.01	0.00	-4.83E-05	3.80E-05	0.00E+00	6.15E-05
58.08	15.06	0.00	-5.51E-05	2.52E-05	0.00E+00	6.06E-05
57.73	14.00	0.00	-5.94E-05	1.09E-05	0.00E+00	6.04E-05
57.62	12.90	0.00	-6.14E-05	-4.28E-06	0.00E+00	6.16E-05
57.86	11.56	0.00	-6.10E-05	-2.14E-05	0.00E+00	6.47E-05
58.36	10.33	0.00	-5.62E-05	-3.56E-05	0.00E+00	6.65E-05
59.36	8.97	0.00	-4.40E-05	-4.99E-05	0.00E+00	6.65E-05
60.26	8.32	0.00	-3.27E-05	-5.83E-05	0.00E+00	6.68E-05
61.27	7.86	0.00	-2.02E-05	-6.36E-05	0.00E+00	6.68E-05
62.35	7.63	0.00	-6.96E-06	-6.61E-05	0.00E+00	6.65E-05
63.45	7.63	0.00	6.71E-06	-6.58E-05	0.00E+00	6.61E-05
64.54	7.86	0.00	2.02E-05	-6.25E-05	0.00E+00	6.57E-05
65.55	8.31	0.00	3.37E-05	-5.64E-05	0.00E+00	6.56E-05
67.19	9.78	0.00	5.18E-05	-3.99E-05	0.00E+00	6.53E-05
67.74	10.73	0.00	5.91E-05	-2.69E-05	0.00E+00	6.49E-05
68.08	11.79	0.00	6.38E-05	-1.36E-05	0.00E+00	6.53E-05

Table 7.4. (Continuing) Optimized Model Displacement Results at the Border of Excavation 2 - Case 1

Mid-Side Nodes						
Node Coordinates (m)			Displacements (m)			Vector Magnitude
x	y	z	Ux	Uy	Uz	
68.14	13.44	0.00	6.55E-05	7.00E-06	0.00E+00	6.58E-05
68.14	12.34	0.00	6.38E-05	1.76E-05	0.00E+00	6.62E-05
68.00	14.26	0.00	6.18E-05	2.41E-05	0.00E+00	6.63E-05
67.83	14.78	0.00	5.77E-05	3.37E-05	0.00E+00	6.69E-05
67.47	15.52	0.00	5.02E-05	4.49E-05	0.00E+00	6.74E-05
66.83	16.41	0.00	4.06E-05	5.43E-05	0.00E+00	6.78E-05
66.01	17.15	0.00	2.71E-05	6.26E-05	0.00E+00	6.82E-05
64.78	17.81	0.00	8.63E-06	6.54E-05	0.00E+00	6.60E-05
63.31	18.23	0.00	-1.07E-05	6.48E-05	0.00E+00	6.56E-05
61.96	18.13	0.00	-2.44E-05	6.11E-05	0.00E+00	6.58E-05
60.78	17.71	0.00	-3.49E-05	5.40E-05	0.00E+00	6.43E-05
59.82	17.16	0.00	-4.46E-05	4.40E-05	0.00E+00	6.26E-05
59.00	16.42	0.00	-5.22E-05	3.20E-05	0.00E+00	6.13E-05
58.36	15.53	0.00	-5.79E-05	1.83E-05	0.00E+00	6.07E-05
57.91	14.53	0.00	-6.10E-05	3.43E-06	0.00E+00	6.11E-05
57.68	13.45	0.00	-6.23E-05	-1.33E-05	0.00E+00	6.37E-05
57.74	12.23	0.00	-5.96E-05	-2.89E-05	0.00E+00	6.62E-05
58.11	10.94	0.00	-5.15E-05	-4.36E-05	0.00E+00	6.75E-05
58.86	9.65	0.00	-3.88E-05	-5.47E-05	0.00E+00	6.70E-05
59.81	8.64	0.00	-2.68E-05	-6.16E-05	0.00E+00	6.72E-05
60.76	8.09	0.00	-1.38E-05	-6.56E-05	0.00E+00	6.70E-05
61.81	7.75	0.00	-9.86E-08	-6.67E-05	0.00E+00	6.67E-05
62.90	7.63	0.00	1.37E-05	-6.49E-05	0.00E+00	6.63E-05
63.99	7.74	0.00	2.71E-05	-6.00E-05	0.00E+00	6.58E-05
65.04	8.08	0.00	4.45E-05	-5.02E-05	0.00E+00	6.71E-05
66.37	9.04	0.00	5.59E-05	-3.36E-05	0.00E+00	6.52E-05
67.46	10.26	0.00	6.21E-05	-2.04E-05	0.00E+00	6.54E-05
67.91	11.26	0.00	6.53E-05	-6.69E-06	0.00E+00	6.56E-05

7.2.2 Case 2 Results

The mesh using 16-node transitional hexahedral elements, as the connecting elements, had the same number of elements as in Case 1 with a total of 12934 degrees of freedom. The displacement results at both excavations borders are listed in Tables 7.5 and 7.6.

Table 7.5 Optimized Model Displacement Results at the Border of Excavation 1 - Case 2

Corner Nodes			Displacements (m)			Vector Magnitude
x	y	z	Ux	Uy	Uz	
47.54	17.85	0.00	7.51E-06	9.10E-06	0.00E+00	1.18E-05
46.83	19.88	0.00	4.11E-06	3.03E-05	0.00E+00	3.05E-05
45.94	20.35	0.00	-3.79E-06	3.90E-05	0.00E+00	3.92E-05
44.90	20.52	0.00	-1.31E-05	3.96E-05	0.00E+00	4.17E-05
44.13	20.40	0.00	-2.13E-05	3.60E-05	0.00E+00	4.18E-05
43.51	20.10	0.00	-2.88E-05	3.02E-05	0.00E+00	4.17E-05
42.86	19.40	0.00	-3.68E-05	1.99E-05	0.00E+00	4.19E-05
42.58	18.66	0.00	-4.13E-05	9.80E-06	0.00E+00	4.24E-05
42.50	18.14	0.00	-4.28E-05	2.61E-06	0.00E+00	4.28E-05
42.52	17.61	0.00	-4.32E-05	-5.06E-06	0.00E+00	4.35E-05
42.89	16.63	0.00	-4.06E-05	-1.72E-05	0.00E+00	4.41E-05
43.22	16.22	0.00	-3.72E-05	-2.31E-05	0.00E+00	4.38E-05
43.63	15.88	0.00	-3.30E-05	-2.78E-05	0.00E+00	4.32E-05
44.28	15.60	0.00	-2.73E-05	-3.18E-05	0.00E+00	4.19E-05
44.97	15.48	0.00	-2.09E-05	-3.26E-05	0.00E+00	3.88E-05
45.66	15.55	0.00	-1.43E-05	-3.05E-05	0.00E+00	3.37E-05
46.16	15.74	0.00	-9.32E-06	-2.71E-05	0.00E+00	2.86E-05
46.60	16.02	0.00	-4.77E-06	-2.21E-05	0.00E+00	2.26E-05
46.98	16.40	0.00	-8.10E-07	-1.55E-05	0.00E+00	1.55E-05
47.27	16.84	0.00	2.85E-06	-7.53E-06	0.00E+00	8.05E-06

Table 7.5 (Continuing) Optimized Model Displacement Results at the Border of Excavation 1 - Case 2

Mid-Side Nodes						
Node Coordinates (m)			Displacements (m)			Vector Magnitude
x	y	z	Ux	Uy	Uz	
47.19	18.87	0.00	1.06E-05	2.17E-05	0.00E+00	2.41E-05
46.38	20.12	0.00	7.60E-07	3.62E-05	0.00E+00	3.62E-05
45.42	20.44	0.00	-8.35E-06	4.07E-05	0.00E+00	4.16E-05
44.51	20.46	0.00	-1.72E-05	3.85E-05	0.00E+00	4.22E-05
43.82	20.25	0.00	-2.51E-05	3.36E-05	0.00E+00	4.20E-05
43.19	19.75	0.00	-3.36E-05	2.57E-05	0.00E+00	4.23E-05
42.72	19.03	0.00	-3.98E-05	1.50E-05	0.00E+00	4.25E-05
42.54	18.40	0.00	-4.23E-05	6.31E-06	0.00E+00	4.28E-05
42.51	17.88	0.00	-4.33E-05	-1.32E-06	0.00E+00	4.34E-05
42.47	15.99	0.00	-4.29E-05	-1.15E-05	0.00E+00	4.45E-05
43.06	16.42	0.00	-3.91E-05	-2.03E-05	0.00E+00	4.41E-05
43.43	16.05	0.00	-3.52E-05	-2.57E-05	0.00E+00	4.36E-05
43.95	15.74	0.00	-3.03E-05	-3.04E-05	0.00E+00	4.29E-05
44.62	15.54	0.00	-2.42E-05	-3.29E-05	0.00E+00	4.08E-05
45.31	15.51	0.00	-1.76E-05	-3.23E-05	0.00E+00	3.67E-05
45.91	15.64	0.00	-1.18E-05	-2.92E-05	0.00E+00	3.15E-05
46.38	15.88	0.00	-6.96E-06	-2.49E-05	0.00E+00	2.59E-05
46.79	16.21	0.00	-2.67E-06	-1.91E-05	0.00E+00	1.93E-05
47.12	16.62	0.00	1.25E-06	-1.17E-05	0.00E+00	1.18E-05
47.40	17.35	0.00	6.19E-06	4.65E-07	0.00E+00	6.21E-06

Table 7.6 Optimized Model Displacement Results at the Border of Excavation 2 - Case 2

Corner Nodes						
Node Coordinates (m)			Displacements (m)			Vector Magnitude
x	y	z	Ux	Uy	Uz	
68.20	12.89	0.00	6.41E-05	-2.01E-07	0.00E+00	6.41E-05
68.09	13.99	0.00	6.34E-05	1.36E-05	0.00E+00	6.48E-05
67.91	14.53	0.00	6.19E-05	2.06E-05	0.00E+00	6.52E-05
67.75	15.04	0.00	5.94E-05	2.68E-05	0.00E+00	6.52E-05
67.20	16.00	0.00	5.31E-05	3.88E-05	0.00E+00	6.57E-05
66.46	16.82	0.00	4.45E-05	4.91E-05	0.00E+00	6.62E-05
65.56	17.47	0.00	3.42E-05	5.72E-05	0.00E+00	6.67E-05
64.00	18.14	0.00	1.68E-05	6.36E-05	0.00E+00	6.58E-05
62.63	18.33	0.00	-1.91E-06	6.36E-05	0.00E+00	6.36E-05
61.28	17.93	0.00	-1.90E-05	6.25E-05	0.00E+00	6.53E-05
60.27	17.48	0.00	-2.98E-05	5.71E-05	0.00E+00	6.44E-05
59.37	16.83	0.00	-3.99E-05	4.86E-05	0.00E+00	6.29E-05
58.63	16.01	0.00	-4.83E-05	3.78E-05	0.00E+00	6.14E-05
58.08	15.06	0.00	-5.50E-05	2.51E-05	0.00E+00	6.05E-05
57.73	14.00	0.00	-5.93E-05	1.10E-05	0.00E+00	6.03E-05
57.62	12.90	0.00	-6.12E-05	-4.14E-06	0.00E+00	6.14E-05
57.86	11.56	0.00	-6.08E-05	-2.11E-05	0.00E+00	6.44E-05
58.36	10.33	0.00	-5.59E-05	-3.52E-05	0.00E+00	6.61E-05
59.36	8.97	0.00	-4.39E-05	-4.94E-05	0.00E+00	6.61E-05
60.26	8.32	0.00	-3.26E-05	-5.78E-05	0.00E+00	6.63E-05
61.27	7.86	0.00	-2.03E-05	-6.31E-05	0.00E+00	6.63E-05
62.35	7.63	0.00	-7.09E-06	-6.56E-05	0.00E+00	6.60E-05
63.45	7.63	0.00	6.45E-06	-6.53E-05	0.00E+00	6.56E-05
64.54	7.86	0.00	1.98E-05	-6.21E-05	0.00E+00	6.52E-05
65.55	8.31	0.00	3.31E-05	-5.60E-05	0.00E+00	6.51E-05
67.19	9.78	0.00	5.10E-05	-3.97E-05	0.00E+00	6.47E-05
67.74	10.73	0.00	5.82E-05	-2.69E-05	0.00E+00	6.41E-05
68.08	11.79	0.00	6.29E-05	-1.37E-05	0.00E+00	6.44E-05

Table 7.6. (Continuing) Optimized Model Displacement Results at the Border of Excavation 2 - Case 2

Mid-Side Nodes						
Node Coordinates (m)			Displacements (m)			Vector Magnitude
x	y	z	Ux	Uy	Uz	
68.14	13.44	0.00	6.45E-05	6.73E-06	0.00E+00	6.48E-05
68.14	12.34	0.00	6.28E-05	1.72E-05	0.00E+00	6.51E-05
68.00	14.26	0.00	6.08E-05	2.37E-05	0.00E+00	6.53E-05
67.83	14.78	0.00	5.68E-05	3.33E-05	0.00E+00	6.58E-05
67.47	15.52	0.00	4.93E-05	4.44E-05	0.00E+00	6.63E-05
66.83	16.41	0.00	3.97E-05	5.37E-05	0.00E+00	6.68E-05
66.01	17.15	0.00	2.63E-05	6.19E-05	0.00E+00	6.73E-05
64.78	17.81	0.00	8.03E-06	6.48E-05	0.00E+00	6.53E-05
63.31	18.23	0.00	-1.11E-05	6.42E-05	0.00E+00	6.51E-05
61.96	18.13	0.00	-2.47E-05	6.06E-05	0.00E+00	6.54E-05
60.78	17.71	0.00	-3.51E-05	5.35E-05	0.00E+00	6.40E-05
59.82	17.16	0.00	-4.47E-05	4.37E-05	0.00E+00	6.25E-05
59.00	16.42	0.00	-5.22E-05	3.18E-05	0.00E+00	6.12E-05
58.36	15.53	0.00	-5.78E-05	1.83E-05	0.00E+00	6.06E-05
57.91	14.53	0.00	-6.09E-05	3.50E-06	0.00E+00	6.10E-05
57.68	13.45	0.00	-6.21E-05	-1.31E-05	0.00E+00	6.34E-05
57.74	12.23	0.00	-5.93E-05	-2.85E-05	0.00E+00	6.59E-05
58.11	10.94	0.00	-5.13E-05	-4.32E-05	0.00E+00	6.71E-05
58.86	9.65	0.00	-3.86E-05	-5.42E-05	0.00E+00	6.66E-05
59.81	8.64	0.00	-2.67E-05	-6.11E-05	0.00E+00	6.67E-05
60.76	8.09	0.00	-1.39E-05	-6.51E-05	0.00E+00	6.65E-05
61.81	7.75	0.00	-2.89E-07	-6.62E-05	0.00E+00	6.62E-05
62.90	7.63	0.00	1.34E-05	-6.45E-05	0.00E+00	6.59E-05
63.99	7.74	0.00	2.66E-05	-5.96E-05	0.00E+00	6.53E-05
65.04	8.08	0.00	4.39E-05	-5.00E-05	0.00E+00	6.65E-05
66.37	9.04	0.00	5.51E-05	-3.36E-05	0.00E+00	6.45E-05
67.46	10.26	0.00	6.13E-05	-2.05E-05	0.00E+00	6.46E-05
67.91	11.26	0.00	6.43E-05	-6.86E-06	0.00E+00	6.47E-05

7.3 Non-optimized and Optimized Models Comparison

After testing both the non-optimized and optimized models, the displacement results were compared at nodes located at the borders of excavations 1 and 2 where those nodes were defined by their coordinates as shown in Tables 7.7 and 7.8.

Table 7.7 Comparison of displacement results for Non-optimized Model and Optimized Model Case 1 at the Borders of Excavation 1

Corner Nodes						
Node Coordinates (m)			Difference (%)			
x	y	z	Ux	Uy	Uz	Magnitude
47.54	17.85	0.00	0.97	2.29	0.00	1.01
46.83	19.88	0.00	2.94	0.79	0.00	0.72
45.94	20.35	0.00	4.72	0.65	0.00	0.68
44.90	20.52	0.00	1.88	0.66	0.00	0.78
44.13	20.40	0.00	1.40	0.74	0.00	0.91
43.51	20.10	0.00	1.19	0.88	0.00	1.02
42.86	19.40	0.00	1.07	1.2	0.00	1.11
42.58	18.66	0.00	1.00	2.46	0.00	1.08
42.50	18.14	0.00	0.99	8.85	0.00	1.02
42.52	17.61	0.00	1.00	4.48	0.00	0.92
42.89	16.63	0.00	0.90	1.27	0.00	0.57
43.22	16.22	0.00	0.84	1.10	0.00	0.30
43.63	15.88	0.00	0.84	0.82	0.00	0.16
44.28	15.60	0.00	0.82	0.71	0.00	0.06
44.97	15.48	0.00	0.76	0.66	0.00	0.24
45.66	15.55	0.00	1.01	0.60	0.00	0.31
46.16	15.74	0.00	1.33	0.67	0.00	0.45
46.60	16.02	0.00	2.26	0.80	0.00	0.65
46.98	16.40	0.00	10.33	1.17	0.00	1.13
47.27	16.84	0.00	3.22	2.59	0.00	2.67

Table 7.7. (Continuing) Comparison of Displacement Results for Non-optimized Model and Optimized Model Case 1 at the Borders of Excavation 1

Mid-Side Nodes						
Node Coordinates (m)			Difference (%)			
x	y	z	Ux	Uy	Uz	Magnitude
47.19	18.87	0.00	0.74	1.05	0.00	0.71
46.38	20.12	0.00	20.28	0.68	0.00	0.67
45.42	20.44	0.00	2.57	0.64	0.00	0.72
44.51	20.46	0.00	1.59	0.70	0.00	0.84
43.82	20.25	0.00	1.28	0.80	0.00	0.97
43.19	19.75	0.00	1.11	1.02	0.00	1.08
42.72	19.03	0.00	1.03	1.64	0.00	1.10
42.54	18.40	0.00	1.00	3.75	0.00	1.06
42.51	17.88	0.00	1.00	18.96	0.00	0.98
42.47	15.99	0.00	0.90	2.06	0.00	0.71
43.06	16.42	0.00	0.86	1.19	0.00	0.43
43.43	16.05	0.00	0.83	0.96	0.00	0.21
43.95	15.74	0.00	0.80	0.81	0.00	0.00
44.62	15.54	0.00	0.73	0.70	0.00	0.19
45.31	15.51	0.00	0.86	0.63	0.00	0.28
45.91	15.64	0.00	1.14	0.62	0.00	0.37
46.38	15.88	0.00	1.66	0.71	0.00	0.53
46.79	16.21	0.00	3.72	0.93	0.00	0.83
47.12	16.62	0.00	8.37	1.60	0.00	1.67
47.40	17.35	0.00	1.27	28.39	0.00	0.94

Table 7.8 Comparison of Displacement Results for Non-optimized Model and Optimized Model Case 1 at the Borders of Excavation 2

Corner Nodes						
Node Coordinates (m)			Difference (%)			
x	y	z	Ux	Uy	Uz	Magnitude
68.20	12.89	0.00	0.50	97.02	0.00	0.50
68.09	13.99	0.00	0.55	4.40	0.00	0.73
67.91	14.53	0.00	0.57	3.07	0.00	0.83
67.75	15.04	0.00	0.60	2.45	0.00	0.92
67.20	16.00	0.00	0.65	1.79	0.00	1.05
66.46	16.82	0.00	0.72	1.47	0.00	1.13
65.56	17.47	0.00	0.82	1.28	0.00	1.15
64.00	18.14	0.00	1.23	1.13	0.00	1.13
62.63	18.33	0.00	11.37	1.06	0.00	1.06
61.28	17.93	0.00	0.42	0.98	0.00	0.87
60.27	17.48	0.00	0.09	0.94	0.00	0.73
59.37	16.83	0.00	0.07	0.93	0.00	0.59
58.63	16.01	0.00	0.17	0.95	0.00	0.47
58.08	15.06	0.00	0.26	1.04	0.00	0.39
57.73	14.00	0.00	0.34	1.53	0.00	0.38
57.62	12.90	0.00	0.44	2.00	0.00	0.43
57.86	11.56	0.00	0.56	0.01	0.00	0.50
58.36	10.33	0.00	0.69	0.13	0.00	0.53
59.36	8.97	0.00	0.92	0.13	0.00	0.47
60.26	8.32	0.00	1.19	0.08	0.00	0.35
61.27	7.86	0.00	1.71	0.02	0.00	0.18
62.35	7.63	0.00	4.07	0.06	0.00	0.01
63.45	7.63	0.00	3.41	0.15	0.00	0.19
64.54	7.86	0.00	0.68	0.28	0.00	0.32
65.55	8.31	0.00	0.11	0.45	0.00	0.36
67.19	9.78	0.00	0.25	1.00	0.00	0.21
67.74	10.73	0.00	0.36	1.78	0.00	0.00
68.08	11.79	0.00	0.43	4.10	0.00	0.25

Table 7.8. (Continuing) Comparison of Displacement Results for Non-optimized Model and Optimized Model Case 1 at the Borders of Excavation 2

Mid-Side Nodes						
Node Coordinates (m)			Difference (%)			
x	y	z	Ux	Uy	Uz	Magnitude
68.14	13.44	0.00	0.52	8.11	0.00	0.62
68.14	12.34	0.00	0.56	3.59	0.00	0.78
68.00	14.26	0.00	0.58	2.73	0.00	0.87
67.83	14.78	0.00	0.62	2.04	0.00	0.99
67.47	15.52	0.00	0.68	1.60	0.00	1.09
66.83	16.41	0.00	0.76	1.35	0.00	1.14
66.01	17.15	0.00	0.94	1.18	0.00	1.14
64.78	17.81	0.00	2.08	1.08	0.00	1.10
63.31	18.23	0.00	1.03	1.01	0.00	0.96
61.96	18.13	0.00	0.22	0.96	0.00	0.80
60.78	17.71	0.00	0.00	0.93	0.00	0.66
59.82	17.16	0.00	0.12	0.93	0.00	0.52
59.00	16.42	0.00	0.21	0.98	0.00	0.42
58.36	15.53	0.00	0.30	1.17	0.00	0.38
57.91	14.53	0.00	0.39	3.49	0.00	0.40
57.68	13.45	0.00	0.49	0.27	0.00	0.46
57.74	12.23	0.00	0.62	0.09	0.00	0.52
58.11	10.94	0.00	0.78	0.14	0.00	0.51
58.86	9.65	0.00	1.03	0.11	0.00	0.42
59.81	8.64	0.00	1.38	0.05	0.00	0.27
60.76	8.09	0.00	2.32	0.01	0.00	0.09
61.81	7.75	0.00	72.56	0.10	0.00	0.10
62.90	7.63	0.00	1.33	0.21	0.00	0.26
63.99	7.74	0.00	0.33	0.36	0.00	0.35
65.04	8.08	0.00	0.11	0.64	0.00	0.31
66.37	9.04	0.00	0.31	1.31	0.00	0.12
67.46	10.26	0.00	0.40	2.53	0.00	0.12
67.91	11.26	0.00	0.47	9.22	0.00	0.38

As can be seen from Tables 7.7 and 7.8, the maximum difference found in the displacement magnitude between the non-optimized mesh and the optimized mesh using 12-node transitional hexahedral elements was 2.67% for both corner and mid-side nodes at the borders of Excavation 1 and 1.15% for both corner and mid-side nodes at the borders of Excavation 2.

Table 7.9 Comparison of Displacement Results for Non-optimized Model and Optimized Model Case 2 at the Borders of Excavation 1

Corner Nodes						
Node Coordinates (m)			Difference (%)			
x	y	z	Ux	Uy	Uz	Magnitude
47.54	17.85	0.00	0.16	3.65	0.00	2.16
46.83	19.88	0.00	0.24	1.91	0.00	1.88
45.94	20.35	0.00	1.82	1.64	0.00	1.64
44.90	20.52	0.00	1.37	1.55	0.00	1.54
44.13	20.40	0.00	1.34	1.53	0.00	1.48
43.51	20.10	0.00	1.36	1.54	0.00	1.45
42.86	19.40	0.00	1.45	1.61	0.00	1.48
42.58	18.66	0.00	1.49	2.03	0.00	1.52
42.50	18.14	0.00	1.54	4.74	0.00	1.55
42.52	17.61	0.00	1.61	0.75	0.00	1.58
42.89	16.63	0.00	1.56	0.48	0.00	1.40
43.22	16.22	0.00	1.53	0.37	0.00	1.21
43.63	15.88	0.00	1.61	0.56	0.00	1.18
44.28	15.60	0.00	1.69	0.53	0.00	1.03
44.97	15.48	0.00	1.73	0.48	0.00	0.85
45.66	15.55	0.00	2.23	0.47	0.00	0.79
46.16	15.74	0.00	2.81	0.32	0.00	0.60
46.60	16.02	0.00	4.32	0.12	0.00	0.32
46.98	16.40	0.00	16.62	0.37	0.00	0.31
47.27	16.84	0.00	3.76	2.09	0.00	2.29

Table 7.9. (Continuing) Comparison of Displacement Results for Non-optimized Model and Optimized Model Case 2 at the Borders of Excavation 1

Mid-Side Nodes						
Node Coordinates (m)			Difference (%)			
x	y	z	Ux	Uy	Uz	Magnitude
47.19	18.87	0.00	0.37	2.21	0.00	1.86
46.38	20.12	0.00	3.40	1.72	0.00	1.71
45.42	20.44	0.00	1.45	1.57	0.00	1.57
44.51	20.46	0.00	1.34	1.54	0.00	1.51
43.82	20.25	0.00	1.35	1.53	0.00	1.47
43.19	19.75	0.00	1.40	1.55	0.00	1.45
42.72	19.03	0.00	1.47	1.71	0.00	1.50
42.54	18.40	0.00	1.52	2.55	0.00	1.54
42.51	17.88	0.00	1.58	6.71	0.00	1.57
42.47	15.99	0.00	1.54	0.09	0.00	1.44
43.06	16.42	0.00	1.53	0.40	0.00	1.30
43.43	16.05	0.00	1.56	0.45	0.00	1.18
43.95	15.74	0.00	1.62	0.49	0.00	1.06
44.62	15.54	0.00	1.66	0.49	0.00	0.91
45.31	15.51	0.00	1.95	0.48	0.00	0.82
45.91	15.64	0.00	2.47	0.41	0.00	0.71
46.38	15.88	0.00	3.37	0.24	0.00	0.48
46.79	16.21	0.00	6.60	0.06	0.00	0.08
47.12	16.62	0.00	11.71	0.90	0.00	1.01
47.40	17.35	0.00	0.82	34.94	0.00	0.43

Table 7.10 Comparison of Displacement Results for Non-optimized Model and Optimized Model Case 2 at the Borders of Excavation 2

Corner Nodes						
Node Coordinates (m)			Difference (%)			
x	y	z	Ux	Uy	Uz	Magnitude
68.20	12.89	0.00	1.95	132.92	0.00%	1.96
68.09	13.99	0.00	2.05	6.67	0.00%	2.27
67.91	14.53	0.00	2.11	4.85	0.00%	2.39
67.75	15.04	0.00	2.19	4.00	0.00%	2.50
67.20	16.00	0.00	2.37	3.09	0.00%	2.62
66.46	16.82	0.00	2.64	2.63	0.00%	2.64
65.56	17.47	0.00	3.10	2.36	0.00%	2.56
64.00	18.14	0.00	5.01	2.13	0.00%	2.32
62.63	18.33	0.00	52.73	2.01	0.00%	1.98
61.28	17.93	0.00	2.41	1.84	0.00%	1.50
60.27	17.48	0.00	0.98	1.75	0.00%	1.19
59.37	16.83	0.00	0.31	1.67	0.00%	0.89
58.63	16.01	0.00	0.06	1.60	0.00%	0.65
58.08	15.06	0.00	0.33	1.53	0.00%	0.54
57.73	14.00	0.00	0.54	1.47	0.00%	0.57
57.62	12.90	0.00	0.72	1.23	0.00%	0.72
57.86	11.56	0.00	0.91	1.27	0.00%	0.95
58.36	10.33	0.00	1.07	1.18	0.00%	1.10
59.36	8.97	0.00	1.27	1.05	0.00%	1.15
60.26	8.32	0.00	1.43	0.93	0.00%	1.05
61.27	7.86	0.00	1.63	0.82	0.00%	0.89
62.35	7.63	0.00	2.28	0.69	0.00%	0.71
63.45	7.63	0.00	0.51	0.54	0.00%	0.54
64.54	7.86	0.00	1.24	0.35	0.00%	0.44
65.55	8.31	0.00	1.43	0.11	0.00%	0.46
67.19	9.78	0.00	1.67	0.67	0.00%	0.80
67.74	10.73	0.00	1.76	1.74	0.00%	1.17
68.08	11.79	0.00	1.85	4.91	0.00%	1.57

Table 7.10. (Continuing) Comparison of Displacement Results for Non-optimized Model and Optimized Model Case 2 at the Borders of Excavation 2

Mid-Side Nodes						
Node Coordinates (m)			Difference (%)			
x	y	z	Ux	Uy	Uz	Magnitude
68.14	13.44	0.00	1.99	11.73	0.00	2.11
68.14	12.34	0.00	2.08	5.55	0.00	2.33
68.00	14.26	0.00	2.15	4.38	0.00	2.45
67.83	14.78	0.00	2.26	3.43	0.00	2.56
67.47	15.52	0.00	2.48	2.82	0.00	2.63
66.83	16.41	0.00	2.83	2.47	0.00	2.60
66.01	17.15	0.00	3.67	2.21	0.00	2.43
64.78	17.81	0.00	8.87	2.05	0.00	2.16
63.31	18.23	0.00	5.23	1.91	0.00	1.72
61.96	18.13	0.00	1.51	1.79	0.00	1.34
60.78	17.71	0.00	0.59	1.71	0.00	1.03
59.82	17.16	0.00	0.10	1.63	0.00	0.76
59.00	16.42	0.00	0.21	1.56	0.00	0.58
58.36	15.53	0.00	0.44	1.48	0.00	0.54
57.91	14.53	0.00	0.63	1.44	0.00	0.64
57.68	13.45	0.00	0.82	1.31	0.00	0.84
57.74	12.23	0.00	0.99	1.23	0.00	1.03
58.11	10.94	0.00	1.16	1.11	0.00	1.14
58.86	9.65	0.00	1.34	0.99	0.00	1.11
59.81	8.64	0.00	1.51	0.87	0.00	0.98
60.76	8.09	0.00	1.82	0.75	0.00	0.80
61.81	7.75	0.00	19.56	0.62	0.00	0.62
62.90	7.63	0.00	1.04	0.45	0.00	0.48
63.99	7.74	0.00	1.34	0.24	0.00	0.43
65.04	8.08	0.00	1.54	0.18	0.00	0.58
66.37	9.04	0.00	1.71	1.09	0.00	0.98
67.46	10.26	0.00	1.80	2.77	0.00	1.37
67.91	11.26	0.00	1.89	11.89	0.00	1.76

As can be observed from Tables 7.9 and 7.10, the maximum difference found in the displacement magnitude between the non-optimized mesh and the optimized mesh using

16-node transitional hexahedral elements was 2.29% for both the corner and mid-side nodes at the borders of Excavation 1 and 2.64% for both corner and mid-side nodes at the borders of Excavation 2.

The compared results indicated that both optimized and non-optimized meshes using both kinds of transitional elements 12-node and 16-node led to very close results with small differences.

7.4 Benefits of Mesh Optimization

In the previous section, a comparison between the optimized and non-optimized mesh was conducted to study the behavior of the transition elements and their effects on solution accuracy. Because the essence of applying the p-type mesh technique is to reduce computation time and resource requirements, a cost of computation was performed using the memory footprint of global stiffness matrix, and the time required to acquire the solution. Also, the model characteristics such as number of nodes or elements and the number of degrees of freedom were compared.

The analysis of all of the models was conducted using a computer with 32 GB RAM, Intel Xeon W3565 3.2GHz processor and Mac OSX 10.9 as the operating system. Tables 7.11 and 7.12 summarize the effect of p-type mesh optimization on computational resources.

The first entry is the non-optimized model that consisted of second-order hexahedral elements. It required un-compressed matrix storage of 6.64 GB and solution time of 2093 seconds.

The models with transition elements needed less than half as much memory and solution time as non-optimized models with all second-order hexahedral elements.

A more illustrative summary of requirements and solution times is shown in Table 7.12, where all quantities were made relative to the non-optimized model. Models with transition zones possess the benefits of relatively fast solution times and solution accuracy of second-order elements translating into savings in memory usage of around 82% (Case 1 compared to the non-optimized model) and around 81% (Case 2 compared to the non-optimized model) while solution times were reduced by around 82% (Case 1 compared to the non-optimized model) and around 81% (Case 2 compared to the non-optimized model) as shown in Figure 7.6.

Table 7.11 Use of Computational Resources Comparison for Underground Excavation Models

Model	No. of Nodes	No. of Elements	No. of Degrees of Freedom	Size of Global Stiffness Matrix (Bytes)	Solution Time (CPU) (sec)
Non-optimized Model	14738	2005	29861	7,133,434,568	2093
Optimized Model					
Case 1	6248	2005	12622	1,274,519,072	367
Case 2	6350	2005	12934	1,338,306,848	388

Table 7.12 Ratio of Computational Resource Requirements for Underground Excavation Models

Model	Size of Global Stiffness Matrix Ratio	Solution Time (CPU) Ratio
Non-optimized Model	1.00	1.00
Optimized Model		
Case 1	5.6	5.7
Case 2	5.33	5.39

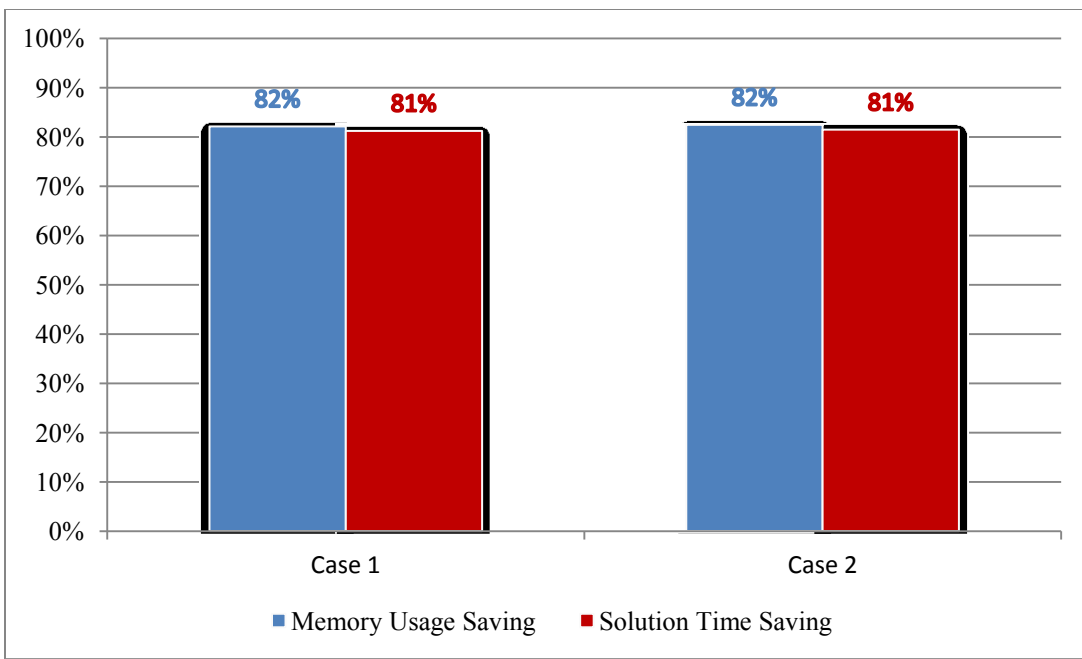


Figure 7.6 Memory Usage and Solution Time Savings for Cases 1 and 2 in Comparison to the Non-optimized Model

8. Conclusion

The behavior of 12-node and 16-node transitional hexahedral elements was tested and verified, and the p-type mesh optimization method was applied to underground excavations problems with successful results implementing the ability of using these elements without affecting the solution accuracy, as presented in the previous chapter. Therefore, it can be said that this thesis presented a reliable approach for stress analysis optimization problems in geomechanics field concluding the following points:

- It is possible to use mixed meshes with transitional elements connecting linear and quadratic elements in a finite element method (FEM) to solve stress analysis problems in geomechanics problems.
- Using sim|FEM software, which includes the formulation of transition elements and allows the application of mesh optimization in finite element analysis, leads to noticeable savings in computational resources needed to solve the problems. Hence, improving the commercial software available can be a powerful tool in solving geomechanics problems.
- Future researchers interested in studying transitional elements or mesh optimization process can rely on this thesis as a reference. In addition to the possibility of using sim|FEM code as it is capable of dealing with mixed meshes.
- Applying p-type method to underground excavation example lead to considerable saving in computational resources as concluded in Chapter 7, where a maximum of around 82% saving in memory usage and a maximum of around 82% saving in solution times were obtained of optimized models compared to non-optimized model.

9. Recommendations for Further Work

This thesis studied 3D transitional element behavior through the application of a p-type method of mesh optimization to an underground excavation problem using a finite element method (FEM) with hexahedral elements and two kinds of transitional hexahedral elements: 12-node and 16-node elements.

By implementing the same concept of mesh optimization and maybe by using different numerical analysis methods, future work can be done by investigating different problems in geotechnical engineering. For example, in foundation problems, the change in the stress status in the soil profile due to the construction of a foundation can be found and the optimization may be applied to the zones of the mesh that are undergoing not more than 5% disturbance in the medium in comparison to the initial stress field existed prior the construction process.

In addition, other formulations of transitional elements can be tested depending on the studied model or even a completely different shape of elements such as tetrahedral elements.

Also, as sim|FEM code does not yet support 3D visualization of the tested problems, a script was written in TCL to allow the visualization of 3D linear and quadratic elements only. Hence, sim|FEM code can be improved to include that feature of 3D visualization or another supported code can be written to enable the 3D visualization of meshes with transitional elements.

10. List of References

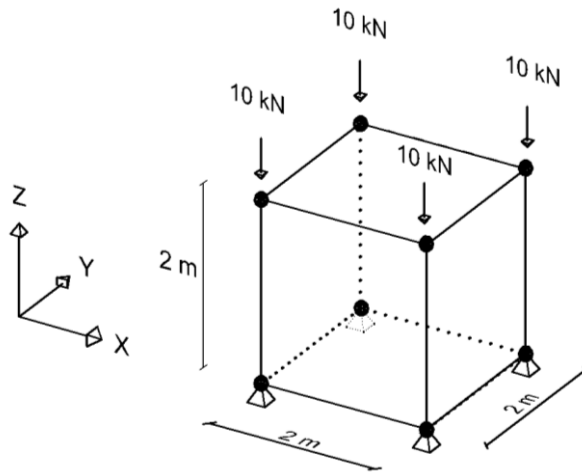
1. Abaqus. (2007). “Abaqus/Standard user's manual”. Version 6.7 (Student Version), Hibbit, Karlsson, & Sorensen, Inc.
2. Davis, R. O. and Selvadurai, A. P. S. (1996). *Elasticity and Geomechanics*. New York: Cambridge University Press.
3. Desai, C. S. and Christian, J. T. (1977). *Numerical methods in geotechnical engineering*. New York: McGraw-Hill Inc.
4. Desai, C. S. and Gioda, G. (1990). *Numerical methods and constitutive modelling in geomechanics*. New York: Springer.
5. Dhondt, G. (2004). *The Finite Element Method for Three-dimensional Thermomechanical Applications*. Munich: John Wiley & Sons Ltd.
6. Felippa, C. (2013). Ch.11 (Hexahedron Elements) Advanced Finite Element Methods Course. Advanced Finite Element Methods Course. <<http://www.colorado.edu/engineering/CAS/courses.d/AFEM.d>> (May. 8, 2013).
7. Felippa, C. (2010). Introduction to Finite Element Method cours. *University of Boulder, Colorado*. <www.colorado.edu/engineering/CAS/courses.d/IFEM.d/Home.html> (Dec. 9, 2013).

8. Garcia Rosero, D.F. (2011). *Finite element mesh optimization using the partial p-adaptive method for stress analysis of underground excavations*. M.A.Sc. Thesis, Dept. BCEE, Montreal, Canada: Concordia University.
9. Gupta, A. K. (1978). A finite element for transition from a fine to a coarse grid. *International Journal for Numerical Methods in Engineering*, 12, 35-45.
10. Hutton, D.V. (2005). *Fundamentals of finite element analysis*. India: McGraw-Hill Education, Pvt Limited.
11. Hoek, E. (2007). *Practical Rock Engineering*. Vancouver: Rocscience inc.
12. Jaeger, J.C, Cook, N.G.W, and Zimmerman, R.W. (2007). *Fundamentals of Rock Mechanics* (4th ed.). Oxford: Blackwell.
13. Jing, L., and Stephansson. (2007). *Fundamentals of Discrete Element Methods for Rock Engineering: Theory and Application*. Amsterdam: Elsevier B.V.
14. Katsikadelis, J.T. (2002). *Boundary elements: Theory and Applications*. Elsevier Science Ltd.
15. Kitware, Inc. (2010). *VTK User's Guide, 11th edition*. Kitware, Inc.
16. LISA, (2012). LISA Version 7.7.1. LISA-Finite Element Technologies (Sonnenhof Holdings). <<http://www.lisa-fet.com>>
17. Liu, G.R, and Quek, S.S. (2003). *The Finite Element Method: A Practical Course*. Department of Mechanical Engineering, National University of Singapore. Oxford: Elsevier Science Ltd.

18. Logan, D.L. (2007). *A First Course in the Finite Element Method* (4 ed.). Delhi: Nelson.
19. Maidl, B., Leonhard, S., Ritz, W., and Herrenknecht, M. (2008). *Hardrock tunnel Boring Machines*. Berlin: Ernst and Sohn.
20. Morton, D.J, Tyler, J. M., and Dorroh J. R. (1995). A New 3D Finite Element for Adaptive h-Refinement 1-Irrigular Meshes. *International Journal for Numerical Methods in Engineering*, 38, 3989-4008.
21. Potts, D. M. and Zdravkovic, L. (1999). *Finite Element Analysis in Geotechnical Engineering*. Heron Quay, (T. a. Imperial College of Science, Ed.) Thomas Telford.
22. Smith, I. M. and Griffiths, D. (2004). *Programming the finite element method* (4 ed.). Chichester: John Wiley & Sons Ltd.
23. Ramamurthy, T. (2007). *Engineering in rocks for slopes, foundations and tunnels*, 2nd Ed., Delhi: PHI.
24. Zsaki, A.M. (2010). sim|FEM [Software]. Montreal: Concordia University.
25. Zienkiewicz, O.C., Taylor, R.L. and Zhu, J.Z. (2013). *The Finite Element Method: its Basis and Fundamentals*, 6th Ed., Burlington: Elsevier Ltd.
26. Zsaki, A.M and Curran, J.H. (2005). A continuum mechanics based framework for optimizing boundary and finite element meshes associated with underground excavations – framework. *International Journal for Numerical and Analytical Methods in Geomechanics*, 29 (13), 1271-1298.

Appendix 1

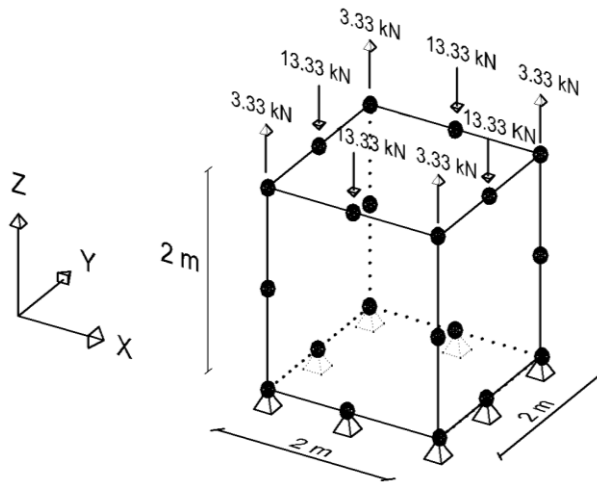
Type I Models Using (STRHEX08L) - Results



NAME	SOFTWARE	DISPLACEMENTS				
		Node Location	Ux (m)	Uy (m)	Uz (m)	Vector Magnitude
STRHEX08LR	sim FEM	(0,0,0)	0.000000E+00	0.000000E+00	0.000000E+00	0.000000E+00
		(2,0,0)	0.000000E+00	0.000000E+00	0.000000E+00	0.000000E+00
		(2,2,0)	0.000000E+00	0.000000E+00	0.000000E+00	0.000000E+00
		(0,2,0)	0.000000E+00	0.000000E+00	0.000000E+00	0.000000E+00
		(0,0,2)	-6.000000E-03	-6.000000E-03	-2.000000E-02	2.1725561E-02
		(2,0,2)	6.000000E-03	-6.000000E-03	-2.000000E-02	2.1725561E-02
		(2,2,2)	6.000000E-03	6.000000E-03	-2.000000E-02	2.1725561E-02
		(0,2,2)	-6.000000E-03	6.000000E-03	-2.000000E-02	2.1725561E-02
STRHEX08LR	ABAQUS	Node Location	Ux (m)	Uy (m)	Uz (m)	Vector Magnitude
		(0,0,0)	0.000000E+00	0.000000E+00	0.000000E+00	0.000000E+00
		(2,0,0)	0.000000E+00	0.000000E+00	0.000000E+00	0.000000E+00
		(2,2,0)	0.000000E+00	0.000000E+00	0.000000E+00	0.000000E+00
		(0,2,0)	0.000000E+00	0.000000E+00	0.000000E+00	0.000000E+00
		(0,0,2)	-5.9848100E-03	-5.9848100E-03	-1.9987000E-02	2.1705208E-02
		(2,0,2)	5.9848100E-03	-5.9848100E-03	-1.9987000E-02	2.1705208E-02
		(2,2,2)	5.9848100E-03	5.9848100E-03	-1.9987000E-02	2.1705208E-02
		(0,2,2)	-5.9848100E-03	5.9848100E-03	-1.9987000E-02	2.1705208E-02

		Node Location	Ux (m)	Uy (m)	Uz (m)	Vector Magnitude
STRHEX08LF	sim FEM	(0,0,0)	0.0000000E+00	0.0000000E+00	0.0000000E+00	0.0000000E+00
		(2,0,0)	0.0000000E+00	0.0000000E+00	0.0000000E+00	0.0000000E+00
		(2,2,0)	0.0000000E+00	0.0000000E+00	0.0000000E+00	0.0000000E+00
		(0,2,0)	0.0000000E+00	0.0000000E+00	0.0000000E+00	0.0000000E+00
		(0,0,2)	-3.9000000E-03	-3.9000000E-03	-1.8200000E-02	1.9017360E-02
		(2,0,2)	3.9000000E-03	-3.9000000E-03	-1.8200000E-02	1.9017360E-02
		(2,2,2)	3.9000000E-03	3.9000000E-03	-1.8200000E-02	1.9017360E-02
		(0,2,2)	-3.9000000E-03	3.9000000E-03	-1.8200000E-02	1.9017360E-02
STRHEX08LF	ABAQUS	Node Location	Ux (m)	Uy (m)	Uz (m)	Vector Magnitude
		(0,0,0)	0.0000000E+00	0.0000000E+00	0.0000000E+00	0.0000000E+00
		(2,0,0)	0.0000000E+00	0.0000000E+00	0.0000000E+00	0.0000000E+00
		(2,2,0)	0.0000000E+00	0.0000000E+00	0.0000000E+00	0.0000000E+00
		(0,2,0)	0.0000000E+00	0.0000000E+00	0.0000000E+00	0.0000000E+00
		(0,0,2)	-5.2193300E-03	-5.2193300E-03	-1.9330900E-02	2.0692185E-02
		(2,0,2)	5.2193300E-03	-5.2193300E-03	-1.9330900E-02	2.0692185E-02
		(2,2,2)	5.2193300E-03	5.2193300E-03	-1.9330900E-02	2.0692185E-02
		(0,2,2)	-5.2193300E-03	5.2193300E-03	-1.9330900E-02	2.0692185E-02
STRHEX08LF	LISA	Node Location	Ux (m)	Uy (m)	Uz (m)	Vector Magnitude
		(0,0,0)	0.0000000E+00	0.0000000E+00	0.0000000E+00	0.0000000E+00
		(2,0,0)	0.0000000E+00	0.0000000E+00	0.0000000E+00	0.0000000E+00
		(2,2,0)	0.0000000E+00	0.0000000E+00	0.0000000E+00	0.0000000E+00
		(0,2,0)	0.0000000E+00	0.0000000E+00	0.0000000E+00	0.0000000E+00
		(0,0,2)	-3.9000000E-03	-3.9000000E-03	-1.8200000E-02	1.9017360E-02
		(2,0,2)	3.9000000E-03	-3.9000000E-03	-1.8200000E-02	1.9017360E-02
		(2,2,2)	3.9000000E-03	3.9000000E-03	-1.8200000E-02	1.9017360E-02
		(0,2,2)	-3.9000000E-03	3.9000000E-03	-1.8200000E-02	1.9017360E-02

Type I Models Using (STRHEX20Q) - Results



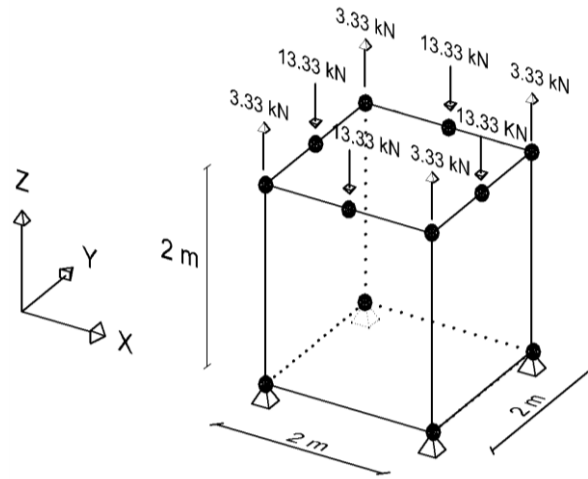
NAME	SOFTWARE	DISPLACEMENTS				
		Node Location	Ux (m)	Uy (m)	Uz (m)	Vector Magnitude
STRHEX20QR	sim FEM	(0,0,0)	0.000000E+00	0.000000E+00	0.000000E+00	0.000000E+00
		(2,0,0)	0.000000E+00	0.000000E+00	0.000000E+00	0.000000E+00
		(2,2,0)	0.000000E+00	0.000000E+00	0.000000E+00	0.000000E+00
		(0,2,0)	0.000000E+00	0.000000E+00	0.000000E+00	0.000000E+00
		(0,0,2)	-1.6470588E-03	-1.6470588E-03	-1.8352941E-02	1.8500163E-02
		(2,0,2)	1.6470588E-03	-1.6470588E-03	-1.8352941E-02	1.8500163E-02
		(2,2,2)	1.6470588E-03	1.6470588E-03	-1.8352941E-02	1.8500163E-02
		(0,2,2)	-1.6470588E-03	1.6470588E-03	-1.8352941E-02	1.8500163E-02
		(1,0,0)	0.000000E+00	0.000000E+00	0.000000E+00	0.000000E+00
		(2,1,0)	0.000000E+00	0.000000E+00	0.000000E+00	0.000000E+00
		(1,2,0)	0.000000E+00	0.000000E+00	0.000000E+00	0.000000E+00
		(0,1,0)	0.000000E+00	0.000000E+00	0.000000E+00	0.000000E+00
		(1,0,2)	0.000000E+00	-1.6470588E-03	-1.9058824E-02	1.9129861E-02
		(2,1,2)	1.6470588E-03	0.000000E+00	-1.9058824E-02	1.9129861E-02
		(1,2,2)	0.000000E+00	1.6470588E-03	-1.9058824E-02	1.9129861E-02
		(0,1,2)	-1.6470588E-03	0.000000E+00	-1.9058824E-02	1.9129861E-02
		(0,0,1)	-3.4705882E-03	-3.4705882E-03	-8.8235294E-03	1.0096764E-02
		(2,0,1)	3.4705882E-03	-3.4705882E-03	-8.8235294E-03	1.0096764E-02
		(2,2,1)	3.4705882E-03	3.4705882E-03	-8.8235294E-03	1.0096764E-02
		(0,2,1)	-3.4705882E-03	3.4705882E-03	-8.8235294E-03	1.0096764E-02

		Node Location	Ux (m)	Uy (m)	Uz (m)	Vector Magnitude
STRHEX20QR	ABAQUS	(0,0,0)	0.0000000E+00	0.0000000E+00	0.0000000E+00	0.0000000E+00
		(2,0,0)	0.0000000E+00	0.0000000E+00	0.0000000E+00	0.0000000E+00
		(2,2,0)	0.0000000E+00	0.0000000E+00	0.0000000E+00	0.0000000E+00
		(0,2,0)	0.0000000E+00	0.0000000E+00	0.0000000E+00	0.0000000E+00
		(0,0,2)	-2.0542500E-03	-1.8352900E-02	-1.2398700E-03	1.8509083E-02
		(2,0,2)	2.0542500E-03	-1.8352900E-02	-1.2398700E-03	1.8509083E-02
		(2,2,2)	2.0542500E-03	-1.8352900E-02	1.2398700E-03	1.8509083E-02
		(0,2,2)	-2.0542500E-03	-1.8352900E-02	1.2398700E-03	1.8509083E-02
		(1,0,0)	0.0000000E+00	0.0000000E+00	0.0000000E+00	0.0000000E+00
		(2,1,0)	0.0000000E+00	0.0000000E+00	0.0000000E+00	0.0000000E+00
		(1,2,0)	0.0000000E+00	0.0000000E+00	0.0000000E+00	0.0000000E+00
		(0,1,0)	0.0000000E+00	0.0000000E+00	0.0000000E+00	0.0000000E+00
		(1,0,2)	3.5236600E-18	-1.9058800E-02	-1.8506500E-03	1.9148440E-02
		(2,1,2)	1.4434600E-03	-1.9058800E-02	0.0000000E+00	1.9113384E-02
		(1,2,2)	1.6371500E-17	-1.9058800E-02	1.8506500E-03	1.9148440E-02
		(0,1,2)	-1.4434600E-03	-1.9058800E-02	0.0000000E+00	1.9113384E-02
		(0,0,1)	-3.6741800E-03	-8.8235300E-03	-3.2669900E-03	1.0100866E-02
		(2,0,1)	3.6741800E-03	-8.8235300E-03	-3.2669900E-03	1.0100866E-02
		(2,2,1)	3.6741800E-03	-8.8235300E-03	3.2669900E-03	1.0100866E-02
		(0,2,1)	-3.6741800E-03	-8.8235300E-03	3.2669900E-03	1.0100866E-02
STRHEX20QF	Sim FEM	Node Location	Ux (m)	Uy (m)	Uz (m)	Vector Magnitude
		(0,0,0)	0.0000000E+00	0.0000000E+00	0.0000000E+00	0.0000000E+00
		(2,0,0)	0.0000000E+00	0.0000000E+00	0.0000000E+00	0.0000000E+00
		(2,2,0)	0.0000000E+00	0.0000000E+00	0.0000000E+00	0.0000000E+00
		(0,2,0)	0.0000000E+00	0.0000000E+00	0.0000000E+00	0.0000000E+00
		(0,0,2)	-2.8239842E-03	-2.8239842E-03	-1.9346317E-02	1.9754234E-02
		(2,0,2)	2.8239842E-03	-2.8239842E-03	-1.9346317E-02	1.9754234E-02
		(2,2,2)	2.8239842E-03	2.8239842E-03	-1.9346317E-02	1.9754234E-02
		(0,2,2)	-2.8239842E-03	2.8239842E-03	-1.9346317E-02	1.9754234E-02
		(1,0,0)	0.0000000E+00	0.0000000E+00	0.0000000E+00	0.0000000E+00
		(2,1,0)	0.0000000E+00	0.0000000E+00	0.0000000E+00	0.0000000E+00
		(1,2,0)	0.0000000E+00	0.0000000E+00	0.0000000E+00	0.0000000E+00
		(0,1,0)	0.0000000E+00	0.0000000E+00	0.0000000E+00	0.0000000E+00
		(1,0,2)	0.0000000E+00	-2.8038739E-03	-1.9100525E-02	1.9305226E-02
		(2,1,2)	2.8038739E-03	0.0000000E+00	-1.9100525E-02	1.9305226E-02
		(1,2,2)	0.0000000E+00	2.8038739E-03	-1.9100525E-02	1.9305226E-02

		Node Location	Ux (m)	Uy (m)	Uz (m)	Vector Magnitude
STRHEX20QF	Sim FEM	(0,1,2)	-2.8038739E-03	0.0000000E+00	-1.9100525E-02	1.9305226E-02
		(0,0,1)	-2.9453288E-03	-2.9453288E-03	-9.0708922E-03	9.9815334E-03
		(2,0,1)	2.9453288E-03	-2.9453288E-03	-9.0708922E-03	9.9815334E-03
		(2,2,1)	2.9453288E-03	2.9453288E-03	-9.0708922E-03	9.9815334E-03
		(0,2,1)	-2.9453288E-03	2.9453288E-03	-9.0708922E-03	9.9815334E-03
		Node Location	Ux (m)	Uy (m)	Uz (m)	Vector Magnitude
STRHEX20QF	ABAQUS	(0,0,0)	0.0000000E+00	0.0000000E+00	0.0000000E+00	0.0000000E+00
		(2,0,0)	0.0000000E+00	0.0000000E+00	0.0000000E+00	0.0000000E+00
		(2,2,0)	0.0000000E+00	0.0000000E+00	0.0000000E+00	0.0000000E+00
		(0,2,0)	0.0000000E+00	0.0000000E+00	0.0000000E+00	0.0000000E+00
		(0,0,2)	-2.8239800E-03	-1.9346300E-02	-2.8239800E-03	1.9754216E-02
		(2,0,2)	2.8239800E-03	-1.9346300E-02	-2.8239800E-03	1.9754216E-02
		(2,2,2)	2.8239800E-03	-1.9346300E-02	2.8239800E-03	1.9754216E-02
		(0,2,2)	-2.8239800E-03	-1.9346300E-02	2.8239800E-03	1.9754216E-02
		(1,0,0)	0.0000000E+00	0.0000000E+00	0.0000000E+00	0.0000000E+00
		(2,1,0)	0.0000000E+00	0.0000000E+00	0.0000000E+00	0.0000000E+00
		(1,2,0)	0.0000000E+00	0.0000000E+00	0.0000000E+00	0.0000000E+00
		(0,1,0)	0.0000000E+00	0.0000000E+00	0.0000000E+00	0.0000000E+00
STRHEX20QF	ABAQUS	Node Location	Ux (m)	Uy (m)	Uz (m)	Vector Magnitude
		(1,0,2)	0.0000000E+00	-1.9100500E-02	-2.8038700E-03	1.9305201E-02
		(2,1,2)	2.8038700E-03	-1.9100500E-02	0.0000000E+00	1.9305201E-02
		(1,2,2)	-5.4210100E-17	-1.9100500E-02	2.8038700E-03	1.9305201E-02
		(0,1,2)	-2.8038700E-03	-1.9100500E-02	0.0000000E+00	1.9305201E-02
		(0,0,1)	-2.9453300E-03	-9.0708900E-03	-2.9453300E-03	9.9815321E-03
		(2,0,1)	2.9453300E-03	-9.0708900E-03	-2.9453300E-03	9.9815321E-03
		(2,2,1)	2.9453300E-03	-9.0708900E-03	2.9453300E-03	9.9815321E-03
		(0,2,1)	-2.9453300E-03	-9.0708900E-03	2.9453300E-03	9.9815321E-03
		Node Location	Ux (m)	Uy (m)	Uz (m)	Vector Magnitude
STRHEX20QF	LISA	(0,0,0)	0.0000000E+00	0.0000000E+00	0.0000000E+00	0.0000000E+00
		(2,0,0)	0.0000000E+00	0.0000000E+00	0.0000000E+00	0.0000000E+00
		(2,2,0)	0.0000000E+00	0.0000000E+00	0.0000000E+00	0.0000000E+00
		(0,2,0)	0.0000000E+00	0.0000000E+00	0.0000000E+00	0.0000000E+00
		(0,0,2)	-2.8242240E-03	-1.9347060E-02	-2.8242240E-03	1.9755030E-02
		(2,0,2)	-2.8242240E-03	-1.9347060E-02	2.8242240E-03	1.9755030E-02
		(2,2,2)	2.8242240E-03	-1.9347060E-02	2.8242240E-03	1.9755030E-02
		(0,2,2)	2.8242240E-03	-1.9347060E-02	-2.8242240E-03	1.9755030E-02

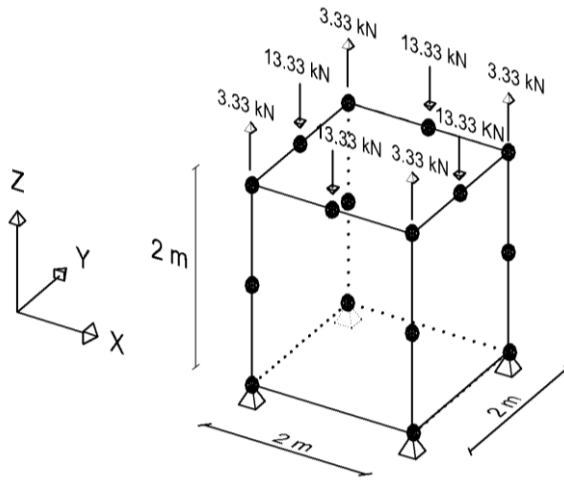
		Node Location	Ux (m)	Uy (m)	Uz (m)	Vector Magnitude
STRHEX20QF	LISA	(1,0,0)	0.0000000E+00	0.0000000E+00	0.0000000E+00	0.0000000E+00
		(2,1,0)	0.0000000E+00	0.0000000E+00	0.0000000E+00	0.0000000E+00
		(1,2,0)	0.0000000E+00	0.0000000E+00	0.0000000E+00	0.0000000E+00
		(0,1,0)	0.0000000E+00	0.0000000E+00	0.0000000E+00	0.0000000E+00
		(1,0,2)	-2.9452980E-03	-9.0712170E-03	-2.9452980E-03	9.9818104E-03
		(2,1,2)	-2.9452980E-03	-9.0712170E-03	2.9452980E-03	9.9818104E-03
		(1,2,2)	2.9452980E-03	-9.0712170E-03	2.9452980E-03	9.9818104E-03
		(0,1,2)	2.9452980E-03	-9.0712170E-03	-2.9452980E-03	9.9818104E-03
		(0,0,1)	-2.8040690E-03	-1.9100720E-02	0.0000000E+00	1.9305448E-02
		(2,0,1)	0.0000000E+00	-1.9100720E-02	2.8040690E-03	1.9305448E-02
		(2,2,1)	2.8040690E-03	-1.9100720E-02	0.0000000E+00	1.9305448E-02
		(0,2,1)	0.0000000E+00	-1.9100720E-02	-2.8040690E-03	1.9305448E-02

Type I Models Using (STRHEX12T) – Results



NAME	SOFTWARE	DISPLACEMENTS				
		Node Location	Ux (m)	Uy (m)	Uz (m)	Vector Magnitude
STRHEX12T	sim FEM	(0,0,0)	0.0000000E+00	0.0000000E+00	0.0000000E+00	0.0000000E+00
		(2,0,0)	0.0000000E+00	0.0000000E+00	0.0000000E+00	0.0000000E+00
		(2,2,0)	0.0000000E+00	0.0000000E+00	0.0000000E+00	0.0000000E+00
		(0,2,0)	0.0000000E+00	0.0000000E+00	0.0000000E+00	0.0000000E+00
		(0,0,2)	-3.3011094E-03	-3.3011094E-03	-1.3595637E-02	1.4374839E-02
		(2,0,2)	3.3011094E-03	-3.3011094E-03	-1.3595637E-02	1.4374839E-02
		(2,2,2)	3.3011094E-03	3.3011094E-03	-1.3595637E-02	1.4374839E-02
		(0,2,2)	-3.3011094E-03	3.3011094E-03	-1.3595637E-02	1.4374839E-02
		(1,0,2)	-3.9243065E-18	-3.7493436E-03	-1.7878766E-02	1.8267672E-02
		(2,1,2)	3.7493436E-03	-9.7074325E-20	-1.7878766E-02	1.8267672E-02
		(1,2,2)	3.4539219E-18	3.7493436E-03	-1.7878766E-02	1.8267672E-02
		(0,1,2)	-3.7493436E-03	1.4665951E-18	-1.7878766E-02	1.8267672E-02

Type I Models Using (STRHEX16T) - Results



NAME	SOFTWARE	DISPLACEMENTS				
		Node Location	Ux (m)	Uy (m)	Uz (m)	Vector Magnitude
STRHEX16T	sim FEM	(0,0,0)	0.0000000E+00	0.0000000E+00	0.0000000E+00	0.0000000E+00
		(2,0,0)	0.0000000E+00	0.0000000E+00	0.0000000E+00	0.0000000E+00
		(2,2,0)	0.0000000E+00	0.0000000E+00	0.0000000E+00	0.0000000E+00
		(0,2,0)	0.0000000E+00	0.0000000E+00	0.0000000E+00	0.0000000E+00
		(0,0,2)	-1.3455588E-03	-1.3455588E-03	-1.2953556E-02	1.3092581E-02
		(2,0,2)	1.3455588E-03	-1.3455588E-03	-1.2953556E-02	1.3092581E-02
		(2,2,2)	1.3455588E-03	1.3455588E-03	-1.2953556E-02	1.3092581E-02
		(0,2,2)	-1.3455588E-03	1.3455588E-03	-1.2953556E-02	1.3092581E-02
		(1,0,2)	0.0000000E+00	-1.9468619E-03	-1.8699344E-02	1.8800419E-02
		(2,1,2)	1.9468619E-03	0.0000000E+00	-1.8699344E-02	1.8800419E-02
		(1,2,2)	0.0000000E+00	1.9468619E-03	-1.8699344E-02	1.8800419E-02
		(0,1,2)	-1.9468619E-03	0.0000000E+00	-1.8699344E-02	1.8800419E-02
		(0,0,1)	-3.5091374E-03	-3.5091374E-03	-6.1240188E-03	7.8823662E-03
		(2,0,1)	3.5091374E-03	-3.5091374E-03	-6.1240188E-03	7.8823662E-03
		(2,2,1)	3.5091374E-03	3.5091374E-03	-6.1240188E-03	7.8823662E-03
		(0,2,1)	-3.5091374E-03	3.5091374E-03	-6.1240188E-03	7.8823662E-03

Appendix 2

Type II Models – Results

(3x3x3) Element Mesh Model Results						
NAME	Integration Scheme	DISPLACEMENTS				
		Node Location	Ux (m)	Uy (m)	Uz (m)	Vector Magnitude
MHex08L_sim FEM	Reduced	(0,0,3)	-5.1683430E-03	-5.1683430E-03	-2.8447676E-02	2.9371650E-02
		(3,0,3)	5.1683430E-03	-5.1683430E-03	-2.8447676E-02	2.9371650E-02
		(3,3,3)	5.1683430E-03	5.1683430E-03	-2.8447676E-02	2.9371650E-02
		(0,3,3)	-5.1683430E-03	5.1683430E-03	-2.8447676E-02	2.9371650E-02
		(2,0,3)	4.7446804E-04	-5.1030111E-03	-2.8945314E-02	2.9395528E-02
		(2,3,3)	4.7446804E-04	5.1030111E-03	-2.8945314E-02	2.9395528E-02
		(0,1,3)	-5.1030111E-03	-4.7446804E-04	-2.8945314E-02	2.9395528E-02
		(3,1,3)	5.1030111E-03	-4.7446804E-04	-2.8945314E-02	2.9395528E-02
MHex08L_sim FEM	Full	Node Location	Ux (m)	Uy (m)	Uz (m)	Vector Magnitude
		(0,0,3)	-4.6487028E-03	-4.6487028E-03	-2.8863095E-02	2.9602350E-02
		(3,0,3)	4.6487028E-03	-4.6487028E-03	-2.8863095E-02	2.9602350E-02
		(3,3,3)	4.6487028E-03	4.6487028E-03	-2.8863095E-02	2.9602350E-02
		(0,3,3)	-4.6487028E-03	4.6487028E-03	-2.8863095E-02	2.9602350E-02
		(2,0,3)	1.5701019E-03	-4.6527417E-03	-2.8693367E-02	2.9110523E-02
		(2,3,3)	1.5701019E-03	4.6527417E-03	-2.8693367E-02	2.9110523E-02
		(0,1,3)	-4.6527417E-03	-1.5701019E-03	-2.8693367E-02	2.9110523E-02
		(3,1,3)	4.6527417E-03	-1.5701019E-03	-2.8693367E-02	2.9110523E-02
		Node Location	Ux (m)	Uy (m)	Uz (m)	Vector Magnitude
MHex08L_ABAQUS	Reduced	(0,0,3)	-5.1459100E-03	-5.1459100E-03	-2.8463200E-02	2.9378811E-02
		(3,0,3)	5.1459100E-03	-5.1459100E-03	-2.8463200E-02	2.9378811E-02
		(3,3,3)	5.1459100E-03	5.1459100E-03	-2.8463200E-02	2.9378811E-02
		(0,3,3)	-5.1459100E-03	5.1459100E-03	-2.8463200E-02	2.9378811E-02
		(2,0,3)	5.2360200E-04	-5.0609700E-03	-2.8938500E-02	2.9382382E-02
		(2,3,3)	5.2360200E-04	5.0609700E-03	-2.8938500E-02	2.9382382E-02
		(0,1,3)	-5.0609700E-03	-5.2360200E-04	-2.8938500E-02	2.9382382E-02
		(3,1,3)	5.0609700E-03	-5.2360200E-04	-2.8938500E-02	2.9382382E-02

		Node Location	Ux (m)	Uy (m)	Uz (m)	Vector Magnitude
MHex08L_ABAQUS	Full	(0,0,3)	-4.7284300E-03	-4.7284300E-03	-2.8903100E-02	2.9666569E-02
		(3,0,3)	4.7284300E-03	-4.7284300E-03	-2.8903100E-02	2.9666569E-02
		(3,3,3)	4.7284300E-03	4.7284300E-03	-2.8903100E-02	2.9666569E-02
		(0,3,3)	-4.7284300E-03	4.7284300E-03	-2.8903100E-02	2.9666569E-02
		(2,0,3)	1.4611700E-03	-4.6076000E-03	-2.8880100E-02	2.9281823E-02
		(2,3,3)	1.4611700E-03	4.6076000E-03	-2.8880100E-02	2.9281823E-02
		(0,1,3)	-4.6076000E-03	-1.4611700E-03	-2.8880100E-02	2.9281823E-02
		(3,1,3)	4.6076000E-03	-1.4611700E-03	-2.8880100E-02	2.9281823E-02
MHex20Q_sim FEM	Reduced	Node Location	Ux (m)	Uy (m)	Uz (m)	Vector Magnitude
		(0,0,3)	-4.6160289E-03	-4.6160289E-03	-2.9197429E-02	2.9918311E-02
		(3,0,3)	4.6160289E-03	-4.6160289E-03	-2.9197429E-02	2.9918311E-02
		(3,3,3)	4.6160289E-03	4.6160289E-03	-2.9197429E-02	2.9918311E-02
		(0,3,3)	-4.6160289E-03	4.6160289E-03	-2.9197429E-02	2.9918311E-02
		(2,0,3)	1.5849714E-03	-4.6138146E-03	-2.9045175E-02	2.9452022E-02
		(2,3,3)	1.5849714E-03	4.6138146E-03	-2.9045175E-02	2.9452022E-02
		(0,1,3)	-4.6138146E-03	-1.5849714E-03	-2.9045175E-02	2.9452022E-02
		(3,1,3)	4.6138146E-03	-1.5849714E-03	-2.9045175E-02	2.9452022E-02
MHex20Q_sim FEM	Full	Node Location	Ux (m)	Uy (m)	Uz (m)	Vector Magnitude
		(0,0,3)	-4.6301436E-03	-4.6301436E-03	-2.9143326E-02	2.9869883E-02
		(3,0,3)	4.6301436E-03	-4.6301436E-03	-2.9143326E-02	2.9869883E-02
		(3,3,3)	4.6301436E-03	4.6301436E-03	-2.9143326E-02	2.9869883E-02
		(0,3,3)	-4.6301436E-03	4.6301436E-03	-2.9143326E-02	2.9869883E-02
		(2,0,3)	1.5801419E-03	-4.6098787E-03	-2.8979624E-02	2.9386501E-02
		(2,3,3)	1.5801419E-03	4.6098787E-03	-2.8979624E-02	2.9386501E-02
		(0,1,3)	-4.6098787E-03	-1.5801419E-03	-2.8979624E-02	2.9386501E-02
		(3,1,3)	4.6098787E-03	-1.5801419E-03	-2.8979624E-02	2.9386501E-02

		Node Location	Ux (m)	Uy (m)	Uz (m)	Vector Magnitude
MHex20Q_ABAQUS	Reduced	(0,0,3)	-4.6234700E-03	-4.6234700E-03	-2.9238200E-02	2.9960395E-02
		(3,0,3)	4.6234700E-03	-4.6234700E-03	-2.9238200E-02	2.9960395E-02
		(3,3,3)	4.6234700E-03	4.6234700E-03	-2.9238200E-02	2.9960395E-02
		(0,3,3)	-4.6234700E-03	4.6234700E-03	-2.9238200E-02	2.9960395E-02
		(2,0,3)	1.5867800E-03	-4.6213400E-03	-2.9084400E-02	2.9491982E-02
		(2,3,3)	1.5867800E-03	4.6213400E-03	-2.9084400E-02	2.9491982E-02
		(0,1,3)	-4.6213400E-03	-1.5867800E-03	-2.9084400E-02	2.9491982E-02
		(3,1,3)	4.6213400E-03	-1.5867800E-03	-2.9084400E-02	2.9491982E-02
MHex20Q_ABAQUS	Full	Node Location	Ux (m)	Uy (m)	Uz (m)	Vector Magnitude
		(0,0,3)	-4.6369400E-03	-4.6369400E-03	-2.9182100E-02	2.9909821E-02
		(3,0,3)	4.6369400E-03	-4.6369400E-03	-2.9182100E-02	2.9909821E-02
		(3,3,3)	4.6369400E-03	4.6369400E-03	-2.9182100E-02	2.9909821E-02
		(0,3,3)	-4.6369400E-03	4.6369400E-03	-2.9182100E-02	2.9909821E-02
		(2,0,3)	1.5821100E-03	-4.6167700E-03	-2.9017400E-02	2.9424941E-02
		(2,3,3)	1.5821100E-03	4.6167700E-03	-2.9017400E-02	2.9424941E-02
		(0,1,3)	-4.6167700E-03	-1.5821100E-03	-2.9017400E-02	2.9424941E-02
		(3,1,3)	4.6167700E-03	-1.5821100E-03	-2.9017400E-02	2.9424941E-02
MHex12T_sim FEM		Node Location	Ux (m)	Uy (m)	Uz (m)	Vector Magnitude
		(0,0,3)	-4.6448742E-03	-4.6448742E-03	-2.9781597E-02	3.0497430E-02
		(3,0,3)	4.6448742E-03	-4.6448742E-03	-2.9781597E-02	3.0497430E-02
		(3,3,3)	4.6448742E-03	4.6448742E-03	-2.9781597E-02	3.0497430E-02
		(0,3,3)	-4.6448742E-03	4.6448742E-03	-2.9781597E-02	3.0497430E-02
		(2,0,3)	1.4831197E-03	-4.6453626E-03	-2.9571262E-02	2.9970629E-02
		(2,3,3)	1.4831197E-03	4.6453626E-03	-2.9571262E-02	2.9970629E-02
		(0,1,3)	-4.6453626E-03	-1.4831197E-03	-2.9571262E-02	2.9970629E-02
		(3,1,3)	4.6453626E-03	-1.4831197E-03	-2.9571262E-02	2.9970629E-02
MHex16T_sim FEM		Node Location	Ux (m)	Uy (m)	Uz (m)	Vector Magnitude
		(0,0,3)	-4.6259319E-03	-4.6259319E-03	-2.9773321E-02	3.0483588E-02
		(3,0,3)	4.6259319E-03	-4.6259320E-03	-2.9773321E-02	3.0483588E-02
		(3,3,3)	4.6259320E-03	4.6259320E-03	-2.9773321E-02	3.0483588E-02
		(0,3,3)	-4.6259319E-03	4.6259319E-03	-2.9773321E-02	3.0483588E-02
		(2,0,3)	1.4697022E-03	-4.6337918E-03	-2.9584919E-02	2.9981652E-02
		(2,3,3)	1.4697022E-03	4.6337918E-03	-2.9584919E-02	2.9981652E-02
		(0,1,3)	-4.6337918E-03	-1.4697022E-03	-2.9584919E-02	2.9981652E-02
		(3,1,3)	4.6337918E-03	-1.4697022E-03	-2.9584919E-02	2.9981652E-02

Appendix 3
Kirsch Equations Results - Left Excavation

$a_1 = 2.6 \text{ m}, \sigma_H = \sigma_V = 10 \text{ kPa}, \theta = 0^\circ$						
r_1	σ_r	σ_θ	$\tau_{r\theta}$	σ_{xx}	σ_{zz}	τ_{xz}
2.6	0.000	20.000	0.000	0.000	20.000	0.000
5.2	7.500	12.500	0.000	7.500	12.500	0.000
7.8	8.889	11.111	0.000	8.889	11.111	0.000
10.4	9.375	10.625	0.000	9.375	10.625	0.000
13	9.600	10.400	0.000	9.600	10.400	0.000
15.6	9.722	10.278	0.000	9.722	10.278	0.000
18.2	9.796	10.204	0.000	9.796	10.204	0.000
20.8	9.844	10.156	0.000	9.844	10.156	0.000
23.4	9.877	10.123	0.000	9.877	10.123	0.000
26	9.900	10.100	0.000	9.900	10.100	0.000
28.6	9.917	10.083	0.000	9.917	10.083	0.000
31.2	9.931	10.069	0.000	9.931	10.069	0.000
33.8	9.941	10.059	0.000	9.941	10.059	0.000
36.4	9.949	10.051	0.000	9.949	10.051	0.000
39	9.956	10.044	0.000	9.956	10.044	0.000
$a_1 = 2.6 \text{ m}, \sigma_H = \sigma_V = 10 \text{ kPa}, \theta = 10^\circ$						
r_1	σ_r	σ_θ	$\tau_{r\theta}$	σ_{xx}	σ_{zz}	τ_{xz}
2.6	0.000	20.000	0.000	5.919	14.081	-9.129
5.2	7.500	12.500	0.000	8.980	11.020	-2.282
7.8	8.889	11.111	0.000	9.547	10.453	-1.014
10.4	9.375	10.625	0.000	9.745	10.255	-0.571
13	9.600	10.400	0.000	9.837	10.163	-0.365
15.6	9.722	10.278	0.000	9.887	10.113	-0.254
18.2	9.796	10.204	0.000	9.917	10.083	-0.186
20.8	9.844	10.156	0.000	9.936	10.064	-0.143
23.4	9.877	10.123	0.000	9.950	10.050	-0.113
26	9.900	10.100	0.000	9.959	10.041	-0.091
28.6	9.917	10.083	0.000	9.966	10.034	-0.075
31.2	9.931	10.069	0.000	9.972	10.028	-0.063
33.8	9.941	10.059	0.000	9.976	10.024	-0.054
36.4	9.949	10.051	0.000	9.979	10.021	-0.047
39	9.956	10.044	0.000	9.982	10.018	-0.041

$a_1 = 2.6 \text{ m}, \sigma_H = \sigma_V = 10 \text{ kPa}, \theta = 20^\circ$						
r_1	σ_r	σ_θ	$\tau_{r\theta}$	σ_{xx}	σ_{zz}	τ_{xz}
2.6	0.000	20.000	0.000	16.669	3.331	-7.451
5.2	7.500	12.500	0.000	11.667	8.333	-1.863
7.8	8.889	11.111	0.000	10.741	9.259	-0.828
10.4	9.375	10.625	0.000	10.417	9.583	-0.466
13	9.600	10.400	0.000	10.267	9.733	-0.298
15.6	9.722	10.278	0.000	10.185	9.815	-0.207
18.2	9.796	10.204	0.000	10.136	9.864	-0.152
20.8	9.844	10.156	0.000	10.104	9.896	-0.116
23.4	9.877	10.123	0.000	10.082	9.918	-0.092
26	9.900	10.100	0.000	10.067	9.933	-0.075
28.6	9.917	10.083	0.000	10.055	9.945	-0.062
31.2	9.931	10.069	0.000	10.046	9.954	-0.052
33.8	9.941	10.059	0.000	10.039	9.961	-0.044
36.4	9.949	10.051	0.000	10.034	9.966	-0.038
39	9.956	10.044	0.000	10.030	9.970	-0.033
$a_1 = 2.6 \text{ m}, \sigma_H = \sigma_V = 10 \text{ kPa}, \theta = 30^\circ$						
r_1	σ_r	σ_θ	$\tau_{r\theta}$	σ_{xx}	σ_{zz}	τ_{xz}
2.6	0.000	20.000	0.000	19.524	0.476	3.048
5.2	7.500	12.500	0.000	12.381	7.619	0.762
7.8	8.889	11.111	0.000	11.058	8.942	0.339
10.4	9.375	10.625	0.000	10.595	9.405	0.191
13	9.600	10.400	0.000	10.381	9.619	0.122
15.6	9.722	10.278	0.000	10.265	9.735	0.085
18.2	9.796	10.204	0.000	10.194	9.806	0.062
20.8	9.844	10.156	0.000	10.149	9.851	0.048
23.4	9.877	10.123	0.000	10.118	9.882	0.038
26	9.900	10.100	0.000	10.095	9.905	0.030
28.6	9.917	10.083	0.000	10.079	9.921	0.025
31.2	9.931	10.069	0.000	10.066	9.934	0.021
33.8	9.941	10.059	0.000	10.056	9.944	0.018
36.4	9.949	10.051	0.000	10.049	9.951	0.016
39	9.956	10.044	0.000	10.042	9.958	0.014

$a_1 = 2.6 \text{ m}, \sigma_H = \sigma_V = 10 \text{ kPa}, \theta = 40^\circ$						
r_1	σ_r	σ_θ	$\tau_{r\theta}$	σ_{xx}	σ_{zz}	τ_{xz}
2.6	0.000	20.000	0.000	11.104	8.896	9.939
5.2	7.500	12.500	0.000	10.276	9.724	2.485
7.8	8.889	11.111	0.000	10.123	9.877	1.104
10.4	9.375	10.625	0.000	10.069	9.931	0.621
13	9.600	10.400	0.000	10.044	9.956	0.398
15.6	9.722	10.278	0.000	10.031	9.969	0.276
18.2	9.796	10.204	0.000	10.023	9.977	0.203
20.8	9.844	10.156	0.000	10.017	9.983	0.155
23.4	9.877	10.123	0.000	10.014	9.986	0.123
26	9.900	10.100	0.000	10.011	9.989	0.099
28.6	9.917	10.083	0.000	10.009	9.991	0.082
31.2	9.931	10.069	0.000	10.008	9.992	0.069
33.8	9.941	10.059	0.000	10.007	9.993	0.059
36.4	9.949	10.051	0.000	10.006	9.994	0.051
39	9.956	10.044	0.000	10.005	9.995	0.044
$a_1 = 2.6 \text{ m}, \sigma_H = \sigma_V = 10 \text{ kPa}, \theta = 50^\circ$						
r_1	σ_r	σ_θ	$\tau_{r\theta}$	σ_{xx}	σ_{zz}	τ_{xz}
2.6	0.000	20.000	0.000	1.377	18.623	5.064
5.2	7.500	12.500	0.000	7.844	12.156	1.266
7.8	8.889	11.111	0.000	9.042	10.958	0.563
10.4	9.375	10.625	0.000	9.461	10.539	0.316
13	9.600	10.400	0.000	9.655	10.345	0.203
15.6	9.722	10.278	0.000	9.760	10.240	0.141
18.2	9.796	10.204	0.000	9.824	10.176	0.103
20.8	9.844	10.156	0.000	9.865	10.135	0.079
23.4	9.877	10.123	0.000	9.894	10.106	0.063
26	9.900	10.100	0.000	9.914	10.086	0.051
28.6	9.917	10.083	0.000	9.929	10.071	0.042
31.2	9.931	10.069	0.000	9.940	10.060	0.035
33.8	9.941	10.059	0.000	9.949	10.051	0.030
36.4	9.949	10.051	0.000	9.956	10.044	0.026
39	9.956	10.044	0.000	9.962	10.038	0.023

$a_1 = 2.6 \text{ m}, \sigma_H = \sigma_V = 10 \text{ kPa}, \theta = 60^\circ$						
r_1	σ_r	σ_θ	$\tau_{r\theta}$	σ_{xx}	σ_{zz}	τ_{xz}
2.6	0.000	20.000	0.000	1.858	18.142	-5.806
5.2	7.500	12.500	0.000	7.965	12.035	-1.452
7.8	8.889	11.111	0.000	9.095	10.905	-0.645
10.4	9.375	10.625	0.000	9.491	10.509	-0.363
13	9.600	10.400	0.000	9.674	10.326	-0.232
15.6	9.722	10.278	0.000	9.774	10.226	-0.161
18.2	9.796	10.204	0.000	9.834	10.166	-0.118
20.8	9.844	10.156	0.000	9.873	10.127	-0.091
23.4	9.877	10.123	0.000	9.899	10.101	-0.072
26	9.900	10.100	0.000	9.919	10.081	-0.058
28.6	9.917	10.083	0.000	9.933	10.067	-0.048
31.2	9.931	10.069	0.000	9.943	10.057	-0.040
33.8	9.941	10.059	0.000	9.952	10.048	-0.034
36.4	9.949	10.051	0.000	9.958	10.042	-0.030
39	9.956	10.044	0.000	9.964	10.036	-0.026
$a_1 = 2.6 \text{ m}, \sigma_H = \sigma_V = 10 \text{ kPa}, \theta = 70^\circ$						
r_1	σ_r	σ_θ	$\tau_{r\theta}$	σ_{xx}	σ_{zz}	τ_{xz}
2.6	0.000	20.000	0.000	11.978	8.022	-9.802
5.2	7.500	12.500	0.000	10.495	9.505	-2.451
7.8	8.889	11.111	0.000	10.220	9.780	-1.089
10.4	9.375	10.625	0.000	10.124	9.876	-0.613
13	9.600	10.400	0.000	10.079	9.921	-0.392
15.6	9.722	10.278	0.000	10.055	9.945	-0.272
18.2	9.796	10.204	0.000	10.040	9.960	-0.200
20.8	9.844	10.156	0.000	10.031	9.969	-0.153
23.4	9.877	10.123	0.000	10.024	9.976	-0.121
26	9.900	10.100	0.000	10.020	9.980	-0.098
28.6	9.917	10.083	0.000	10.016	9.984	-0.081
31.2	9.931	10.069	0.000	10.014	9.986	-0.068
33.8	9.941	10.059	0.000	10.012	9.988	-0.058
36.4	9.949	10.051	0.000	10.010	9.990	-0.050
39	9.956	10.044	0.000	10.009	9.991	-0.044

$a_1 = 2.6 \text{ m}, \sigma_H = \sigma_V = 10 \text{ kPa}, \theta = 80^\circ$						
r_1	σ_r	σ_θ	$\tau_{r\theta}$	σ_{xx}	σ_{zz}	τ_{xz}
2.6	0.000	20.000	0.000	19.756	0.244	-2.194
5.2	7.500	12.500	0.000	12.439	7.561	-0.549
7.8	8.889	11.111	0.000	11.084	8.916	-0.244
10.4	9.375	10.625	0.000	10.610	9.390	-0.137
13	9.600	10.400	0.000	10.390	9.610	-0.088
15.6	9.722	10.278	0.000	10.271	9.729	-0.061
18.2	9.796	10.204	0.000	10.199	9.801	-0.045
20.8	9.844	10.156	0.000	10.152	9.848	-0.034
23.4	9.877	10.123	0.000	10.120	9.880	-0.027
26	9.900	10.100	0.000	10.098	9.902	-0.022
28.6	9.917	10.083	0.000	10.081	9.919	-0.018
31.2	9.931	10.069	0.000	10.068	9.932	-0.015
33.8	9.941	10.059	0.000	10.058	9.942	-0.013
36.4	9.949	10.051	0.000	10.050	9.950	-0.011
39	9.956	10.044	0.000	10.043	9.957	-0.010
$a_1 = 2.6 \text{ m}, \sigma_H = \sigma_V = 10 \text{ kPa}, \theta = 90^\circ$						
r_1	σ_r	σ_θ	$\tau_{r\theta}$	σ_{xx}	σ_{zz}	τ_{xz}
2.6	0.000	20.000	0.000	15.985	4.015	8.012
5.2	7.500	12.500	0.000	11.496	8.504	2.003
7.8	8.889	11.111	0.000	10.665	9.335	0.890
10.4	9.375	10.625	0.000	10.374	9.626	0.501
13	9.600	10.400	0.000	10.239	9.761	0.320
15.6	9.722	10.278	0.000	10.166	9.834	0.223
18.2	9.796	10.204	0.000	10.122	9.878	0.164
20.8	9.844	10.156	0.000	10.094	9.906	0.125
23.4	9.877	10.123	0.000	10.074	9.926	0.099
26	9.900	10.100	0.000	10.060	9.940	0.080
28.6	9.917	10.083	0.000	10.049	9.951	0.066
31.2	9.931	10.069	0.000	10.042	9.958	0.056
33.8	9.941	10.059	0.000	10.035	9.965	0.047
36.4	9.949	10.051	0.000	10.031	9.969	0.041
39	9.956	10.044	0.000	10.027	9.973	0.036

Kirsch Equations Results - Right Excavation

$a_2 = 5.4 \text{ m}, \sigma_H = \sigma_V = 10 \text{ kPa}, \theta = 0^\circ$						
r_2	σ_r	σ_θ	$\tau_{r\theta}$	σ_{xx}	σ_{zz}	τ_{xz}
5.4	0.000	20.000	0.000	0.000	20.000	0.000
10.8	7.500	12.500	0.000	7.500	12.500	0.000
16.2	8.889	11.111	0.000	8.889	11.111	0.000
21.6	9.375	10.625	0.000	9.375	10.625	0.000
27	9.600	10.400	0.000	9.600	10.400	0.000
32.4	9.722	10.278	0.000	9.722	10.278	0.000
37.8	9.796	10.204	0.000	9.796	10.204	0.000
43.2	9.844	10.156	0.000	9.844	10.156	0.000
48.6	9.877	10.123	0.000	9.877	10.123	0.000
54	9.900	10.100	0.000	9.900	10.100	0.000
59.4	9.917	10.083	0.000	9.917	10.083	0.000
64.8	9.931	10.069	0.000	9.931	10.069	0.000
70.2	9.941	10.059	0.000	9.941	10.059	0.000
75.6	9.949	10.051	0.000	9.949	10.051	0.000
81	9.956	10.044	0.000	9.956	10.044	0.000
$a_2 = 5.4 \text{ m}, \sigma_H = \sigma_V = 10 \text{ kPa}, \theta = 10^\circ$						
r_2	σ_r	σ_θ	$\tau_{r\theta}$	σ_{xx}	σ_{zz}	τ_{xz}
5.4	0.000	20.000	0.000	5.919	14.081	-9.129
10.8	7.500	12.500	0.000	8.980	11.020	-2.282
16.2	8.889	11.111	0.000	9.547	10.453	-1.014
21.6	9.375	10.625	0.000	9.745	10.255	-0.571
27	9.600	10.400	0.000	9.837	10.163	-0.365
32.4	9.722	10.278	0.000	9.887	10.113	-0.254
37.8	9.796	10.204	0.000	9.917	10.083	-0.186
43.2	9.844	10.156	0.000	9.936	10.064	-0.143
48.6	9.877	10.123	0.000	9.950	10.050	-0.113
54	9.900	10.100	0.000	9.959	10.041	-0.091
59.4	9.917	10.083	0.000	9.966	10.034	-0.075
64.8	9.931	10.069	0.000	9.972	10.028	-0.063
70.2	9.941	10.059	0.000	9.976	10.024	-0.054
75.6	9.949	10.051	0.000	9.979	10.021	-0.047
81	9.956	10.044	0.000	9.982	10.018	-0.041

$a_2 = 5.4 \text{ m}, \sigma_H = \sigma_V = 10 \text{ kPa}, \theta = 20^\circ$						
r_2	σ_r	σ_θ	$\tau_{r\theta}$	σ_{xx}	σ_{zz}	τ_{xz}
5.4	0.000	20.000	0.000	16.669	3.331	-7.451
10.8	7.500	12.500	0.000	11.667	8.333	-1.863
16.2	8.889	11.111	0.000	10.741	9.259	-0.828
21.6	9.375	10.625	0.000	10.417	9.583	-0.466
27	9.600	10.400	0.000	10.267	9.733	-0.298
32.4	9.722	10.278	0.000	10.185	9.815	-0.207
37.8	9.796	10.204	0.000	10.136	9.864	-0.152
43.2	9.844	10.156	0.000	10.104	9.896	-0.116
48.6	9.877	10.123	0.000	10.082	9.918	-0.092
54	9.900	10.100	0.000	10.067	9.933	-0.075
59.4	9.917	10.083	0.000	10.055	9.945	-0.062
64.8	9.931	10.069	0.000	10.046	9.954	-0.052
70.2	9.941	10.059	0.000	10.039	9.961	-0.044
75.6	9.949	10.051	0.000	10.034	9.966	-0.038
81	9.956	10.044	0.000	10.030	9.970	-0.033
$a_2 = 5.4 \text{ m}, \sigma_H = \sigma_V = 10 \text{ kPa}, \theta = 30^\circ$						
r_2	σ_r	σ_θ	$\tau_{r\theta}$	σ_{xx}	σ_{zz}	τ_{xz}
5.4	0.000	20.000	0.000	19.524	0.476	3.048
10.8	7.500	12.500	0.000	12.381	7.619	0.762
16.2	8.889	11.111	0.000	11.058	8.942	0.339
21.6	9.375	10.625	0.000	10.595	9.405	0.191
27	9.600	10.400	0.000	10.381	9.619	0.122
32.4	9.722	10.278	0.000	10.265	9.735	0.085
37.8	9.796	10.204	0.000	10.194	9.806	0.062
43.2	9.844	10.156	0.000	10.149	9.851	0.048
48.6	9.877	10.123	0.000	10.118	9.882	0.038
54	9.900	10.100	0.000	10.095	9.905	0.030
59.4	9.917	10.083	0.000	10.079	9.921	0.025
64.8	9.931	10.069	0.000	10.066	9.934	0.021
70.2	9.941	10.059	0.000	10.056	9.944	0.018
75.6	9.949	10.051	0.000	10.049	9.951	0.016
81	9.956	10.044	0.000	10.042	9.958	0.014

$a_2 = 5.4 \text{ m}, \sigma_H = \sigma_V = 10 \text{ kPa}, \theta = 40^\circ$						
r_2	σ_r	σ_θ	$\tau_{r\theta}$	σ_{xx}	σ_{zz}	τ_{xz}
5.4	0.000	20.000	0.000	11.104	8.896	9.939
10.8	7.500	12.500	0.000	10.276	9.724	2.485
16.2	8.889	11.111	0.000	10.123	9.877	1.104
21.6	9.375	10.625	0.000	10.069	9.931	0.621
27	9.600	10.400	0.000	10.044	9.956	0.398
32.4	9.722	10.278	0.000	10.031	9.969	0.276
37.8	9.796	10.204	0.000	10.023	9.977	0.203
43.2	9.844	10.156	0.000	10.017	9.983	0.155
48.6	9.877	10.123	0.000	10.014	9.986	0.123
54	9.900	10.100	0.000	10.011	9.989	0.099
59.4	9.917	10.083	0.000	10.009	9.991	0.082
64.8	9.931	10.069	0.000	10.008	9.992	0.069
70.2	9.941	10.059	0.000	10.007	9.993	0.059
75.6	9.949	10.051	0.000	10.006	9.994	0.051
81	9.956	10.044	0.000	10.005	9.995	0.044
$a_2 = 2.6 \text{ m}, \sigma_H = \sigma_V = 10 \text{ kPa}, \theta = 50^\circ$						
r_2	σ_r	σ_θ	$\tau_{r\theta}$	σ_{xx}	σ_{zz}	τ_{xz}
5.4	0.000	20.000	0.000	1.377	18.623	5.064
10.8	7.500	12.500	0.000	7.844	12.156	1.266
16.2	8.889	11.111	0.000	9.042	10.958	0.563
21.6	9.375	10.625	0.000	9.461	10.539	0.316
27	9.600	10.400	0.000	9.655	10.345	0.203
32.4	9.722	10.278	0.000	9.760	10.240	0.141
37.8	9.796	10.204	0.000	9.824	10.176	0.103
43.2	9.844	10.156	0.000	9.865	10.135	0.079
48.6	9.877	10.123	0.000	9.894	10.106	0.063
54	9.900	10.100	0.000	9.914	10.086	0.051
59.4	9.917	10.083	0.000	9.929	10.071	0.042
64.8	9.931	10.069	0.000	9.940	10.060	0.035
70.2	9.941	10.059	0.000	9.949	10.051	0.030
75.6	9.949	10.051	0.000	9.956	10.044	0.026
81	9.956	10.044	0.000	9.962	10.038	0.023

$a_2 = 2.6 \text{ m}, \sigma_H = \sigma_V = 10 \text{ kPa}, \theta = 60^\circ$						
r_2	σ_r	σ_θ	$\tau_{r\theta}$	σ_{xx}	σ_{zz}	τ_{xz}
5.4	0.000	20.000	0.000	1.858	18.142	-5.806
10.8	7.500	12.500	0.000	7.965	12.035	-1.452
16.2	8.889	11.111	0.000	9.095	10.905	-0.645
21.6	9.375	10.625	0.000	9.491	10.509	-0.363
27	9.600	10.400	0.000	9.674	10.326	-0.232
32.4	9.722	10.278	0.000	9.774	10.226	-0.161
37.8	9.796	10.204	0.000	9.834	10.166	-0.118
43.2	9.844	10.156	0.000	9.873	10.127	-0.091
48.6	9.877	10.123	0.000	9.899	10.101	-0.072
54	9.900	10.100	0.000	9.919	10.081	-0.058
59.4	9.917	10.083	0.000	9.933	10.067	-0.048
64.8	9.931	10.069	0.000	9.943	10.057	-0.040
70.2	9.941	10.059	0.000	9.952	10.048	-0.034
75.6	9.949	10.051	0.000	9.958	10.042	-0.030
81	9.956	10.044	0.000	9.964	10.036	-0.026
$a_2 = 2.6 \text{ m}, \sigma_H = \sigma_V = 10 \text{ kPa}, \theta = 70^\circ$						
r_2	σ_r	σ_θ	$\tau_{r\theta}$	σ_{xx}	σ_{zz}	τ_{xz}
5.4	0.000	20.000	0.000	11.978	8.022	-9.802
10.8	7.500	12.500	0.000	10.495	9.505	-2.451
16.2	8.889	11.111	0.000	10.220	9.780	-1.089
21.6	9.375	10.625	0.000	10.124	9.876	-0.613
27	9.600	10.400	0.000	10.079	9.921	-0.392
32.4	9.722	10.278	0.000	10.055	9.945	-0.272
37.8	9.796	10.204	0.000	10.040	9.960	-0.200
43.2	9.844	10.156	0.000	10.031	9.969	-0.153
48.6	9.877	10.123	0.000	10.024	9.976	-0.121
54	9.900	10.100	0.000	10.020	9.980	-0.098
59.4	9.917	10.083	0.000	10.016	9.984	-0.081
64.8	9.931	10.069	0.000	10.014	9.986	-0.068
70.2	9.941	10.059	0.000	10.012	9.988	-0.058
75.6	9.949	10.051	0.000	10.010	9.990	-0.050
81	9.956	10.044	0.000	10.009	9.991	-0.044

$a_2 = 2.6 \text{ m}, \sigma_H = \sigma_V = 10 \text{ kPa}, \theta = 80^\circ$						
r_2	σ_r	σ_θ	$\tau_{r\theta}$	σ_{xx}	σ_{zz}	τ_{xz}
5.4	0.000	20.000	0.000	19.756	0.244	-2.194
10.8	7.500	12.500	0.000	12.439	7.561	-0.549
16.2	8.889	11.111	0.000	11.084	8.916	-0.244
21.6	9.375	10.625	0.000	10.610	9.390	-0.137
27	9.600	10.400	0.000	10.390	9.610	-0.088
32.4	9.722	10.278	0.000	10.271	9.729	-0.061
37.8	9.796	10.204	0.000	10.199	9.801	-0.045
43.2	9.844	10.156	0.000	10.152	9.848	-0.034
48.6	9.877	10.123	0.000	10.120	9.880	-0.027
54	9.900	10.100	0.000	10.098	9.902	-0.022
59.4	9.917	10.083	0.000	10.081	9.919	-0.018
64.8	9.931	10.069	0.000	10.068	9.932	-0.015
70.2	9.941	10.059	0.000	10.058	9.942	-0.013
75.6	9.949	10.051	0.000	10.050	9.950	-0.011
81	9.956	10.044	0.000	10.043	9.957	-0.010
$a_2 = 2.6 \text{ m}, \sigma_H = \sigma_V = 10 \text{ kPa}, \theta = 90^\circ$						
r_2	σ_r	σ_θ	$\tau_{r\theta}$	σ_{xx}	σ_{zz}	τ_{xz}
5.4	0.000	20.000	0.000	15.985	4.015	8.012
10.8	7.500	12.500	0.000	11.496	8.504	2.003
16.2	8.889	11.111	0.000	10.665	9.335	0.890
21.6	9.375	10.625	0.000	10.374	9.626	0.501
27	9.600	10.400	0.000	10.239	9.761	0.320
32.4	9.722	10.278	0.000	10.166	9.834	0.223
37.8	9.796	10.204	0.000	10.122	9.878	0.164
43.2	9.844	10.156	0.000	10.094	9.906	0.125
48.6	9.877	10.123	0.000	10.074	9.926	0.099
54	9.900	10.100	0.000	10.060	9.940	0.080
59.4	9.917	10.083	0.000	10.049	9.951	0.066
64.8	9.931	10.069	0.000	10.042	9.958	0.056
70.2	9.941	10.059	0.000	10.035	9.965	0.047
75.6	9.949	10.051	0.000	10.031	9.969	0.041
81	9.956	10.044	0.000	10.027	9.973	0.036